MARIA S. MERIAN-Berichte

SoMARTherm: The Mid-Atlantic Ridge 13-33°S

Cruise No. MSM25

January 24 – March 5, 2013,
Cape Town (South Africa) – Mindelo (Cape Verde)

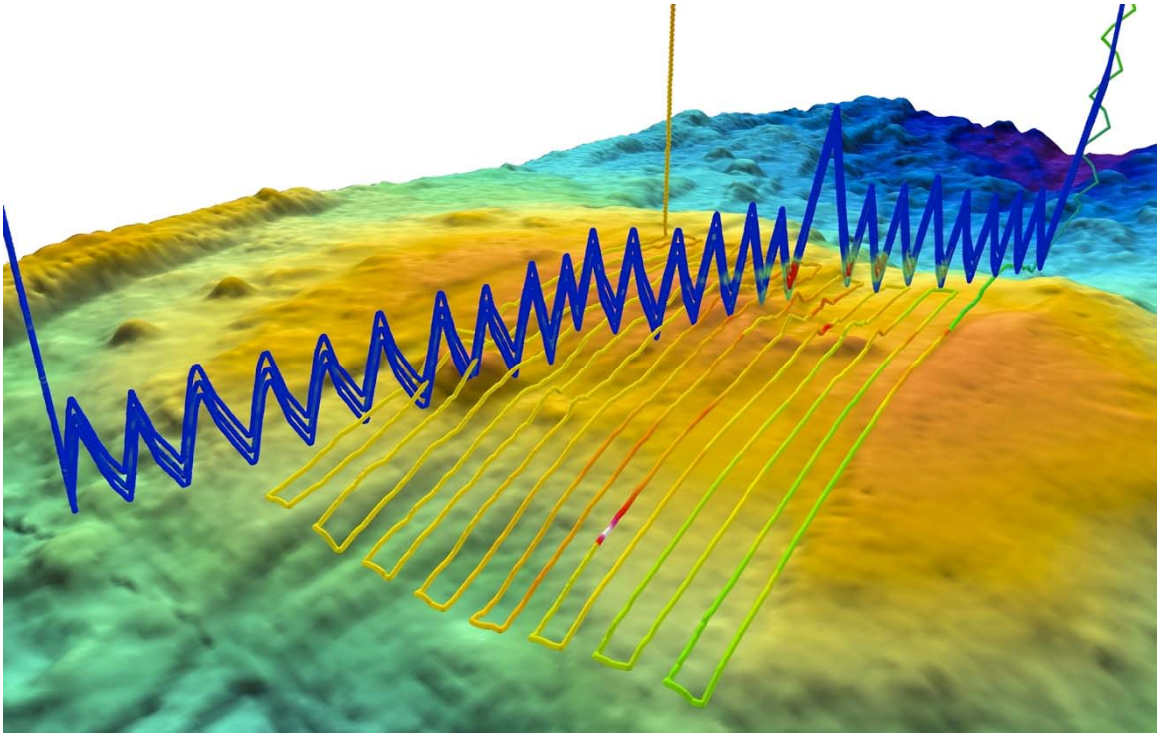

C.W. Devey

Editorial Assistance:

DFG-Senatskommission für Ozeanographie
MARUM – Zentrum für Marine Umweltwissenschaften der Universität Bremen

2014

The MARIA S. MERIAN-Berichte are published at irregular intervals. They are working papers for people who are occupied with the respective expedition and are intended as reports for the funding institutions. The opinions expressed in the MARIA S. MERIAN-Berichte are only those of the authors.

The MARIA S. MERIAN expeditions are funded by the *Deutsche Forschungsgemeinschaft (DFG)* and the *Bundesministerium für Bildung und Forschung (BMBF)*.

Editor:
DFG-Senatskommission für Ozeanographie
c/o MARUM – Zentrum für Marine Umweltwissenschaften
Universität Bremen
Leobener Strasse
28359 Bremen

Author:
Prof. Dr. Colin Devey
Helmholtz-Zentrum für Ozeanforschung
Kiel
GEOMAR
Wischhofstr. 1-3
24118 Kiel

Telefon: +49 431 600-2257
Telefax: +49 431 600-2924
E-mail: cdevey@geomar.de

Citation: C.W. Devey (2014) SoMARTherm: The Mid-Atlantic Ridge 13-33°S – Cruise No. MSM25 – January 24 – March 5, 2013 – Cape Town (South Africa) – Mindelo (Cape Verde). MARIA S. MERIAN-Berichte, MSM25, 80 pp., DFG-Senatskommission für Ozeanographie, DOI:10.2312/cr_msm25

ISSN 2195-8483

Table of Contents

1 Summary

Before the present cruise, no hydrothermal vent sites had been explored in the south Atlantic south of 13°S. As a result of the work in SPP1144 (From Mantle to Ocean: Energy-, Material- and Lifecycles at Spreading Axes), Devey et al. (2010) proposed a model for the relation between volcanism and hydrothermalism. The aim of the cruise was to use a systematic approach to explore the Mid-Atlantic Ridge between 13° and 33°S for hydrothermal activity and plume dispersal by using combined AUV deployments and ship-based CTD casts. The cruise had the following scientific goals:

- Testing the link between volcanism and hydrothermalism: The model proposed by Devey et al. (2010) suggests that hydrothermal activity will be almost constant on marked within-axis volcanic highs (as at Turtle Pits) but relatively seldom at deeper parts of the axis. As the time-scale of activity on the deeper parts of the ridges is likely to be on the order of 1000's of years we needed to use geography as a proxy for time - surveying multiple segments for hydrothermal activity to find one in the eruptive phase.
- Testing the link between ridge morphology and strength of oceanic diapycnal mixing: The sampling of a large variety of ridge morphology should allow a better understand of the relation between mixing strength, flow properties, and bathymetric roughness. The strength of mixing above the ridge crest and in the axial valley determines to a large extent the vertical exchange of chemical species from the hydrothermal fluids and the ocean interior.
- Large scale mapping of plume dispersal: Combined along-axis CTD (Conductivity, Temperature, Depth), plume chemistry (helium, methane, metals, rare elements), and current measurement can allow characterization of the large scale, particularly along axis, displacement of plume material and identification of possible pathways for larvae dispersal.
- Closing the gap between 10°S and the Antarctic ridges of ridge crest explored for hydrothermal activity, a region of high importance for the definition of biogeographical boundaries.
- Refining hydrothermal plume hunting techniques: The long-range AUV (Autonomous Underwater Vehicles) deployments coupled with ship-based CTD casts offered the possibility to survey whole segments in relatively short time-periods.

Although a thorough analysis of the cruise results (particularly for physical oceanography) will require extensive post-cruise work, it is already clear that:

1. **The marked within-axis highs show the expected chronic hydrothermal activity, confirming and reinforcing the proposed model**. In addition we found the most southerly-known axial oceanic core complex and found it also to be associated with high-temperature venting.
2. **Using co-registered AUV and CTD data over these highs we were able to map, for the first time, the 3D extent of hydrothermal plumes (see cover illustration)**. The combination of the vertical resolution of the CTD Tow-Yo with the horizontal resolution of a near-bottom (50m altitude) AUV raster gave an almost synoptic view of the venting over the entire summit. Together with the high-resolution side-scan data recorded by the AUV (which allowed us to identify and locate individual chimneys associated with the hydrothermal plumes and determine their geological setting) this provides the ideal basis for preparing to return to these biogeographically important sites to sample the ecosystems they sustain and determine the oceanographic features relevant for local larval dispersal.
3. **On ridges without within-axis highs we also found occasional signs of hydrothermal activity, proving the efficiency of the combined AUV+CTD exploration method**. An

additional bonus from the AUV deployments was that we were able to simultaneously collect a single swath of high-frequency side-scan sonar data along the axial valley and hence derive information about the style and relative age of volcanism along-axis.

Zusammenfassung

Vor der Fahrt MSM25 waren im Südatlantik keine Hydrothermalquellen südlich von 13°S bekannt. Aufbauend auf den Ergebnissen des SPP1144 (Vom Mantel zum Ozean: Energie-, Stoff- und Lebenszyklen an Spreizungsachsen) wurde von Devey et al. (2010) ein Model für den Zusammenhang zwischen Vulkanismus und Hydrothermalismus im Atlantik entwickelt. Wir haben während MSM25 eine systematische Untersuchung des Mittelatlantischen Rückens zwischen 13° und 33°S auf hydrothermale Aktivität durchgeführt und dabei dieses Modell getestet. Dabei sind die Kartierung des Rückens und der Plumes mittels eines kombinierten Einsatzes von AUV und schiffsgestützen CTD Stationen erfolgt. Die Reise hatte die folgenden wissenschaftlichen Ziele:

- Überprüfung des Zusammenhangs zwischen Vulkanismus und dem Auftreten von Hydrothermalismus: Das Modell, das von Devey et al. (2010) entwickelt wurde, sagt aus, dass zeitlich relativ konstante hydrothermale Aktivität an "in-axis volcanic highs" zu erwarten ist, im Gegensatz zu dem sehr seltenen Auftreten an tieferen Teilen der Spreizungsachse. Hier liegt die zu erwartende Zeitskala für die Beobachtung eines Events in der Größenordnung von 1000 Jahren. Darum muss die räumliche Ausdehnung als Proxy für die Zeit verwendet werden, indem eine hinreichend große Anzahl von solchen Segmenten untersucht wird, um eines in einer vulkanisch aktiven Phase zu finden.
- Überprüfung des Zusammenhangs zwischen Rückenmorphologie und Stärke der ozeanischen diapyknischen Vermischung: Die quasi-synoptische Untersuchung der Vermischung an einer großen Vielfalt von morphologisch unterschiedlichen Rückensegmenten erlaubt es, bessere Aussagen über den Zusammenhang zwischen Stärke von Vermischung, Eigenschaften des Strömungsfeldes, sowie Rauhigkeit der Bathymetrie zu treffen. Die Stärke der Vermischung oberhalb des Rückens und im Achsengraben ist zudem von großer Bedeutung für den Eintrag von chemischen Spezies aus hydrothermalen Fluiden in den Ozean.
- Großräumige Kartierung der Ausbreitung hydrothermaler Plumes: Die Kombination von hydrographischen Messungen, chemischen Analysen des Plumes (Helium, Methan, Metalle, Spurenelemente), so wie Strömungsmessungen erlauben eine genaue Charakterisierung der Plume Ausbreitung entlang der Spreizungsachse, und eröffnen damit die Möglichkeit, den Eintrag von Plume Material in die ozeanische Zirkulation sowie die möglichen Ausbreitungspfade für Larven zu untersuchen.
- Schließen der Lücke in den bisher auf hydrothermale Aktivität untersuchten Rückensegmenten im Südatlantik südlich von 13°S, um so die Beschreibung biogeographischer Provinzen zwischen dem südlichen Ozean und dem äquatorialen Atlantik voranzutreiben.
- Verbesserung der Techniken zur Entdeckung hydrothermaler Quellen. Der großräumige Einsatz von autonomen Unterwasserfahrzeugen (Autonomous Underwater Vehicles, AUV) in Kombination mit schiffsgestützen hydrographischen Messungen erlaubt die hydrothermale Erkundung von ganzen Rückensegmenten in relativ kurzen Zeitspannen.

Obwohl eine gründliche Analyse der gewonnen Daten (besonders in Bezug auf die physikalische Ozeanographie) eine Nachprozessieren erfordert und daher erst im Nachhinein an Land durchgeführt werden kann, sind bereits folgende Sachverhalte festzustellen:

1. **Segmente mit ausgeprägten zentralen Vulkanbauten zeigen alle die erwartete chronische hydrothermale Aktivität und validieren damit das Modell**. Zusätzlich

haben wir den südlichsten Mantelgesteinskomplex ("oceanic core complex") gefunden, der ebenfalls hydrothermal aktiv ist.

2. **Die gleichzeitige Aufnahme aus AUV- und CTD-Daten über den zentralen Vulkanbauten erlaubt es erstmals die 3-dimensionale Struktur solche Plumes sichtbar zu machen (siehe Titelbild)**. Die Kombination aus vertikalen CTD-Tow-Yo-Daten mit den bodennahen (50 m über Grund) horizontalen Daten des AUV-Rasters zeigt einen synoptischen Einblick in die Verteilung der Plumes über die Gesamtfläche des Vulkangipfels. Die während der AUV-Tauchgänge ebenfalls aufgezeichneten hochauflösenden Seitensicht-Sonardaten des AUV erlaubten die Identifizierung einzelner Chimneystrukturen und ihres geologischen Umfeldes. Zusammen mit den ozeanographischen Informationen erlaubt dies die Vorbereitung einer Rückkehr zu diesen Hydrothermalfeldern, um die für die globale Biogeographie bedeutenden Vent-Ökosysteme des Südaltantiks zu beproben und die lokalen Ausbreitungswege der Larven zu untersuchen.
3. **Auf Rückensegmenten ohne ausgeprägte Vulkanstruktur wurden gelegentlich ebenfalls Anzeichen für hydrothermale Aktivität gefunden, was die Effizienz der kombiniert eingesetzten Explorationsmethoden zeigt**. Als Bonus wurde während der AUV-Tauchgänge ein Streifen der Rückensegmente hochfrequent mittels Seitensichtsonar kartiert, was zusätzliche Informationen zur Form des Vulkanismus und der relativen Alter der Laven entlang der Rückenachsen ermöglicht.

2 Participants

Name	Discipline	Institution
Devey, Colin, Prof. Dr.	Marine Geology / Chief Scientist	GEOMAR
Buss, Antje	Oceanography/Helium	IUP-HB
Collins, Jane	Bathymetry	GEOMAR
Held, Noelle	Trace metals in seawater	WHOI
Jamieson, John	Marine mineral deposits	UOttawa
Köhler, Janna	Oceanography/currents	IUP-HB
Palgan, Dominik	Seafloor hydrothermalism	GEOMAR
Petersen, Sven, Dr.	Marine mineral deposits/AUV	GEOMAR
Rothenbeck, Marcel, Dipl. Ing.	AUV Team	GEOMAR
Schaefer, Sinah	Oceanography	IUP-HB
Schmid, Florian	Oceanography	IUP-HB
Steinführer, Anja, Dipl. Ing.	AUV Team	GEOMAR
Triebe, Lars	AUV-Team	GEOMAR
Vishiti, Akumbom	MAPR/Petrology	GEOMAR
Walter, Maren, Dr.	Oceanography	IUP-HB
Werdenbach, Philipp	Oceanography	IUP-HB
Yeo, Isobel, Dr.	Bathymetry/side-scan	GEOMAR
Zeng, Jing-Ying	Oceanography	IUP-HB

GEOMAR Helmholtz Centre for Marine Sciences, Kiel
IUP-HB Institut für Umweltphysik, Universität Bremen
WHOI Woods Hole Oceanographic Institution, Woods Hole MA, USA
UOttawa Dept. of Earth Sciences, University of Ottawa, Canada

3 Research Program

The cruise had several important goals:

- Testing the link between volcanism and hydrothermalism: The model proposed by Devey et al. (2010) as a result of the work in SPP1144 suggests that hydrothermal activity will be almost constant on marked within-axis volcanic highs (as at Turtle Pits) but relatively seldom at deeper parts of the axis. As the timescale of activity on the deeper parts of the ridges is likely to be on the order of 1000s of years we needed to use geography as a proxy for time - surveying multiple segments for hydrothermal activity to find one in the eruptive phase. For the present cruise we chose to survey an area comprising at least 18 first- or 13 second-order segments between 13 and 33°S. With an average of 195 volcanoes per 1000 km^2 of ridge valley floor (Smith and Cann, 1990) and an axial valley width of ca. 10km we expected to encounter ca. 1950 volcanoes in the area to be studied. Even if we assume the repeat rate of volcanism on the Southern Mid-Atlantic Ridge to be 1000 years (a very conservative estimate - the repeat rate on the East Pacific Rise appears to be around 15 years at a full spreading rate of 16 cm/yr (see Tolstoy et al., 2006). Assuming 4cm/yr spreading rate in the South Atlantic would imply a 4-fold decrease in eruption rate (= 1 eruption every 60 years) if eruption volumes are comparable) this means that we should encounter at least 2 volcanoes in this area which have erupted within the last year. Evidence from individual volcanoes on other ridges (e.g. Franklin Seamount, Woodlark basin: Binns et al., 1993) suggests that their hydrothermal systems are active for several years at least, adding further weight to our assumption that with the length of axis chosen the search for volcanic-hosted hydrothermal systems even in the deepest parts of the rift valley floor should be successful, allowing us to test the model.
- Testing the link between ridge morphology and strength of oceanic diapycnal mixing: Profiles of stratification allow the estimation of the mixing strength by overturn detection and analysis of fine structure variance. The sampling of a large variety of ridge morphology will enable us to better understand the relation between mixing strength, flow properties, and bathymetry. The strength of mixing above the ridge crest and in the axial valley determines to a large extent the vertical exchange of chemical species from the hydrothermal fluids and the ocean interior.
- Large scale mapping of plume dispersal: Combined along-axis CTD, plume chemistry (helium, methane, metals, rare elements), and current measurement should allow us to characterize the large scale, particularly along axis, displacement of plume material and to identify possible pathways for larval dispersal.
- To close the gap between 13°S and the Antarctic ridges of ridge crest explored for hydrothermal activity, a region of high importance for the definition of biogeographical boundaries.
- Refining hydrothermal plume hunting techniques: The last 5 years have seen huge advances in our ability to predict the location of and to find hydrothermal systems. Particularly long-range AUV deployments coupled with ship-based CTD casts held the possibility to survey whole segments in relatively short time-periods (100 km in 36 hrs).

4 Cruise narrative

(Devey, Yeo)

4.1 Description of work done

The cruise started on schedule on 24.01.13 in Cape Town. After one day steaming towards the working area, however, 3 trespassers were found on board, leading to us having to return to Cape Town to place them in the hands of the relevant authorities. On 28.01.13 this was achieved and we headed back out to sea at maximum speed, reaching the working area early on the morning of 03.02.13, a delay of 4 days compared to the original plan. The working area consisted of a total of 16 spreading segments of which we have bathymetric data from previous cruises for only 8 (see **Fig. 4.1**).

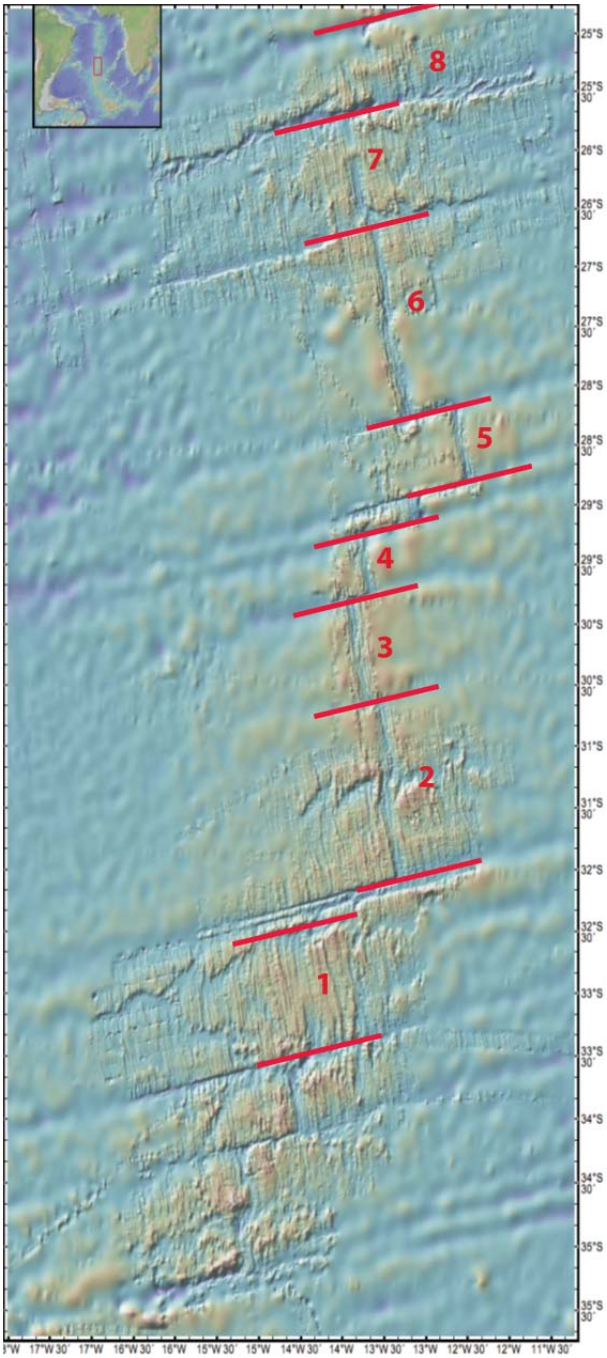

Fig. 4.1 The bathymetry of the previously mapped segments in the southern section of the working area. The segment numbers are used throughout this report and reflect the areas we concentrated on, not necessarily all the segments or sub-segments which could be defined tectonically.

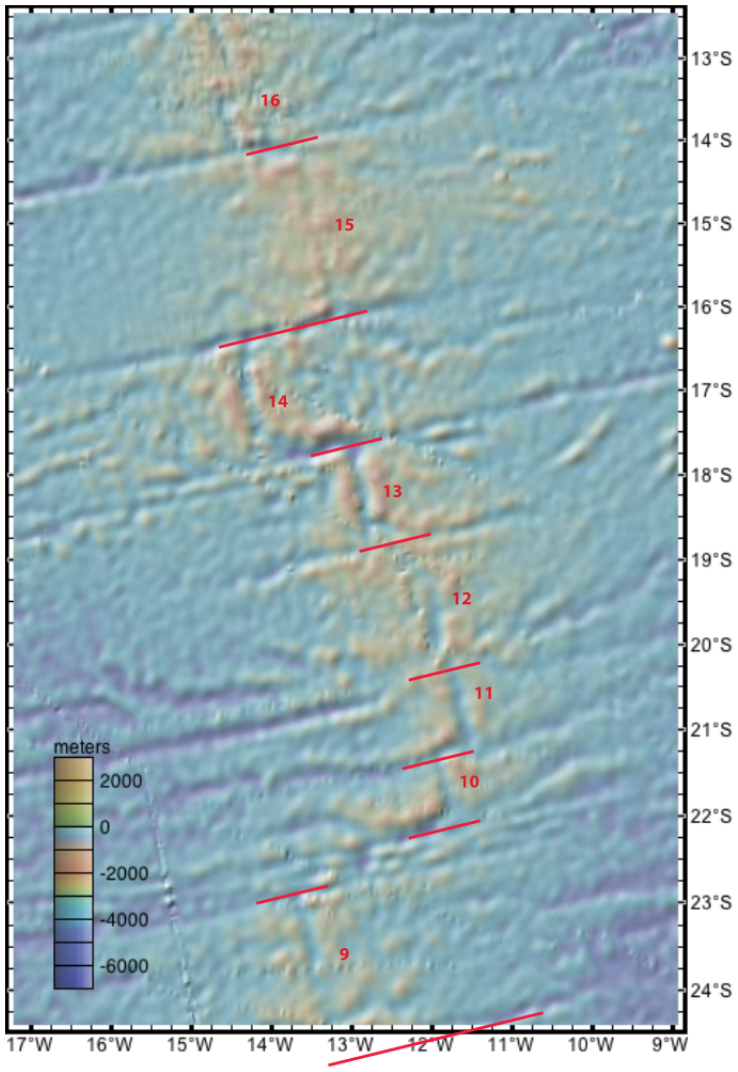

Fig. 4.2 The bathymetric overview of the previously unmapped segments derived from satellite altimetry. For segment numbering see caption to **Fig. 4.1**

For the remaining segments (9-16) the bathymetric information can be derived from satellite altimetry only (see Fig. 4.2). Our work began at the southern end of Segment 1. Our work then consisted of AUV deployments along the axis of the segments. When the AUV was diving, the ship was free to carry out the planned CTD stations to examine both ocean mixing over the complex seafloor topography and to search for traces of hydrothermal activity. This test of the hydrothermal exploration methodology (one of the technical aims of the cruise) was successful and the original time plan was found to be reasonable. This work on the previously-mapped segments 1-8 was completed on 12.02.13 and we began with the somewhat more complicated task of mapping the segments 9-16 for the first time ever AND investigating them with AUV and CTD. Progress was somewhat slower as the mapping and sampling required 3 passes of each segment (rather than the one-time pass required on Segments 1-8) but nevertheless was completed in the available time by 27.02.13 at 19:00 when we began the transit to Mindelo (Cape Verdes). The exact track of the ship during the ridge axis survey is shown in Fig. 5.1. During the survey we maintained a close watch on our level of progress by plotting latitude against time for every new work plan. The results of this are shown in Fig. 4.3.

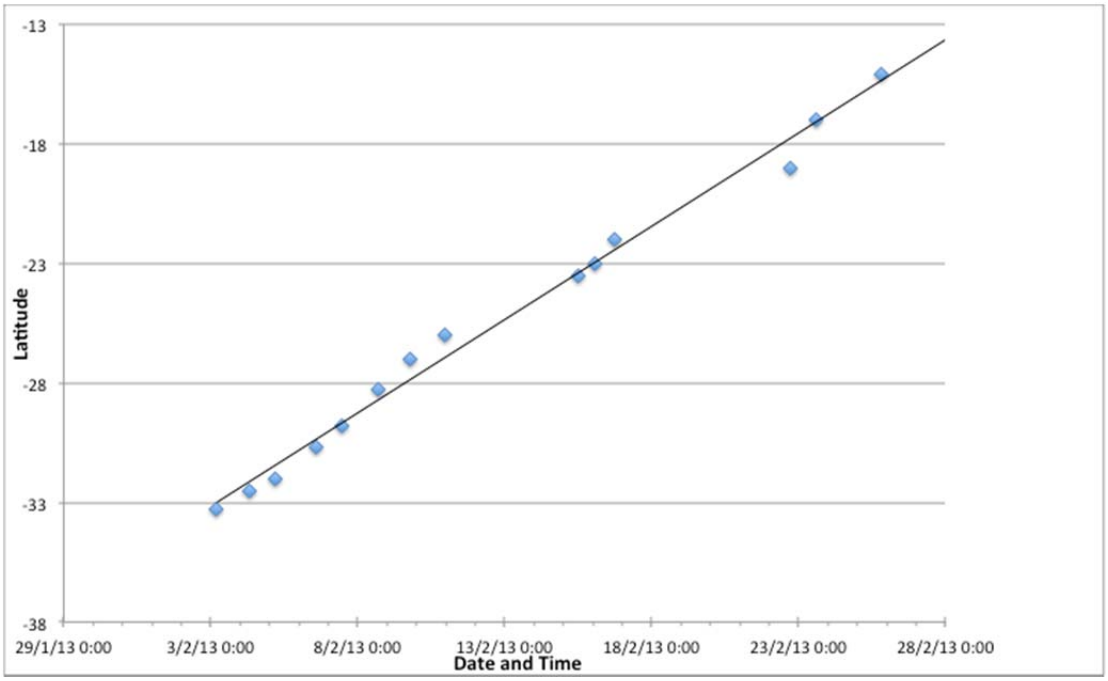

Fig. 4.3 The progress through the working area shown as a plot of latitude vs time.

We arrived in Mindelo and the cruise was completed on 05.03.13.

4.1.1 Literature

Binns, R.A., Scott, S.D., Bogdanov, Y.A., Lisitzin, A.P., Gordeev, V.V., Gurvich, E.G., Finlayson, E.J., Boyd, T., Dotter, L.E., Wheller, G.E. and Muravyev, K.G., 1993. Hydrothermal oxide and gold-rich sulfate deposits on Franklin Seamount, Western Woodlark Basin, Papua New Guinea. Bull. Soc. Econ. Geol. , 88(8): 2122-2153.

Devey, C.W., German, C.R., Haase, K.M., Lackschewitz, K.S., Melchert, B. and Connelly, D.P., 2010. The relationships between volcanism, tectonism and hydrothermal activity on the Southern Equatorial Mid-Atlantic Ridge. In: P. Rona, C.W. Devey, J. Dyment and B.J. Murton (Editors), Diversity of hydrothermal systems on slow spreading ocean ridges. Geophysical Monograph Series. American Geophysical Union, Washington D.C.

Smith, D.K. and Cann, J.R., 1990. Hundreds of small volcanoes on the median valley floor of the Mid-Atlantic Ridge at 24-30°N. Nature, 348: 152-155.

Tolstoy, M., Cowen, J.P., Baker, E.T., Fornari, D.J., RUbin, K.H., Shank, T.M., Waldhauser, F., Bohnenstiehl, D.R., Forsyth, D.W., Holmes, R.C., Love, B., Perfit, M.R., Weekly, R.T., Soule, S.A. and Glazer, B., 2006. A seafloor spreading event captured by seismometers. Science, 314: 1920-1922.

5 Preliminary Results

5.1 EM122 Multibeam Mapping

(Yeo, Jamieson, Collins, Palgan)

5.1.1 Mapping Overview

Multibeam bathymetry data were acquired over all 16 segments surveyed during cruise MSM25. The surveying we carried out during MSM25 covered a total area of 40,000 km^2.

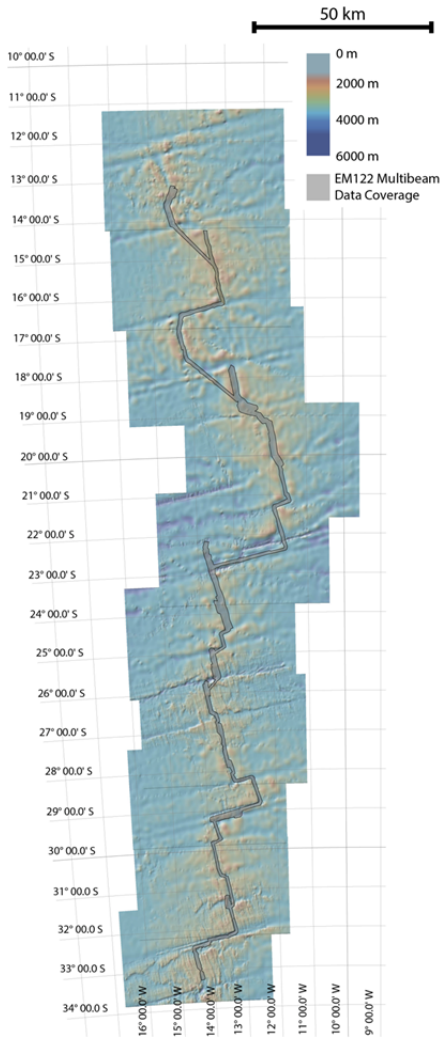

Fig. 5.1 The area surveyed using the ship´s EM-122 multibeam system superimposed on satellite altimetry data

Multibeam and backscatter data were acquired using the Kongsberg EM122 12kHz echosounder. Data were acquired at a variable ping rate dependent on water depth, but never less than 12 pings per minute, which with a ship speed of 10kn yields an absolute maximum along track resolution of 15m (data were typically gridded at 40m). Beam widths were normally kept between 55 and 60° in typical water depths of 4000 – 2500m, but occasionally increased to 65° in shallower water. Narrower beam widths (30° - 45°) were used during CTD Tow-Yos with a typical ship speed of < 1 kn yielding higher resolution datasets where the ship was in a favourable orientation.

Separate files were created for each segment's raw data files, but to avoid data gaps files were not always changed at the end of every segment. In these cases the files have been reorganized into the correct files after the data were collected. One problem noticed during data acquisition

was that pings appeared to be being ‘dropped’ (not recorded) between data file changes resulting in small (50 – 200 m) data gaps in the gridded datasets. After consultation with Kongsberg this is apparently due to lines not being completed as the file changes. Partial lines cannot be read by Fledermaus and so the loaded data contains gaps. Kongsberg have provided a program to correct this and it should be possible to reconnect these lines in post-processing.

Sound velocity profiles were taken from the CTD data and were updated regularly, and at least once every two segments (approximately every 3° of latitude), except in the transits where this was not possible.

Multibeam data were processed and gridded using the Fledermaus package (DMagic and Fledermaus for multibeam data and FMGT for backscatter). A 3σ filter was applied to the backscatter data to emphasize the difference between higher and lower backscattering areas. While all the data has received a first pass processing some artifacts do still remain in some sections and some small areas may require further editing on shore.

5.1.2 Segment Maps and Geological Summary

5.1.2.1 Segment 1 (33°30 S – 32°00 S)

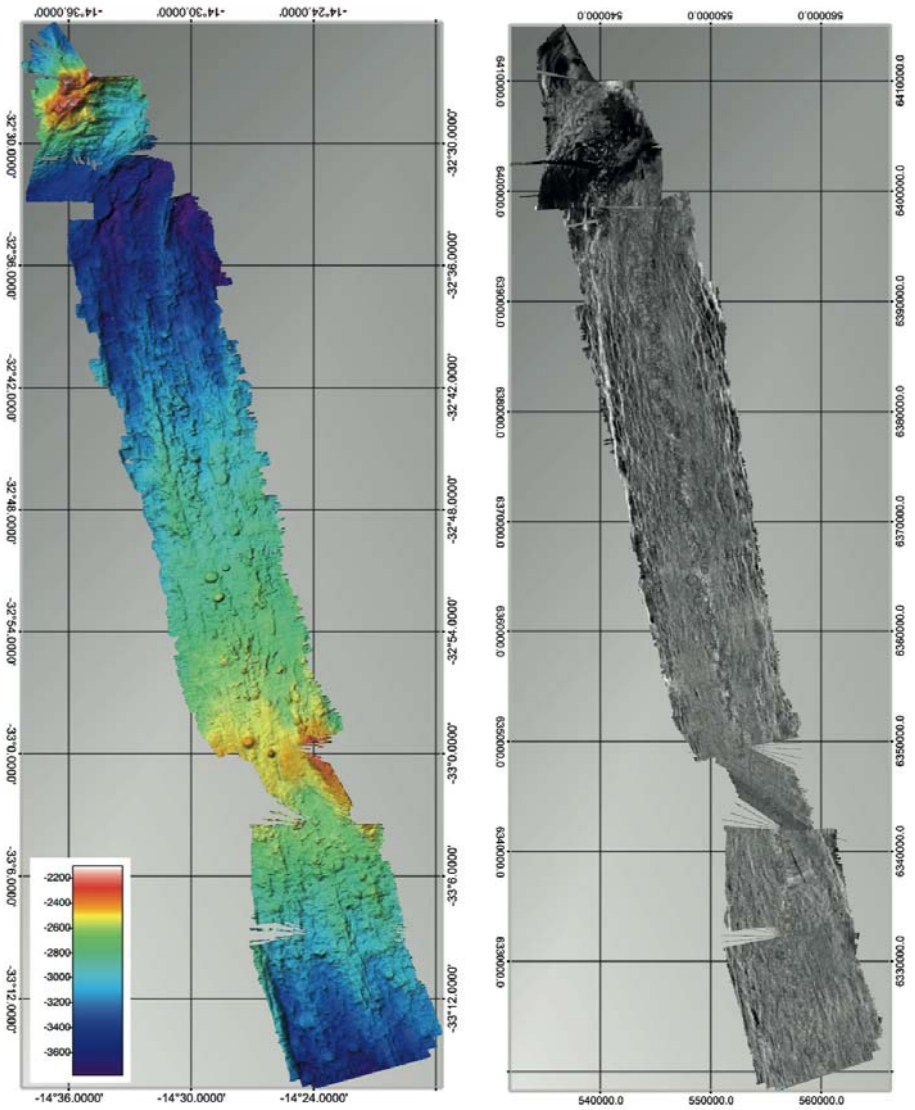

Fig. 5.2 Segment 1 bathymetry data (left hand panel) and backscatter data (right hand panel). Areas of higher backscatter are shown by lighter colours and lower backscatter by darker colours. A 3σ filter was applied to emphasise the difference between high and low backscatter areas. The narrower central section was collected during a Tow-Yo during which the ship was not completely facing the direction of travel.

Segment 1 (Fig. 5.2) extends for 85 km with a strike of 321°. The axial valley is relatively well defined and varies from 4 to 8 km in width, bounded by inward facing normal faults with throws typically around 200 m. The axis is characterized by a smooth central high, which lies 30 km from the southern end of the ridge and 50 km from the north. The shallowest point is at approximately -2450 m water depth and the deepest at -3700 m. Depths shallow smoothly towards the axial high in both the north (for 32 km away from the high) and the south (for 22 km away from the high). A number of flat-top volcanoes (the largest of which has a diameter of 1300 m) can be observed relatively close to the middle of the axis, all to the north of the axial high. We also imaged some areas of rougher textured seafloor, which are probably small areas of hummocky terrain. The surface of the axial high appears fairly smooth, but is cut by several small (< 60 m) throw faults.

The brightest backscatter imagery is centered on the ridge high, suggesting this is the

location of most recent volcanism, although relatively bright backscatter is observed along the length of the ridge suggesting it has all been volcanically active fairly recently. The lowest backscatter is observed outside the axial valley and north of the northern end.

5.1.2.2 Segment 2 (32°00 S – 30°30 S)

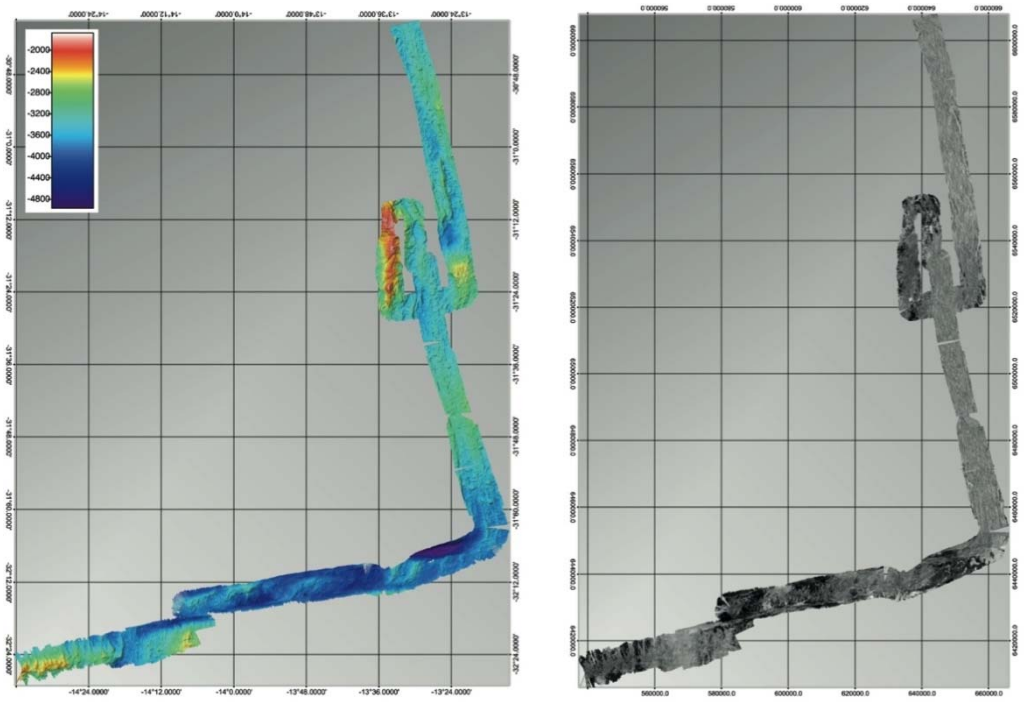

Fig. 5.3 Segment 2 bathymetry data (left hand panel) and backscatter data (right hand panel). The transit from the northern end of segment 1 is also shown. Areas of higher backscatter are shown by lighter colours and lower backscatter by darker colours. A 3σ filter was applied to emphasise the difference between high and low backscatter areas.

Segment 2 (Fig. 5.3) extends for 150 km with a strike of 322°, broken around 75 km along its length by a non-transform offset (NTO), which offsets the axial valley eastwards by 7 km. The axial valley is between 8 and 10 km wide, bounded to the east and west by inward facing normal faults with throws between 200 and 500 m. Within the axis the shallowest depths (3000 m) were observed on two highs, an axial high 65 km north and an axial volcanic ridge (AVR) 40 km south of the NTO. The deepest areas were found at the segment ends, with depths reaching -3800 m.

The AVR displays the typical rough topography associated with hummocky terrain and is associated with several flat-topped seamounts. It is cut by a number of small (throws < 100 m) normal faults, but is topped by a single, 1100 m wide, unfaulted flat-top (30°47.1 S 13°29.1 W) that buries a fault and is probably fairly young. The axial high in the south is also cut by several small (throws < 50 m) faults, which also dissect a number of the flat-tops there. Again some younger edifices can be observed, particularly the flat-top at 31°35.2 S 13°25.9 W which buries two small faults. Just south of this axial high, centred on 31°49 S 13°20 W lies a relatively unfaulted rough (again probably hummocky) area, which may be some of the youngest volcanism on the segment.

The NTO is flanked on its western side by the shallowest terrain in the area, reaching depths of -2100 m. Off the axis and behind this shallow area the seafloor is deeper than at similar distances off the axis elsewhere on the ridge (this deeper terrain is also observed on the eastern side of the valley). The shallow area takes the form of 4 highs, separated by deeper (usually around 300 m from trough to peak) areas. Each of the four highs has probably formed along faults that lie oblique to the ridge axis, although are unusually symmetrical in profile for fault

blocks.

Backscatter was fairly uniformly bright within the whole axial valley, suggesting the whole valley has experienced volcanic activity relatively recently. No difference in backscatter intensity can be seen between the northern and southern portions of the segment. The lowest backscatter was observed in the transform between segments 1 and 2 and on the high near the NTO.

5.1.2.3 Segment 3 (30°30 S – 29°30 S)

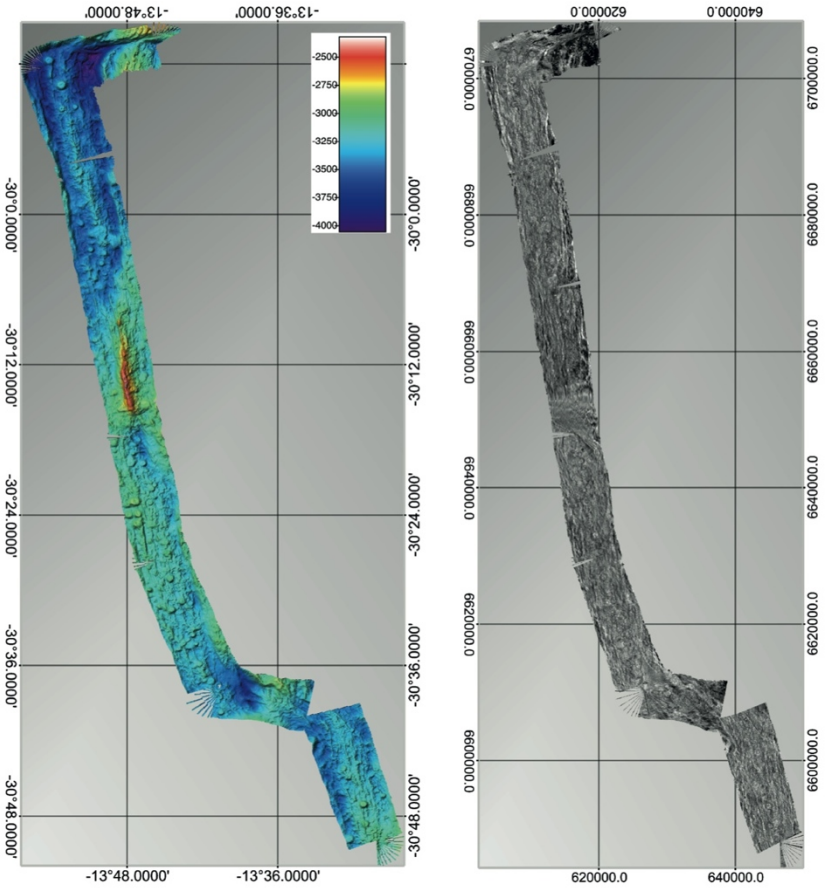

Fig. 5.4 Segment 3 bathymetry data (left hand panel) and backscatter data (right hand panel). The northern end of segment 2 and the offset is also shown. Areas of higher backscatter are shown by lighter colours and lower backscatter by darker colours. A 3σ filter was applied to emphasise the difference between high and low backscatter areas.

Segment 3 (Fig. 5.4) extends for 90 km with a strike of 323°. The axial valley is well defined, varying from 5 to 7 km wide and bounded to the east and west by inward facing normal faults, with throws typically around 250 m. The deepest areas within the axial valley (-3800 m) are found at the northern end, where the valley meets the transform. The shallowest areas are found on a large high in the middle of the segment (45 km from either end), where depths reach -2800 m.

The western side of the central high takes the form of a smooth, ridge parallel fault, with a throw of 600 m and an average slope angle of 33°. The eastern side is shallower, with an average slope angle of 19° and has the rough topography typical of hummocky volcanic terrains. The slope angle on the volcanic terrain is within the range common for AVRs and this, combined with the hummocky appearance and its position in the centre of the valley, suggest the high could be a faulted AVR, in which case the survey did not image the western side. Alternatively it may be a fault block through young volcanic terrain.

South of the central high the axis is characterized by a large number of flat-topped seamounts.

A number of these seamounts cross cut small ridge parallel faults, which cut the underlying hummocky looking seafloor. Four fairly young looking flat-tops can also been seen outside the axial valley near 30°23 S 13°47 W. North of the high fewer flat-tops are observed and the axis is characterized by a 300 m high volcanic ridge extending approximately 11 km north and south of 29°57 S 13°51 W. The ridge is unfaulted and probably hummocky, with a few flat tops. We also observe a conical, cratered seamount at 29°51.6 S 13°53.2 W, which with a diameter of 1100 m is similar in diameter, but very different in form to the flat-top seamounts.

Higher backscatter is observed in the entire axial valley, but appears slightly brighter at the southern end. Lowest backscatter is again observed outside the axial valley and towards the offset.

5.1.2.4 Segment 4 (29°30 S – 29°00 S)

Segment 4 (Fig. 5.5) extends for 55 km with a strike of 319°. The multibeam survey in this area did not always image both sides of the axial valley (particularly at the northern end) but where both sides were covered the 5 – 7 km wide valley is bounded by inward facing normal faults with throws between 250 m and 400 m. The segment does not have a well-defined axial high, but reaches its shallowest point (-3300 m water depth) 15 km from its northern end. The deepest section is at the very northern tip of the segment where it meets the transform, and reaches a water depth of -4000 m.

The segment does not appear very volcanically robust. Some flat top volcanoes can be seen, although these are mostly confined to the segment ends. The largest volcano imaged is a 2.5 km diameter, cratered, flat-topped seamount at 29°23.6 S 13°47.0 W, which lies outside the axial valley. The southern end of the segment displays some rougher texture which may be hummocky terrain but north of 29°31 S the valley is cut by a number of small throw (50 – 100 m) normal faults, which curve in towards the transform. The only volcanoes which appear to bury these faults are found at the very northern end at 29°22.4 S 13°45.7 W.

The transform between segments 4 and 5 has almost 2000 m of relief and is characterized by a deeper zone at 29°02 S 13°04 W bounded on either side by inward facing normal faults. This area also appears brighter in the backscatter imagery, suggesting there may be some volcanism here. A second brighter backscattering area in the transform corresponds to a series of tall, steep sides fault blocks. The segment 4 axial valley all appears bright in the backscatter imagery, although the south may be marginally more strongly backscattering than the north, suggesting this may be the region of most recent volcanic accretion.

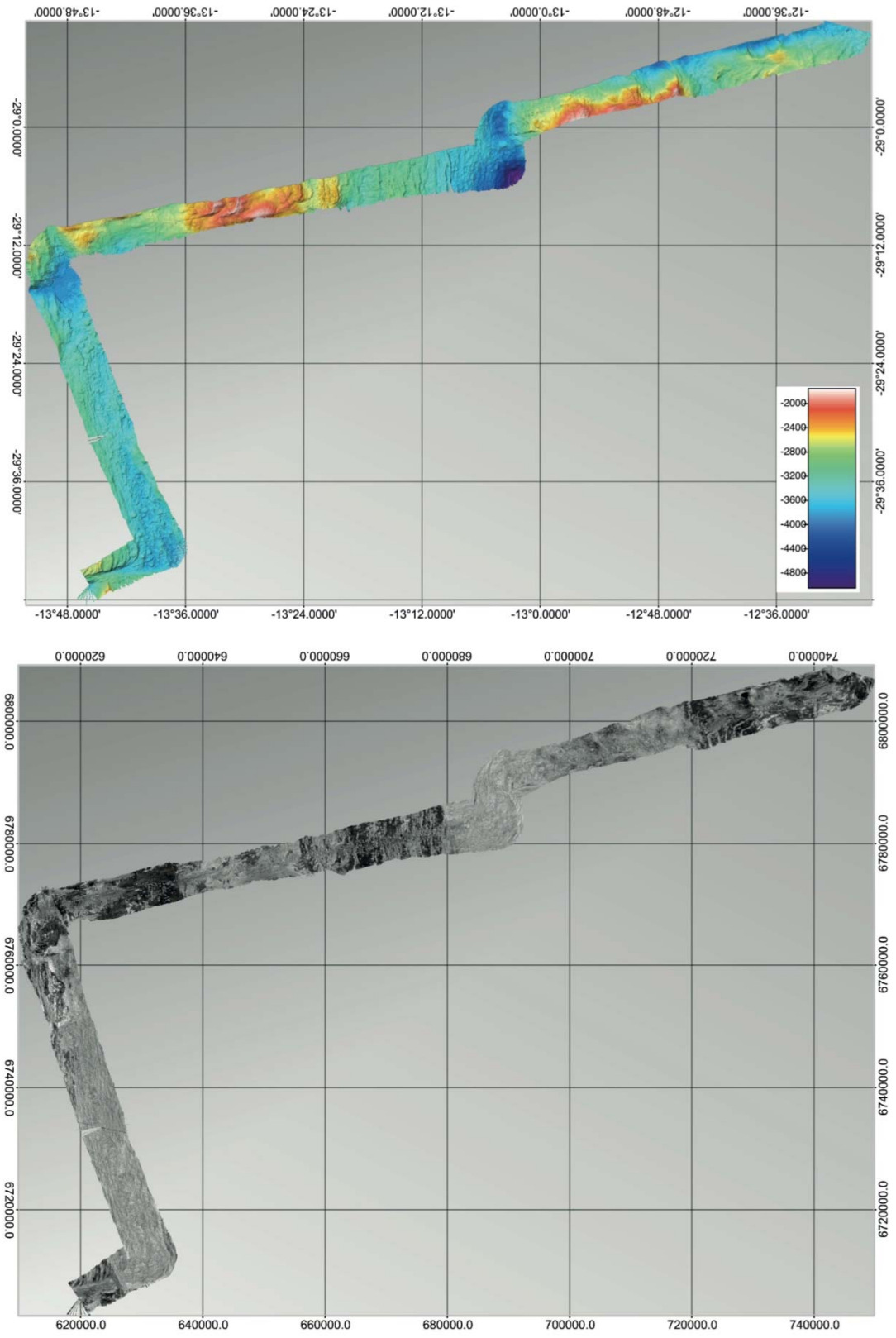

Fig. 5.5 Segment 4 bathymetry data (upper panel) and backscatter data (lower panel). The large transit across the transform between segments 4 and 5 is also shown. Areas of higher backscatter are shown by lighter colours and lower backscatter by darker colours. A 3σ filter was applied to emphasise the difference between high and low backscatter areas.

5.1.2.5 Segment 5 (29°00 S – 28°00 S)

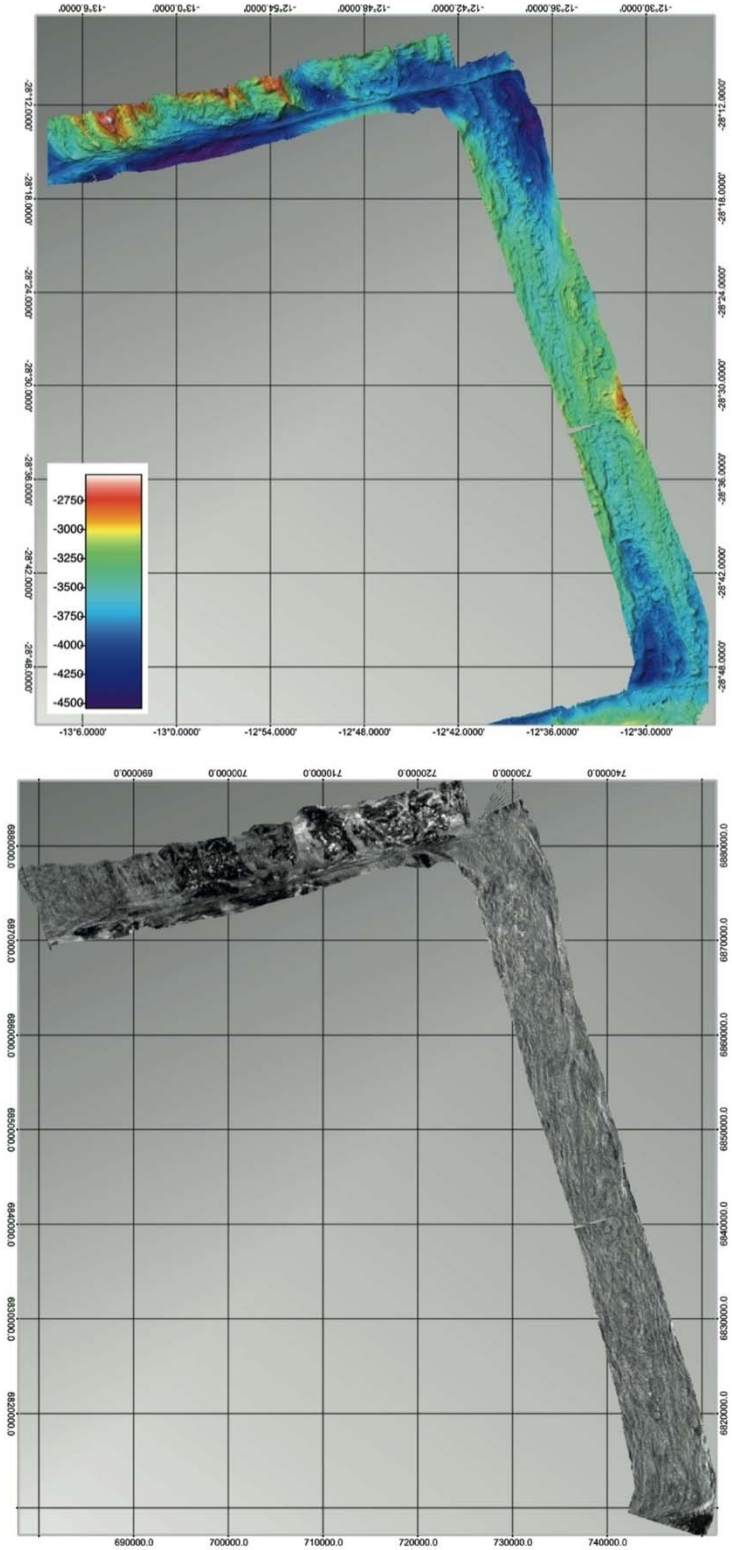

Fig. 5.6 Segment 5 bathymetry data (upper panel) and backscatter data (lower panel). The transform offset between segments 5 and 6 is also shown. Areas of higher backscatter are shown by lighter colours and lower backscatter by darker colours. A 3σ filter was applied to emphasise the difference between high and low backscatter areas.

Segment 5 (Fig. 5.6) extends for 75 km on a strike of 318°. The inner valley is bounded to the east and west by inward facing normal faults with throws typically between 300 m and 400 m,

and varies along its length from 4.5 – 5 km to 2 km at its narrowest point. This narrowing also corresponds to the shallowest water depths (-3200m) observed on the segment. The deepest areas reach -4000 m and are found at the segment ends.

Volcanic morphology can be seen along almost the entire segment length. A 9 km long AVR at 28°36 S 12°32 W characterizes the southern end of the inner valley, south of the narrow section. The AVR reaches a height of approximately 100 – 150 m above the surrounding seafloor and has a rough surface texture, probably corresponding to volcanic hummocks. South of this the seafloor deepens, but flat-topped seamounts and small patches of rough (hummocky) terrain can still be seen. The trend of all the volcanism appears to be parallel to the spreading axis with the exception of a 1.5 km long, 100 m high ridge at 28°39.8 S 12°31.3 W which lies perpendicular to the axis.

North of the narrow central section the inner valley contains a number of flat-topped seamounts and several quite large (5 x 2 km) areas of rough (hummocky) terrain, although not a well-defined AVR.

The narrowing at the centre of the segment is due to the normal faults on the eastern side of the valley stepping in towards the western side. Within these faults a small 400 – 500 m graben has formed lying parallel to the spreading axis. Neither this graben, nor the narrow axial valley, appear to contain volcanic edifices, although this does not mean they cannot be floored by low relief lava flows.

The transform between segments 5 and 6 is a narrow deep flanked to the north by fault blocks, which bend towards the transform. The transform is much darker in the backscatter compared with the segment 5 axis which is fairly uniformly brightly backscattering.

5.1.2.6 Segment 6 (28°00 S – 26°30 S)

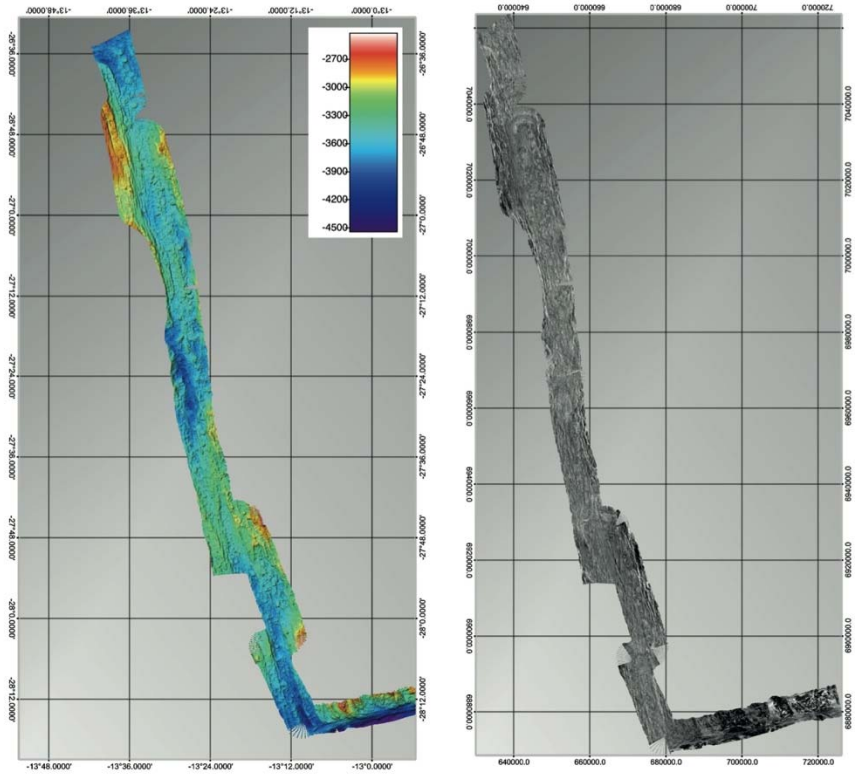

Fig. 5.7 Segment 6 bathymetry data (left hand panel) and backscatter data (right hand panel). A portion of the offset between segments 5 and 6 is also shown. Areas of higher backscatter are shown by lighter colours and lower backscatter by darker colours. A 3σ filter was applied to emphasise the difference between high and low backscatter areas.

Segment 6 (Fig. 5.7) extends for 180 km with a strike of 322°. The inner valley ranges from 5 to 8 km in diameter, bounded on either side by 200 – 600 m throw inward facing normal faults. The

axis is characterized by two highs, which reach a minimum water depth of -3200 m. The deepest section of the segment is at the southern end where it meets the transform with water depths of -4200 m.

The two highs are quite different in character. The southern one, centred on 27°45 S 13°23 W takes the form of a set of normal faults oblique to the trend of the main axis. These faults trend almost North – South and also seem to fall on a small offset or bend in the inner valley (the trend realigns itself with the southern end of the segment north of 27°24 S). Some flat-top volcanoes can be observed on the fault blocks, however the valleys on either side do not contain large volcanic edifices.

The second high is a 45 km long, 400 – 500 m high AVR that is aligned with the spreading axis. The AVR is mostly covered by rough (hummocky) terrain although a number of flat-topped seamounts can be seen both on and to either side of it. The AVR also contains several of the small conical volcanoes described in section 1.2.3, most clearly shown at 27 °12 S 13°28 W, 27°15 S 13°26 W and 26°58 S 13°30.

The middle of the ridge is fairly deep with water depths typically around -3900 m and few volcanic edifices are observed until the southern end of the AVR.

The backscatter is fairly uniformly bright along the length of the inner valley, although is marginally brighter in the area of the AVR, suggesting this is probably the location of most recent volcanism on the segment.

5.1.2.7 Segment 7 (26°30 S – 25°30 S)

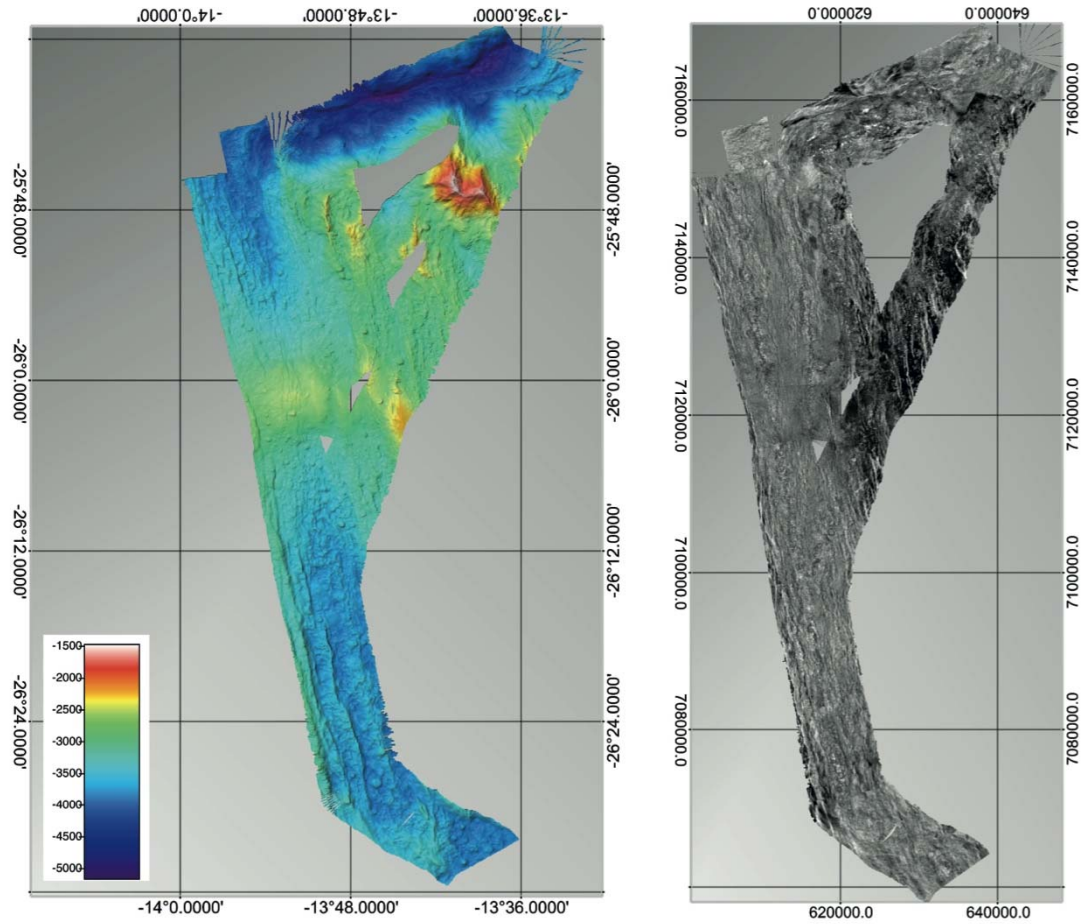

Fig. 5.8 Segment 7 bathymetry data (left hand panel) and backscatter data (right hand panel). The offset between segments 7 and 8, as well as a mapping track covering an off axis area are also shown. Areas of higher backscatter are shown by lighter colours and lower backscatter by darker colours. A 3σ filter was applied to emphasise the difference between high and low backscatter areas.

Segment 7 (Figure 5.8) extends for 85 km with a strike of 324°. The inner valley ranges in width from 7 to 9 km, bounded by inward facing normal faults, although on the eastern side of the valley these faults are not always clear and in places the axial valley may be as wide as 14 km. Fault throws are of the order of 100 – 200 m on the western side and may be as great as 800 m on the eastern side. The inner valley is characterized by a pronounced smooth axial high, which, with a water depth of -2600m, is much shallower than the majority of the segment, lying mostly at 3800 – 3400 m.

The central high is 9 km by 9 km in size and is characterized by a very smooth surface. The summit is cut by a number of small throw (20 – 40 m) normal faults, which form a small axis parallel central graben approximately 60 m deeper than the summit of the high. Rough (hummocky) volcanic terrain with a few flat-topped seamounts is observed directly north and south of the high, but the flat-tops (and probably also the hummocky terrain) becomes less common more than 25 km north and south.

The survey also imaged an off axis area to the east of the spreading axis, which displays typical faulted off axis terrain. Throws of individual faults were mostly less than 200 m, although a faulted block with a relief of almost 1000 m centred on 25°47 S 13°40 W appears to form the western flank of a second small valley. This area also appears slightly brighter than the surrounding off axis seafloor, but no volcanic edifices can be seen within the valley here from the multibeam data. Backscatter in the axial valley is fairly uniform and the axial high is indistinguishable from the surrounding terrain, despite probably being the locus of most of the segments volcanism.

5.1.2.8 Segment 8 (25°30 S – 25°00 S)

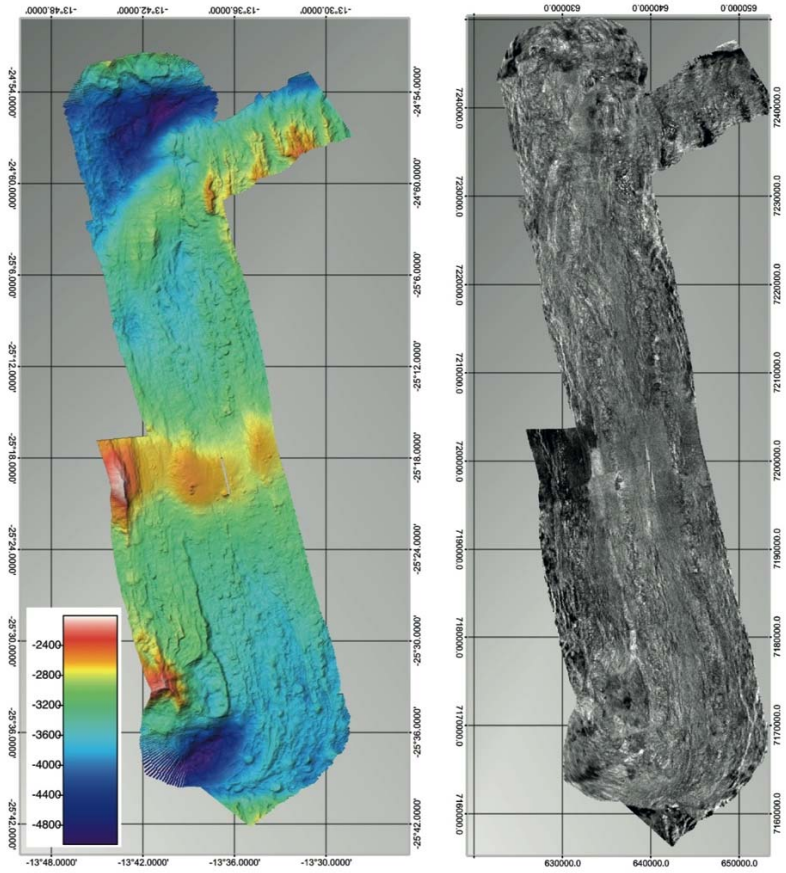

Fig. 5.9 Segment 8 bathymetry data (left hand panel) and backscatter data (right hand panel). Areas of higher backscatter are shown by lighter colours and lower backscatter by darker colours. A 3σ filter was applied to emphasise the difference between high and low backscatter areas.

Segment 8 (Fig. 5.9) is 82 km long and strikes 323°. The depth of the segment steadily decreases from - 4,875 m at the southern end of the segment to - 2,417 m at a central volcanic high and then increases again to a depth of 5,022 mbsl at the northern end of the segment. A secondary volcanic high rises to - 2,887 m just south of the northern end of the segment. The axial valley is bounded on the western side by a series of inward facing fault scarps with up to 85 m of relief and an average slope of 17°. The eastern edge of the axial valley is less well-defined, especially in the southern portion of the segment. The valley floor consists of a series of parallel volcanic or faulted ridges and several flat-top volcanoes of up to 200 m in height. The central volcanic high, located 34 km north of the southern end of the segment, is dome-shaped and gradually rises over 500 m from the valley floor. Compared to the valley floor, the volcanic high is relatively smooth, with the exception of a linear series of three ~100 m high volcanoes that occur near the center of the high and a ~150 m volcano on the southeast edge.

The ridges on the valley floor at the southern terminus of the segment bend westward into the transform fault region between segment 8 and segment 7, which lies to the southwest. A similar gradual bending of the valley floor fabric occurs at the northern terminus of segment 8, but is not as pronounced as at the southern terminus.

Brightest backscatter values are observed within the inner valley and may be marginally brighter in the vicinity of the axial high. The lowest backscattering areas are observed on the fault scarp directly west of the axial high.

5.1.2.9 Segment 9 (25°00 S – 22°30 S)

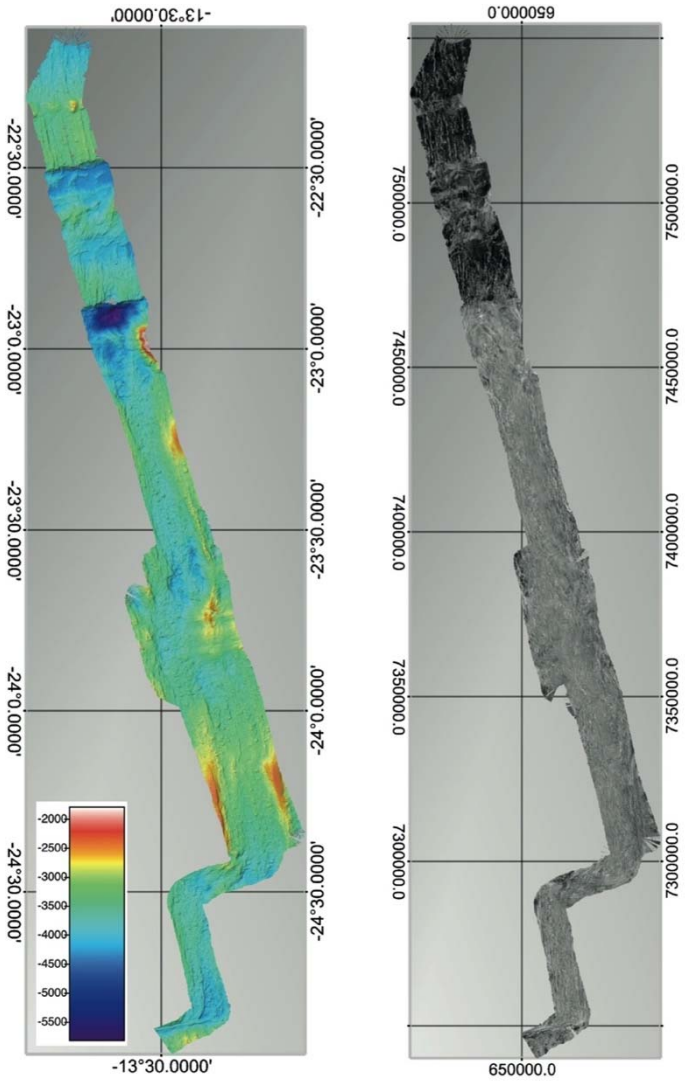

Fig. 5.10 Segment 9 bathymetry data (left hand panel) and backscatter data (right hand panel). Areas of higher backscatter are shown by lighter colours and lower backscatter by darker colours. A 3σ filter was applied to emphasise the difference between high and low backscatter areas.

Segment 9 (Fig. 5.10) is 220 km long and strikes at 321°. It is divided into two sections, separated by a small, 26 km long right-stepping non-transform offset, 43 km north of the southern terminus.

The southern section becomes progressively shallower to the north, from a maximum depth of -4,340 m at the southern end to ~ -3,585 m in the north. The axial valley is 7 to 8 km wide and is bound on both sides by inward-dipping normal faults with throws of >200 m and average slopes of ~10°. The valley floor consists of ridge-parallel fractures and numerous flat top volcanoes, the largest of which has an elevation of 260 m and a basal diameter of 1.2 km.

The axial valley of the northern section varies in width from 7 to over 25 km near the middle of the segment. The valley walls are also variable, ranging from several small inward dipping fault scarps to a single 500 m high fault scrap with an average slope of ~20°. Flat top volcanoes are again abundant, with some that are >300m in height.

The central 40 km of the northern segment appears asymmetric, with no clear axial valley boundary to the west and a large volcanic high on the eastern side that rises 1,500 m from the valley floor and extends to the east beyond the limit of the map area. Unlike the axial valley floor along the rest of the segment, which contains numerous ridge-parallel faults or volcanic ridges, the volcanic high on the eastern side of the valley is marked by parallel striations that are

perpendicular to the ridge axis and continuous over the length of the high. The striations terminate at the western basal edge of the volcanic high, near the axis of the valley. West of the volcanic high, the axial valley floor appears similar to elsewhere along the segment.

The entire inner valley appears relatively brightly backscattering and no clear differences can be seen within it, suggesting relatively uniform volcanism along the segment. The darkest values were observed north of the segment on the transform complex.

5.1.2.10 Segment 10 (22°30 S – 21°00 S)

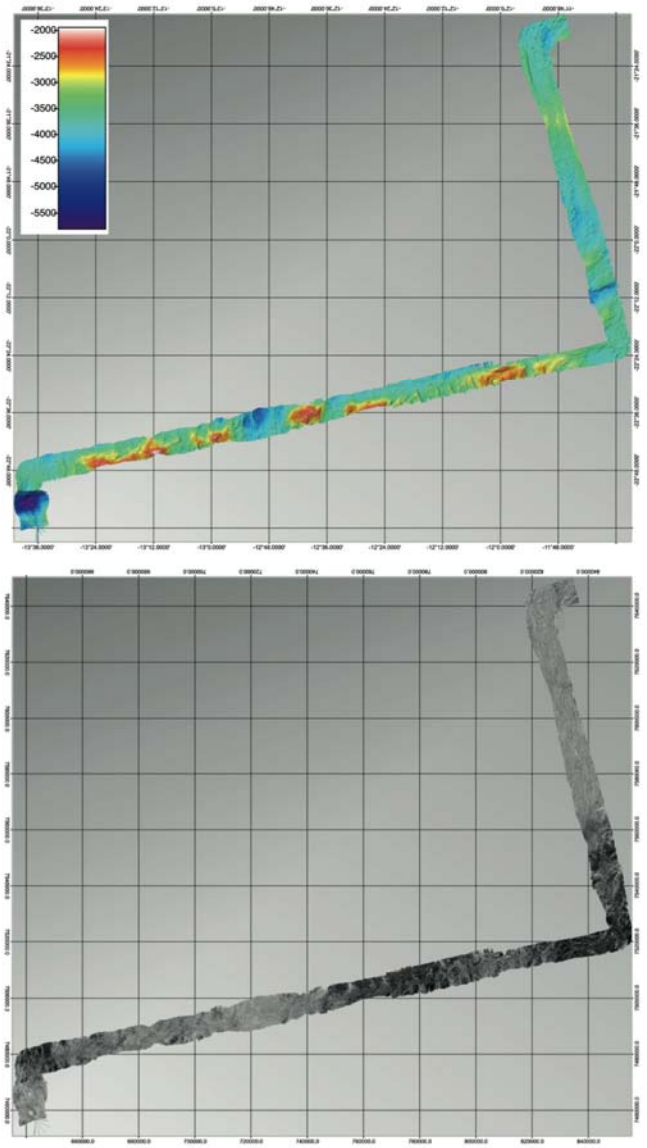

Fig. 5.11 Segment 10 bathymetry data (top panel) and backscatter data (bottom panel). Areas of higher backscatter are shown by lighter colours and lower backscatter by darker colours. A 3σ filter was applied to emphasise the difference between high and low backscatter areas.

Segment 10 (Fig. 5.11) is 85 km long and has a strike of 321°. It rises from a depth of - 4,100 m at the southern end to a high of - 2,960 m at the center of the segment, and steadily becomes deeper to a maximum depth of ~- 4,300 m at the northern end of the segment. Segment 10 is offset 218 km northeast of segment 9, separated by a 40 km transform fault zone. The axial valley is 8-10 km wide, and is bounded by normal faults with surface relief of up to 500 m and an average slope of ~25°. The valley floor is generally rough, with numerous ridge-parallel faults and ~100-200 m tall, 1 km wide flat-top volcanoes. The increase in ridge elevation from the

north and south, towards the center of the segment is gradual. The central volcanic high is bisected by a ridge-parallel fault, with the western block being down-dropped ~250 m from the eastern block. The fault is continuous for at least 18 km along the axial valley floor.

The transform zone is characterized in the centre by a low point bounded on either side by inward facing normal faults. This combined with the brighter backscatter values in the area suggest this could be a small area of seafloor spreading. The lowest backscatter is observed in the transform zone away from these areas.

5.1.2.11 Segment 11 (21°00 S – 20°00 S)

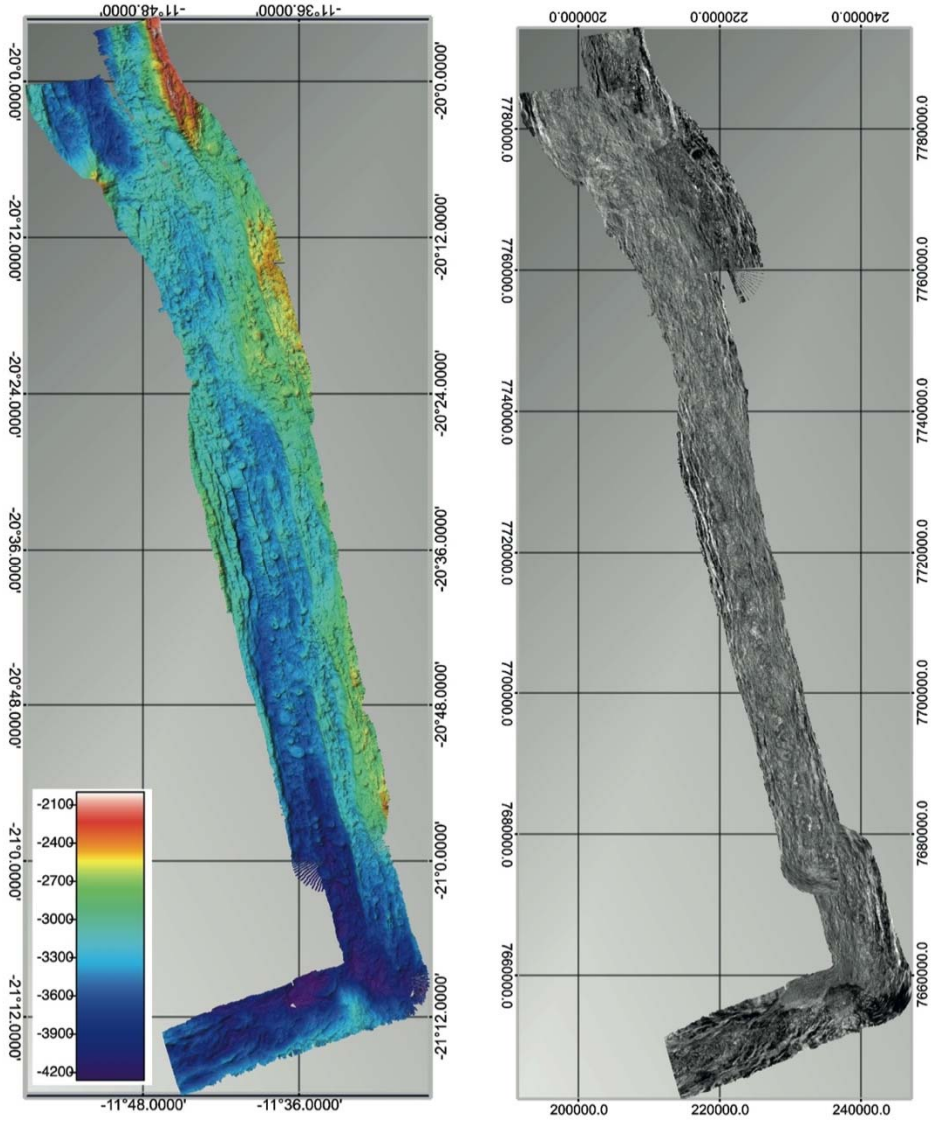

Fig. 5.12 Segment 11 bathymetry data (left hand panel) and backscatter data (right hand panel). Areas of higher backscatter are shown by lighter colours and lower backscatter by darker colours. A 3σ filter was applied to emphasise the difference between high and low backscatter areas.

Segment 11 (Fig. 5.12) extends 126 km, at a bearing of 323° from an dextral transform offset from segment 10 to a slight sinistral offset to segment 12 at the north end. The elevation along the ridge axis is irregular and does not have a central volcanic high typical of other segments along this part of the Mid-Atlantic Ridge. Instead, the segment becomes progressively shallower to the north from a depth of - 4,190 m to a maximum elevation of - 2,950 m, ~12 km south of the northern end of the segment. The axial valley has a relatively consistent width of 7 km, bounded on either side by 300 – 500 m fault scarps that are dipping at an average of 30° towards the

center of the valley. Towards the northern end of the segment, the valley walls change from a single, large fault scarp to a series of smaller, ~100m fault scarps. The axial valley floor consists of a series of ridges parallel to the spreading axis. Volcanic mounds up to 300 m high are common on the axial valley floor. Unlike other nearby segments, where the volcanoes generally have flat tops, many of the volcanoes along segment 11 have craters at their top, with crater depths of up to 75 m. One such volcano ('Brian') was dredged along with a nearby flat-top (see Section 0). The cratered volcanoes are more common in the southern half of the segment. The distribution of cratered volcanoes relative to flat-top volcanoes appears to be random. The cratered volcanoes are generally taller and have steeper sides than the flat-top volcanoes.

The brightest backscatter values were observed within the inner valley, and appear marginally brighter at the northern end, which corresponds with the shallower seafloor in this area. Lowest backscatter values were observed outside the axial valley and in the transform offset at the southern end of the segment.

5.1.2.12 Segment 12 (20°00 S – 18°30 S)

Segment 12 (Fig. 5.13) is 103 km long, and trends at a bearing of 328°. The segment becomes progressively shallower towards the north, from a maximum depth of -4,006 m at the southern end to -2,725 m at the northern end of the segment. The 9km offset between segments 11 and 12 is gradual over 33 km and no abrupt angular offset is present. A ~250m volcanic high occurs in the middle of the transition zone between the two segments.

Axial valley width varies from 5 to over 16 km. Although the segment maintains a relatively constant orientation, the valley walls on both sides are not always parallel to the ridge axis, resulting in the highly variable valley width. In the southern half of the segment, the eastern valley wall consists of two fault scarps with a combined height of over 1,600 m, terminating at the top of a volcanic high that occurs along the eastern edge of the axial valley. The western valley wall in the southern half of the segment is ~1,000 m high and consists of a series of inward dipping normal fault scarps. The valley widens towards the middle of the segment, and then becomes narrower in the northern half of the segment. The innermost valley walls in the northern segment are not as high as those in the southern half of the segment. Fault scarps reach a maximum height of 600 m above the valley floor. The eastern valley walls at the north end of the segment are much higher than the western walls.

The axial valley floor contains several volcanic or fault-related ridges that are parallel to the ridge axis. The valley floor of the southern half of the segment appears to more rough than the northern half. Flat-top and cratered volcanoes are present in the northern half of the segment. The tallest volcano reaches 300 m above the valley floor.

Brightest backscatter values are observed fairly uniformly in the inner valley, while lowest backscatter values were observed at the very northern tip – an area not affected by the complex overlapping, short spreading centres which form the offset between segments 12 and 13 and are described more fully in the next section.

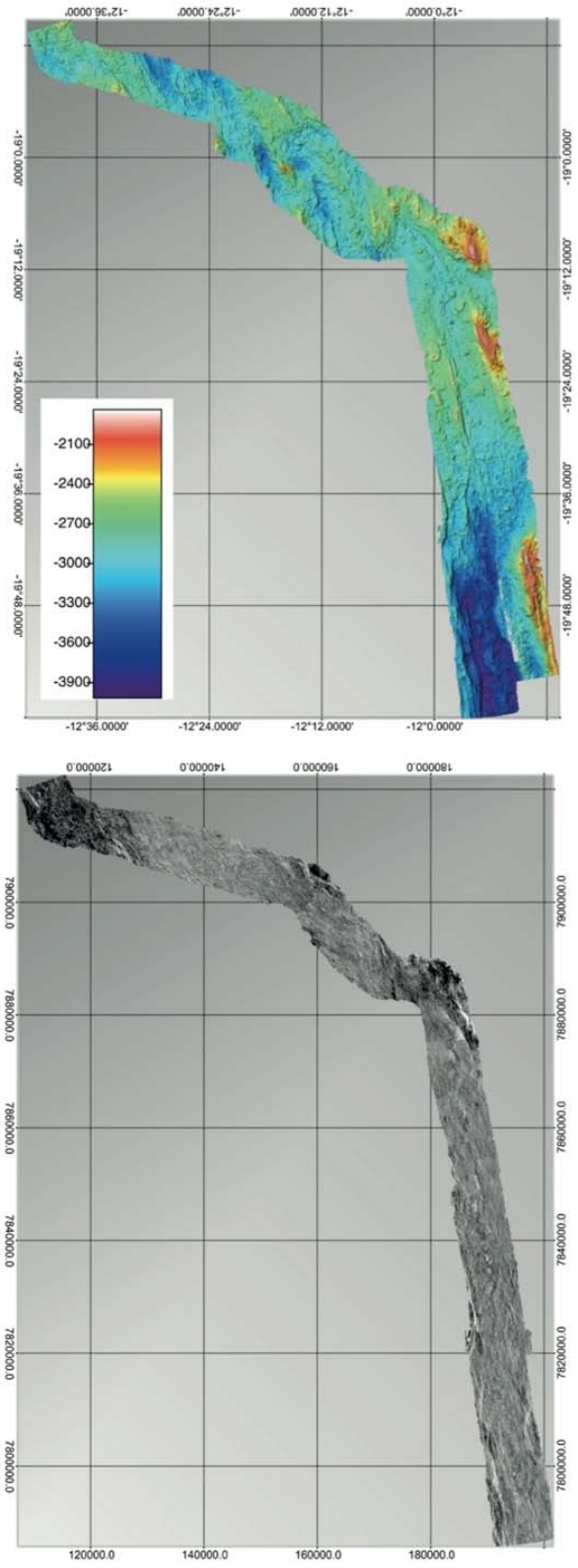

Fig. 5.13 Segment 12 bathymetry data (top panel) and backscatter data (bottom panel). Areas of higher backscatter are shown by lighter colours and lower backscatter by darker colours. A 3σ filter was applied to emphasise the difference between high and low backscatter areas.

5.1.2.13 Segment 13 (18°30 S – 17°00 S)

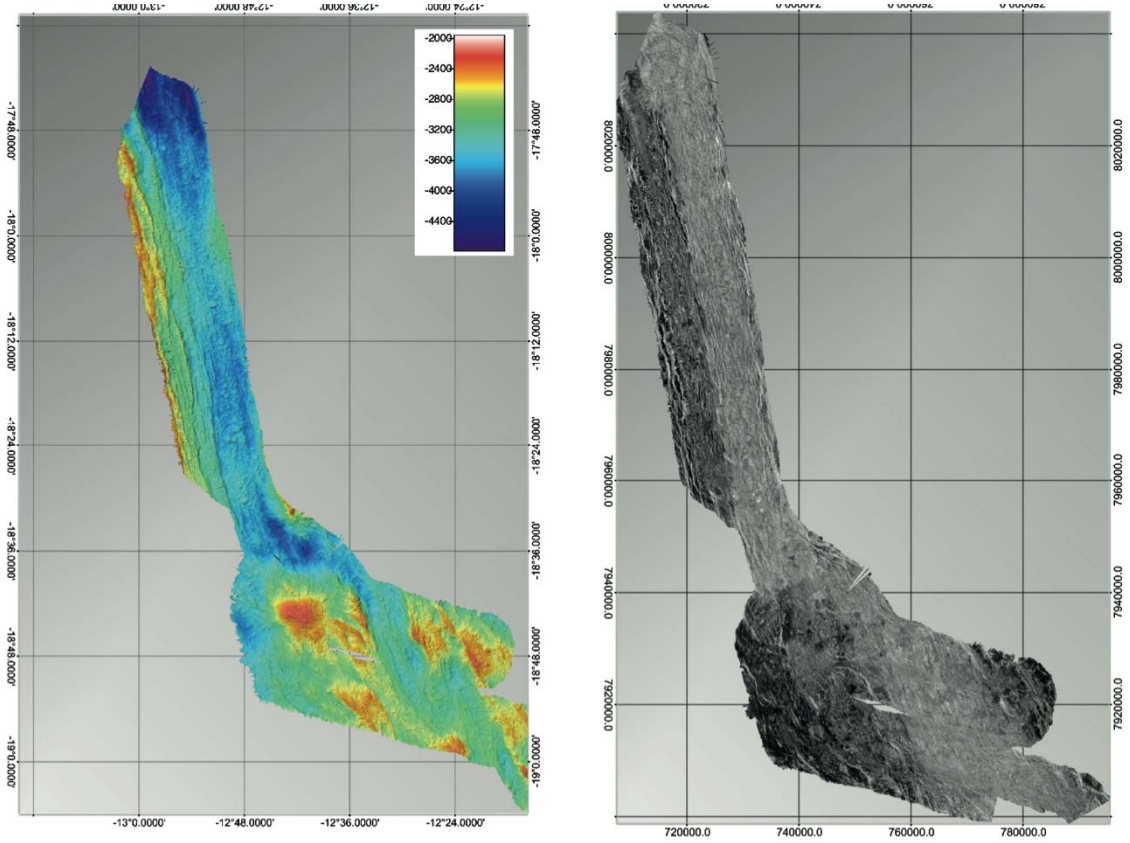

Fig. 5.14 Segment 13 bathymetry data (left hand panel) and backscatter data (right hand panel). The two most westerly overlapping segments in the offset offset are also shown. Areas of higher backscatter are shown by lighter colours and lower backscatter by darker colours. A 3σ filter was applied to emphasise the difference between high and low backscatter areas.

Segment 13 (Fig. 5.14) extends for 110 km on a strike of 326°. The axial valley varies from 7km to 9 km in width and is bounded to the east and west by inward facing normal faults with throws between 300 and 500m. The inner valley lies mostly between -3600 m and -3400 m water depth, with the shallowest point around 40 km from the northern end. The deepest sections are found at the northern end of the segment, reaching a maximum depth of -4200m.

The transform region between segments 12 and 13 is unusual. Between the segments the axial valley is offset westwards by approximately 50 km, however this offset does not take the form of a simple transform fault or a diffuse zone of faulting as observed elsewhere. Instead the offset is taken up across three short, overlapping spreading centres. All three small centres contain volcanic edifices. The most easterly, centred on 19°02 S 12°11 W, contains a number of flat top-seamounts, some of which have large summit craters, as well as areas of rough (hummocky) terrain. The volcanoes form a curved ridge, which aligns with curved, small throw (< 100 m) faults, which also curve into the next small segment. This second segment, centred on 18°55 S 12°21 W, is less well defined on its western side, but still forms a 2 km wide valley containing rough (probably hummocky) terrain and a single flat-topped seamount at its northern end. The third small segment is the straightest and best defined, bounded to the east and west by 200 m – 400 m throw inward facing normal faults. The inner valley contains a 500 m high, rough textured ridge, which may be an AVR, and is cut by a number of faults at its northern end.

Segment 13 itself has volcanic edifices along its entire length, but most of these are probably fairly old being cut by the 50 – 100 m throw normal faults which are common on the inner valley floor north of 18°13 S. South of this point the edifices look younger and a 200m high, 20 km long unfaulted AVR fills the valley.

The brightest backscatter is observed within the segment 13 inner valley and within the small overlapping segments in the offset between segments 12 and 13, suggesting all have been volcanically active relatively recently.

5.1.2.14 Segment 14 (17°00 S – 15°30 S)

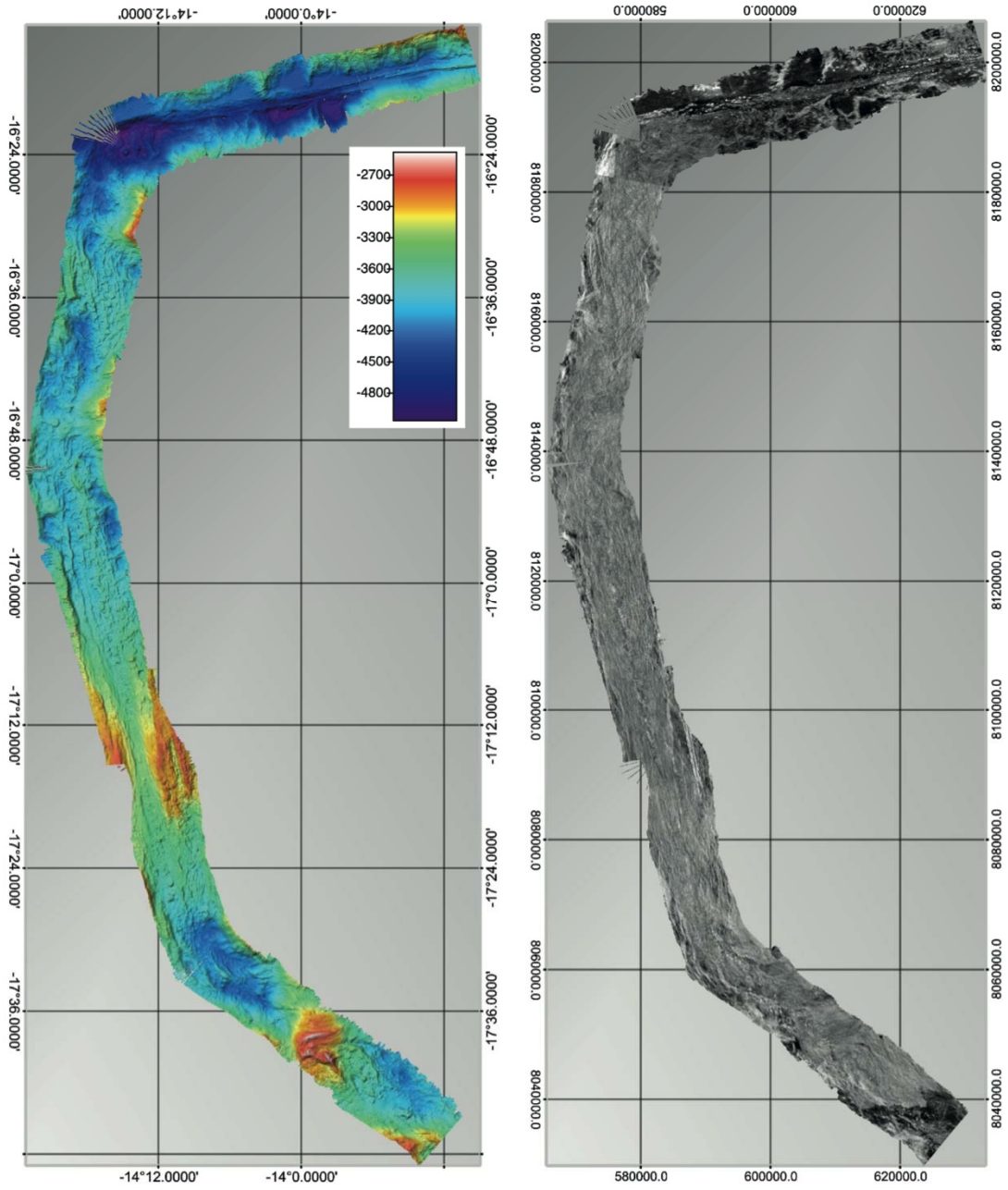

Fig. 5.15 Segment 14 bathymetry data (left hand panel) and backscatter data (right hand panel). Portions of the offsets between segments 13 and 14 and 14 and 15 are also shown. Areas of higher backscatter are shown by lighter colours and lower backscatter by darker colours. A 3σ filter was applied to emphasise the difference between high and low backscatter areas.

Segment 14 (Fig. 5.15) extends for 120 km with a strike of 323°. The ridge axis varies in width from 7 to 10 km and is bounded on either side by inward facing normal faults. Approximately 80 km from its southern end the axis is offset 11 km to the east by a NTO. The shallowest depths (-3400 m) are observed on the longer southern section on the axial high at 17°14 S 14°13 W. The deepest depths (-4100 m) are found at the segment ends.

Few flat-topped seamounts can be observed along the segment, but some small areas of rough, probably hummocky, terrain can be seen in the inner valley. The valley is fairly flat along its length, and is broken up by a number of small throw (<150 m) normal faults, suggesting it is not particularly volcanically robust.

The whole axis is relatively uniformly brightly backscattering, suggesting no part of the segment is currently more active than the rest. The lowest backscatter is found on the transform to the north.

5.1.2.15 Segment 15 (15°30 S – 13°00 S)

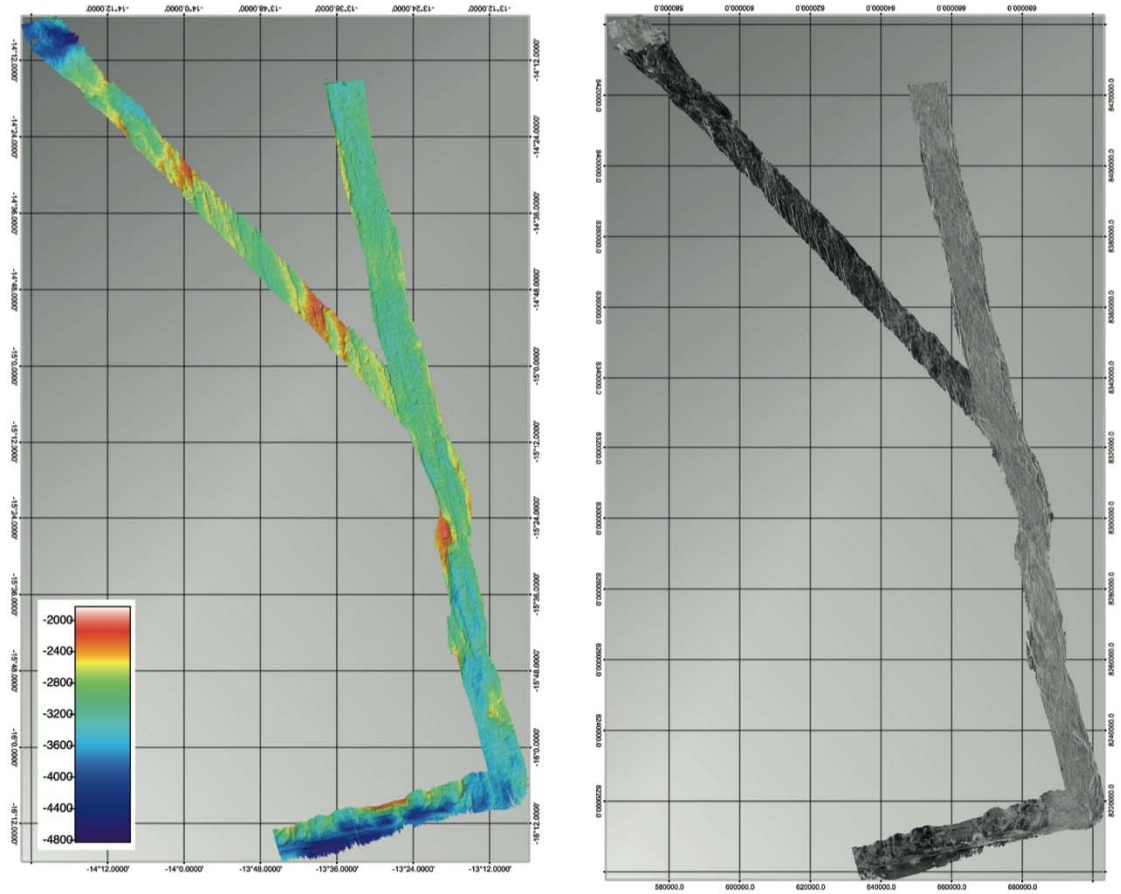

Fig. 5.16 Segment 15 bathymetry data (left hand panel) and backscatter data (right hand panel). Portions of the offsets between segments 15 and 16 and an off axis stripe collected during the transit to 16 are also shown. Areas of higher backscatter are shown by lighter colours and lower backscatter by darker colours. A 3σ filter was applied to emphasise the difference between high and low backscatter areas.

Segment 15 (Fig. 5.16) extends for 200 km on a strike of 326°. The inner valley is bounded to the east and west by inward facing normal faults with throws between 300 m and 400m. The deepest point is at the southern end of the segment where it meets the segment transform, with a depth of -3600 m. The shallowest points within the inner valley reach water depths of around -2700 m on the ridge and are found in the middle of the segment on a 250 m high AVR and at the northern end on what appears to be a small smooth axial high. A second AVR can be seen at the southern end (15°38 S 13°15 W), which has much greater relief above the surrounding seafloor than the one further north, but only reaches water depths of -3100m.

This southern AVR is 13km long and rises 500 m above the surrounding seafloor. The surface is characterized by rough terrain characteristic of volcanic hummocks and the northern end is cut by two relatively small throw (< 150 m) normal faults. This southern end is separated from the rest of the ridge by a small NTO at 15°27 S 13°17 W which offsets the ridge axis 5 km to the east. The ridge north of this is in general around 600 m shallower than the southern section. The

northern AVR (15°12 S 13°21 W) is around 22 km long and is hard to distinguish as it is surrounded on both sides by volcanic terrain. The surface of the AVR displays typical rough hummocky texture and several flat-topped seamounts can be observed along its length. At its northern end it is cut by a 100 m throw, easterly facing normal fault. A nice example of the conical seamounts described in the previous section can be seen at 15°06 S 13°24 W. The only very smooth looking section of the segment is found on the 'axial high' at 14°43 S 13°29 W. This high is much less well defined than those described elsewhere and is flanked by rough terrain on all sides.

The backscatter is uniformly high along the ridge length and darker on the off axis areas and on the transform. No difference can be distinguished in backscatter either side of the NTO.

5.1.2.16 Segment 16 (13°00 S – 12°00 S)

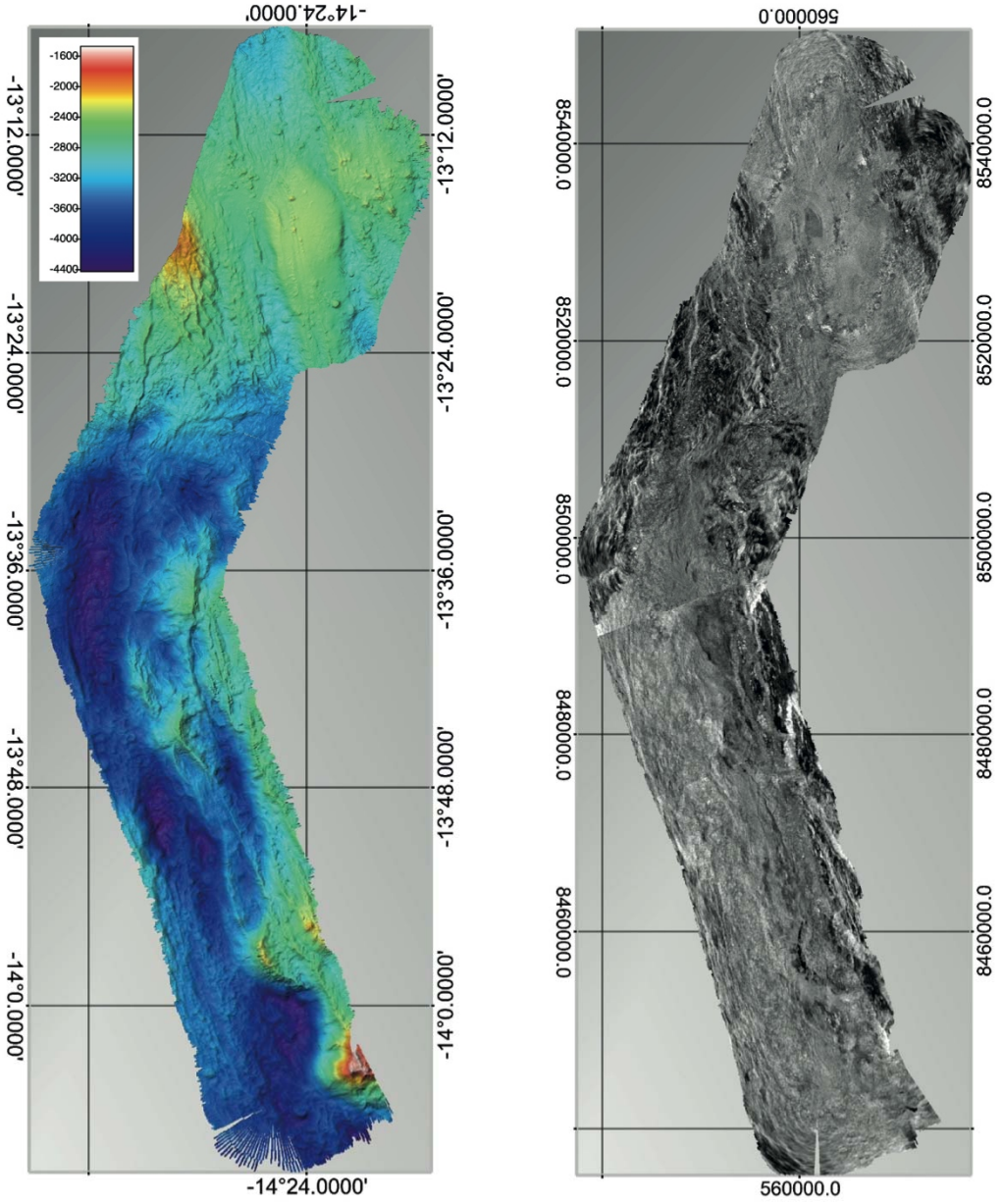

Fig. 5.17 Segment 16 bathymetry data (left hand panel) and backscatter data (right hand panel). Areas of higher backscatter are shown by lighter colours and lower backscatter by darker colours. A 3σ filter was applied to emphasise the difference between high and low backscatter areas.

During MSM 25 we imaged only the southern 90 km of segment 16 (Fig. 5.17). The segment has a strike of 320° and the ridge axis is offset 20 km to the east at 13°31 S 14°30 W by a small

transform. The inner valley is mostly around 9 km wide, although very different in character either side of the offset. The southern end is much deeper, reaching a water depth of -4400 m near the offset. The northern end is much shallower and reaches a water depth of -2400 m at its shallowest point (13°17 S 14°24 W).

The southern end does not appear to be very volcanically robust, although some sparsely distributed flat-topped seamounts can be seen within the valley. In two places the eastern axial valley wall faults have stepped into the valley narrowing it to 5 – 6 km. The northern end is dominated by a large 20 km x 8 km smooth axial volcanic high. The surface of the high is very smooth with the exception of a 600 m wide, 40 m deep, normal-fault-bounded graben, which cuts across its summit on the western side. Some small edifices can be seen along the eastern wall of this graben, which are probably volcanic. The edges of the high are smooth, steep slopes, typically around 30°, and are probably formed volcanically. The high totally fills the axial valley and may even bury the innermost inner valley bounding faults at 13°16 S 14°27 W. Some volcanic edifices and rough terrain can be seen around the axial high, including a conical seamount at 13°12 S 14°26 W.

The backscatter is brighter in both the northern and southern valleys than in the surrounding much darker terrain, however the northern valley appears marginally brighter, suggesting this is the location of most recent volcanism. This would seem likely given how much shallower this section of the segment is and the large axial valley high.

5.2 AUV Mission summary

(Petersen, Rothenbeck, Steinführer, Triebe, Jamieson)

5.2.1 Introduction

The Autonomous Underwater Vehicle (AUV) Abyss (built by HYDROID Inc.) from GEOMAR can be operated in water depths up to 6000 m. The system comprises the AUV itself, a control and workshop container, and a mobile Launch and Recovery System (LARS) with a deployment frame that was installed at the starboard side on the afterdeck of R/V Maria S. Merian. The self-contained LARS was developed by WHOI to support ship-based operations so that no Zodiac or crane is required for launch and recovery. The LARS is mounted on steel plates, which are screwed to the deck of the ship (Fig. **5.18**). The LARS is configured in a way that the AUV can be deployed over the stern or port/starboard side of the German medium and ocean-going research vessels. The AUV Abyss can be launched and recovered at weather conditions with a swell up to 2.5 m and wind speeds of up to 6 Beaufort. For the recovery the nose float pops off when triggered through an acoustic command. The float and the ca. 19 m recovery line drift away from the vehicle so that a grapnel hook can snag the line. The line is then connected to the LARS winch, and the vehicle is pulled up. Finally, the AUV is brought up on deck and secured in the LARS.

During cruise MSM25 13 missions were flown by Abyss (Table 5.1). The missions were flown using the subbottom profiler configuration. Primary sensors used include Eh (for 12 missions) and the microstructure sensor (placed outside the AUV on an outrigger; for 1 mission). The sidescan sensor was collected additional geological data usually with the use of the 120 kHz sonar. Selected missions collected 410 kHz data in order to image hydrothermal fields (Merian Field at 26°S and Baileys Bead at 13°S).

Table 5.1: AUV Mission statistics for cruise MSM25.

Station	*Dive*	*Date*	*Survey time*	*Distance*	*Sensors*	*comment*
001AUV	#122	Jan. 31	1.6 h	12.1 km	---	test
003AUV	#123	Feb. 03	---	4.0 km	Eh + SSS	aborted
004AUV	#124	Feb. 03	14.7 h	96.3 km	Eh + SSS	120kHz
012AUV	#125	Feb. 05	14.3 h	88.1 km	MS + SSS	120kHz
020AUV	#126	Feb. 06	17.3 h	108.7 km	Eh + SSS	120kHz
034AUV	#127	Feb. 08	17.1 h	108.1 km	Eh + SSS	120kHz
049AUV	#128	Feb. 10	17.7 h	108.7 km	Eh + SSS	410kHz
061AUV	#129	Feb. 14	19.2 h	113.1 km	Eh + SSS	120kHz
080AUV	#130	Feb. 18	---	0.7 km	Eh + SSS	aborted
082AUV	#131	Feb. 18	17.6 h	107.5 km	Eh + SSS	120kHz
090AUV	#132	Feb. 20	17.5 h	105.6 km	Eh + SSS	120kHz
101AUV	#133	Feb. 22	15.9 h	102.4 km	Eh + SSS	120kHz
111AUV	#134	Feb. 24	16.3 h	103.4 km	Eh + SSS	120kHz
118AUV	#135	Feb. 26	16.3 h	102.4 km	Eh + SSS	410kHz
		total:	**185.5 h**	**1161.2 km**		

(Survey time = time spent mapping on the seafloor; distance = distance travelled at the seafloor; Eh = Redox-Sensor, MS = microstructure for current measurements, SSS = sidescan sonar survey).

The first dive was a test mission on the transit to the working area. Two missions had to be aborted early in the mission due to technical problems. Eleven missions went fine and collected plume data and sidescan sonar images.

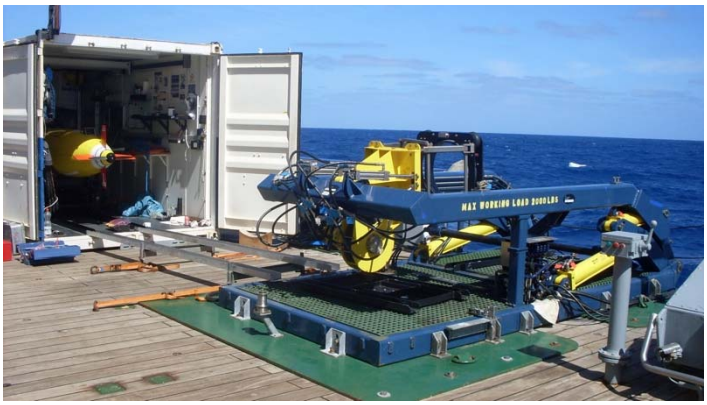

Fig. 5.18 The setup for AUV work on board Maria S. Merian with launch and recovery of the AUV on the starboard side.

Since the missions needed to be flown over long distances, normal transponder navigation was not possible. Instead, we used the Posidonia USBL-navigation system to track the vehicle at the bottom. In order not to hinder the scientific program, tracking was done at the beginning of the survey when the AUV was going down and starting its mission in bottom lock (DVL sees bottom), during CTD casts when the AUV was passing through and at the end of the mission. From mission 131 on, we added a cross-shaped profile line to the start and end of each mission in order to better determine the offset between positions of the inertial navigation system and Posidonia (see Fig. **5.19**). Offsets at the beginning of the surveys is commonly a couple of hundred meters due to current displacement of the vehicle while going down through the water column without GPS (only at surface) and bottom lock (at bottom). During the surveys offsets increased commonly by several hundreds of meters during the 15 to 19 hours of survey time.

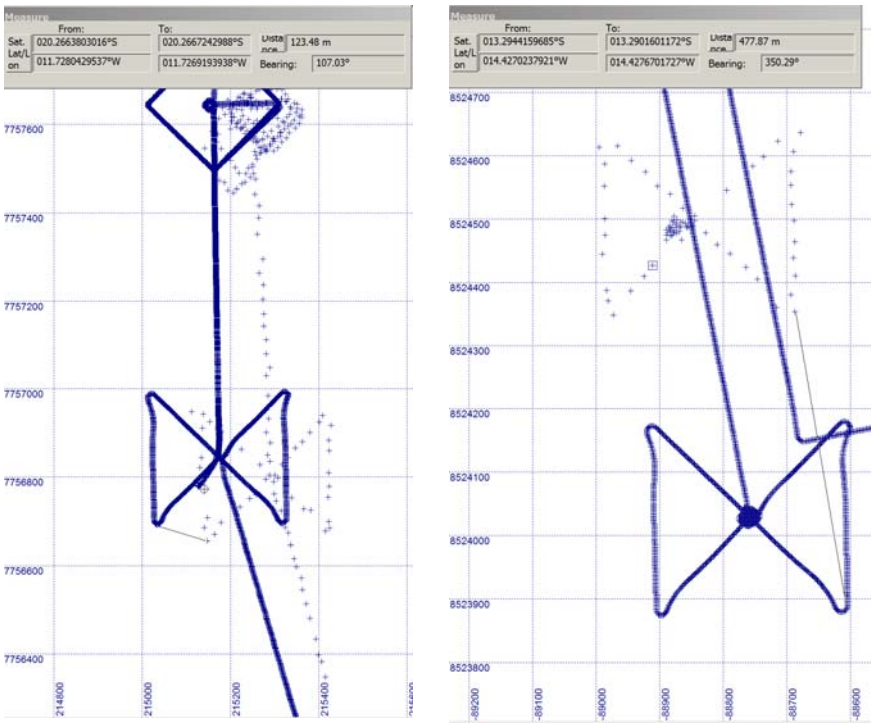

Fig. 5.19 Example for the comparison of Inertial Navigation and USBL (Posidonia) track plot

The main sensor for detection of plumes were the Eh sensor (Redox-Potential) and the turbidity sensor. In total 11 Eh anomalies and associated turbidity anomalies have been documented (Table 5.2). The Eh signal itself varied substantially. This is especially remarkable when comparing the absolute minimum values of Eh measured in the two hydrothermal fields (Merian, 26.9 mV; and Baileys Beads, 76.8) with those of segment 1 and segment 9, where Eh signals are comparable of even lower than those in the vent fields. This could be related to the low altitude flown at the vent fields flying actually below the plume.

Table 5.2: Location of Eh anomalies observed during AUV Abyss dives.

Seg.	*Dive*	*Latitude / Longitude**	*Time*	*AUV depth*	*Altitude*	*Eh (mV)*
1	#124	33°01.29'S/14°26.14'W	18:49	2314m	150m	80.5
1	#124	32°59.55'S/14°26.65'W	19:25	2350m	150m	57.5
1	#124	32°57.93'S/14°27.21'W	19:59	2395m	150m	-1.3
3	#126	29°57.03'S/13°51.27'W	06:49	3229m	150m	71.1
6	#127	27°47.62'S/13°22.38'W	02:24	3067m	150m	57.0
6	#127	27°08.86'S/13°28.52'W	15:37	3191m	150m	75.8
7	#128	Merian Vent Field	06:28	2674m	50m	26.9
9	#129	23°44.57'S/13°23.62'W	14:30	2768m	100m	39.9
12	#133	19°19.81'S/11°56.53'W	07:12	2587m	120m	62.7
15	#134	15°10.00'S /13°21.35'W	07:05	2652m	120m	64.9
16	#135	Baileys Bead's area	21:45	2228m	40m	76.8

** based on inertial navigation system, not corrected. Depth is instrument depth. Altitude given is a goal set for the mission. Eh value given is minimum measured value for that area and only serves as an indication. It has not been corrected to baseline. It does, however, still show the relative size of the anomalies.*

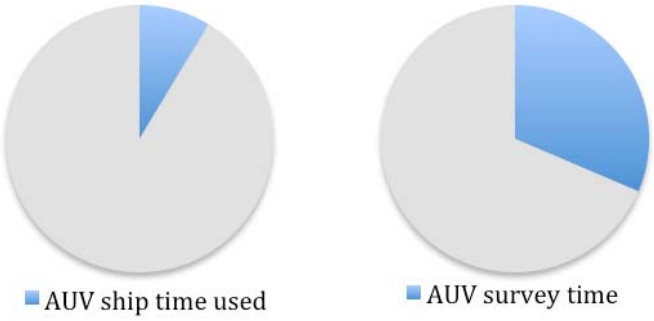

Fig. 5.20 Comparison between the shiptime used for launch, recovery, and tracking of the AUV (no other ship operations possible; time = 51 hours) and the survey time of the AUV. Survey time was 185.5 hours. Total shiptime during MSM25 was 590 hours.

5.2.2 Mission descriptions

The first station (001AUV; dive #122) was a test dive to check communication between AUV and Posidonia. The AUV went down a few hundred meters. Communication was fine and the cruise was continued. The first dive in the working area (station 003AUV; dive #123) on Feb. 3rd was aborted 1 hour into the mission due to difficulties in achieving depth. The remaining dives are described in the Appendix.

5.3 AUV Sidescan Sonar

(Yeo, Jamieson, Petersen, Rothenbeck, Steinführer, Triebe)

5.3.1 Overview

Sidescan sonar imagery of the seafloor was collected during every AUV deployment (segments 1, 2, 3, 6, 7, 9, 11, 12, 13, 15 and 16) covering a total area of 987 km^2 (Fig. **5.21**).

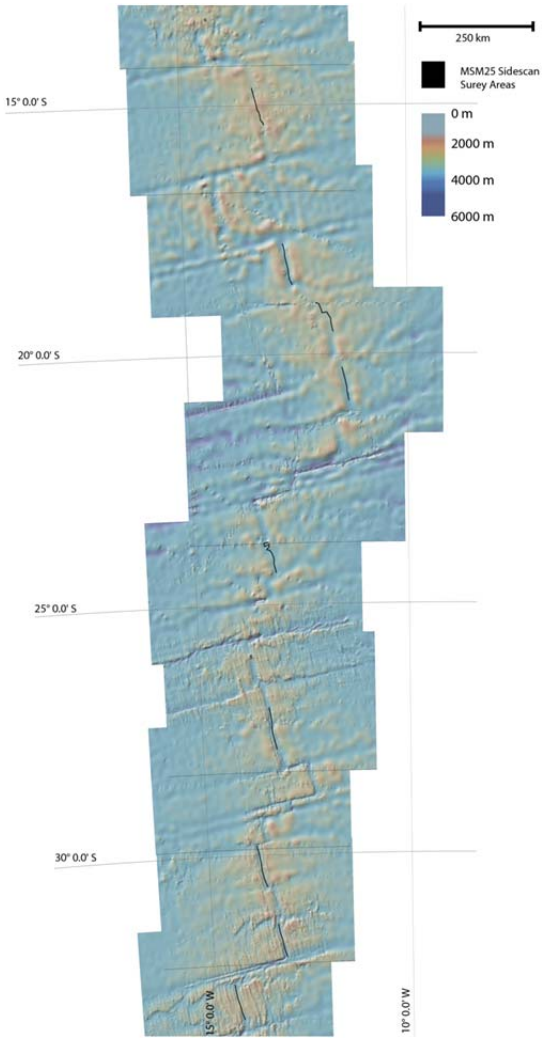

Fig. 5.21 MSM25 AUV sidescan sonar survey areas

All but two surveys (on segments 7 and 16, stations 049AUV and 118AUV) were single track, 120 kHz surveys flown at either 100 m, 120 m, or 150 m altitude. Segments 7 and 16 were surveyed at 410 kHz with altitudes of 50 m and 40 m respectively. In these areas survey lines were laid out in a grid to cover an area of seafloor rather than just a single line. Lines were laid out with a 200 m spacing yielding 100 percent overlap in station 049AUV and with alternating 300 m and 100 m line spacing in 118AUV yielding not only complete overlap but also coverage in the nadir zones. The AUV survey statistics are summarised in Table 5.3.

Table 5.3: AUV Sidescan sonar survey statistics

SEGMENT	STATION NUMBER	SURVEY	AREA SURVEYED (KM^2)
1	004AUV	120 KHZ TRACK	100
2	012AUV	120 KHZ TRACK	90
3	020AUV	120 KHZ TRACK	104
6	034AUV	120 KHZ TRACK	113
7	049AUV	410 KHZ GRID	21
9	061AUV	120 KHZ TRACK	130
11	090AUV	120 KHZ TRACK	111
12	101AUV	120 KHZ TRACK	93
13	082AUV	120 KHZ TRACK	104
15	111AUV	120 KHZ TRACK	102
16	118AUV	410 KHZ GRID	19

The single track, higher altitude surveys are very noisy, making some short sections of the data hard to interpret. Other sections are clear but still cut by quite a large amount of noise. This noise is due to vehicle movement, which is a product of the higher than normal altitude the AUV was flying at. As the sidescan was a secondary objective and the higher altitude was needed to look for plume signals in the water column these high altitudes were used for every single-track dive, despite the problems with noise.

Display and post processing of the sidescan datasets was carried out using SonarWiz. All datasets were slant range corrected and a rough gain correction applied. Further processing of this data will be required on shore to improve the gain correction and apply de-striping. Additionally, as the surveys did not use transponders, the vehicle navigation drifts during each survey. This was measured using the Posodonia at least at the beginning and end of every survey and, where possible, at one or more points in between. More details of these offsets are given in Section 5.2.2

As offsets are not constant along the dive correction of the navigation is not as easy as a simple shift and will need to be done onshore. The renavigated data should then be verified by comparison of geological features seen in both the sidescan survey imagery and the EM122 bathymetry collected over every segment.

5.3.2 Surveys – Volcanology and Hydrothermalism

The following sections provide a very brief volcanological overview of the findings from each sidescan sonar survey. Much closer analysis of the volcanology, backscatter intensities and contact relationships will be carried out on shore. Details of Eh and turbidity data from the AUV can be found in the dive descriptions in the Appendix.

5.3.2.1 Segment 1 (Station 004AUV – Abyss#124)

Survey 004AUV covers an 80 km long track from the southern to the northern end of segment 1. The survey covers both hummocky (composed of dome or cone shaped volcanic edifices from a few tens to a few hundreds of metres in diameter) and smooth seafloor (composed of sheet and lobate flows). A large area of smooth seafloor can be seen beginning around 33°04’ S 24°26’ W and extending to the north for almost 15 km. This area is fairly uniformly backscattering, but some areas are more faulted and fissured than others, suggesting there may be more than one flow of different ages. Young, unfissured hummocky volcanism can also be seen around 32°57’ S 14°27’ W and 32°55’ S 14°28’ W. North of this the backscatter brightness decreases and a mixture of faulted hummocky and small areas of smooth seafloor (both heavily faulted and fissured and relatively untectonised) are observed to the end of the segment.

5.3.2.2 Segment 2 (Station 012AUV – Abyss#125)

Survey 012AUV covers an 80 km track from the southern to the northern end of segment 2. The southern end of the dive covers a mix of old looking (faulted and fissured) and young (relatively undisturbed) hummocks and small patches of smooth seafloor. Around 31°50’ S 13°21’ W some slightly brighter looking hummocky lava flows can be seen truncating fissured terrain to the north (Fig. **5.22**). Similar burial of older terrain by young looking hummocks can be seen at 31°47.2’ S 13°22.2’ W. The survey also covers two relative large area of fairly dark looking, faulted flat-seafloor north of this, at 31°43’ S 13°23’ W (Fig. **5.23**) and 31°37’ S 13°25’ W, and two areas of brighter hummocky terrain at 31°34’ S 13°26’ W and 31°23’ S 13°28’ W.

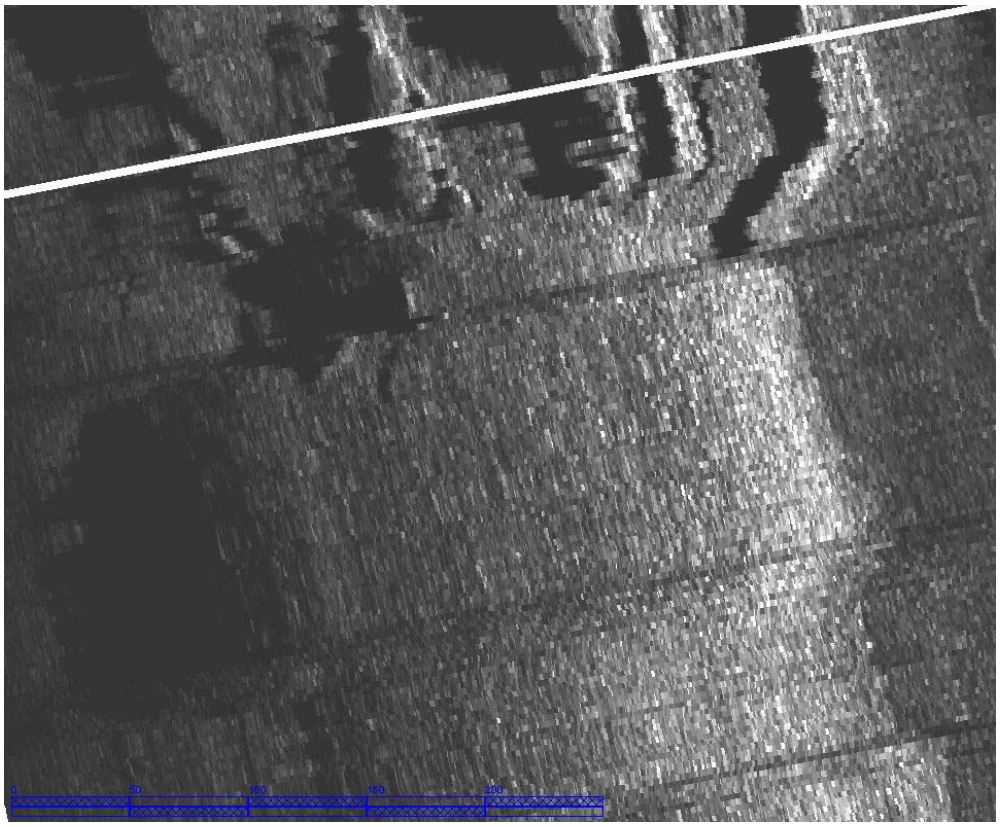

Fig. 5.22 A younger lava flow, flowing northwards buried the faulted, fissured terrain to the north. Illuminated from the RHS. Bright backscatter is white and low backscatter is dark.

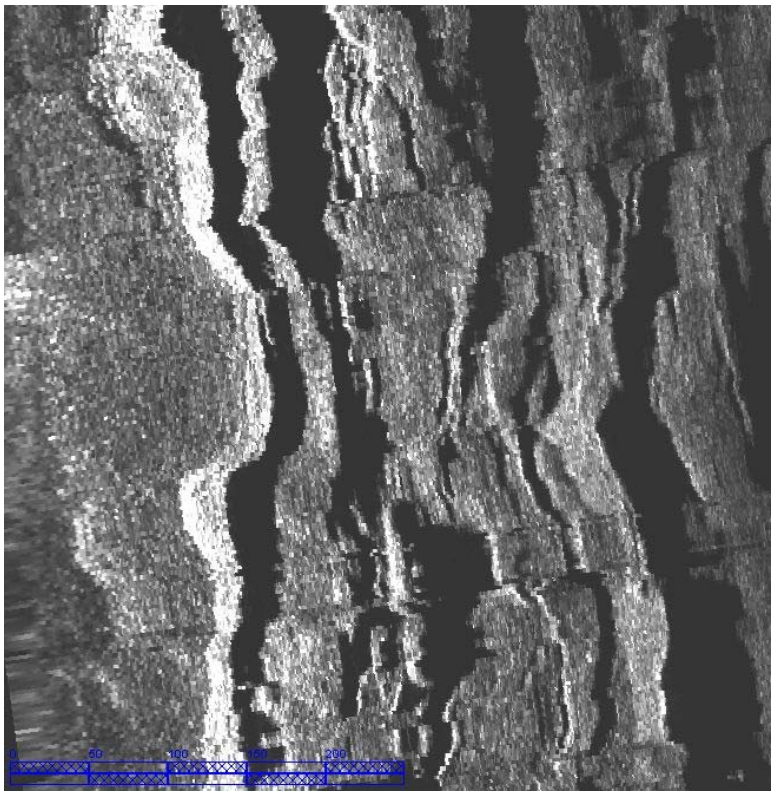

Fig. 5.23 Flat seafloor on the western left hand side of the picture getting progressively more broken up with distance from the axis. Illuminated from the LHS. Bright backscatter is white and low backscatter is dark.

5.3.2.3 Segment 3 (Station 020AUV – Abyss#126)

Survey 020AUV covers an 80 km track from the southern to the northern end of segment 3. The southern end displays moderately backscattering but relatively unfaulted hummocky and flat seafloor, which becomes more broken up around 30°30' S 13°44' W. A large area of smooth seafloor cut by a single large fissure (possibly related to the eruption) is imaged at 30°19' S 13°47' W. North of this flow the seafloor is covered by more brightly backscattering hummocky lavas, which have buried much older, faulted terrain, which can still be seen to the north (Fig. **5.24**). This very broken up seafloor continues to around 30°14' S where smooth, but poorly backscattering seafloor can be observed across almost the whole axial valley. Between this point and 30°08' S the data is very noisy but seems to cover a mixture of hummocky and smooth seafloor, none of which is very brightly backscattering. At 30°05' S 13°50' W a quite bright hummocky flow abuts a poorly backscattering and almost certainly older sheet flow region. The hummocky area also has a 120 m diameter crater on its summit. To the north at 30°01' S 13°50' W the entire survey width is filled by a fairly brightly backscattering area of smooth seafloor. Despite how bright it appears it is cut by at least one small fault. A second bright area can be seen at 29°52' S 13°52' W. A curved, steep sided edifice, which may be one side of a flat-topped seamount, is imaged at 29°49' S 13°53' W and along with a fault opposite appears to have filled the valley, which is narrow at this point, with talus.

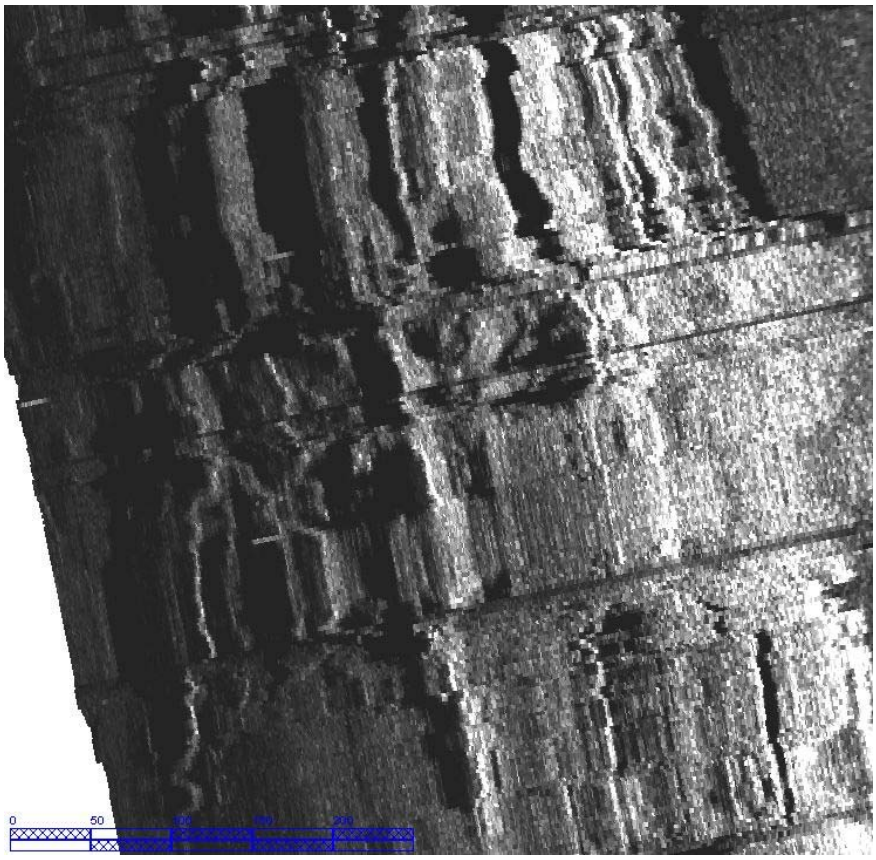

Fig. 5.24 Burial of older faulted terrain by a smoother, more brightly backscattering lava flow. Illuminated from the RHS. Bright backscatter is white and low backscatter is dark.

5.3.2.4 Segment 6 (Station 034AUV – Abyss#127)

Survey 034AUV covers a 93 km long track from the southern to the northern end of segment 6. The very southern end of the valley (to around 27°50' S) is characterised by poorly backscattering, fractured and faulted hummocky seafloor. This becomes moderately backscattering smooth seafloor around 27°49' S. Faulted terrain composed of both hummocks and patches of smooth seafloor then dominates to 27°30' S, broken only at 27°35' S 13°26' W where the faulted terrain is buried by talus which appears to be coming off a flat-topped seamount off on the west side of the survey. North of 27°30' S the AUV images moderately backscattering hummocky terrain on the western side and a steep slope (which may be a fault) with a large talus pile at its base. Backscatter decreases again at 27°26' S, but the survey images a 150 m diameter cratered flat-topped seamount – much smaller than are usually observed (Fig. **5.25**). Between the small seamount and 27°23' S the seafloor is almost entirely covered by smooth flows, which are commonly heavily faulted. North of this, the survey covers a mixture of hummocky terrain and smooth seafloor, none of which is particularly brightly backscattering.

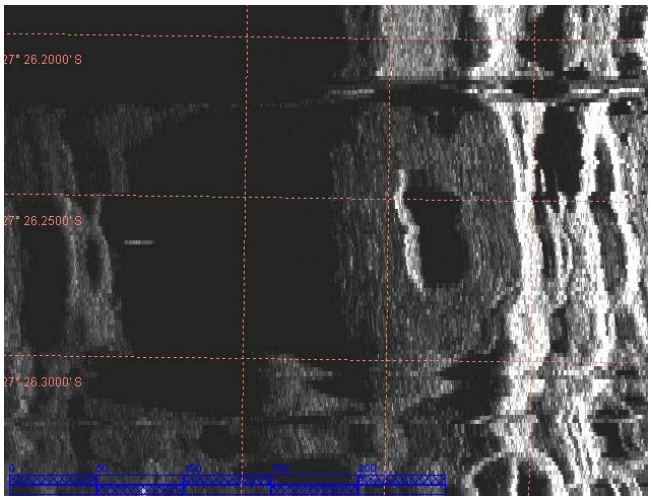

Fig. 5.25 Very small diameter flat-topped, cratered seamount. Illuminated from the RHS. Bright backscatter is white and low backscatter is dark.

5.3.2.5 Segment 7 (Station 049AUV – Abyss#128)

Survey 049AUV is a 410 kHz survey and covers an area of 21 km^2 on the summit of the axial high on segment 7. The seafloor imaged consists almost entirely of flat-seafloor, with fissures and collapse features. The brightest area is in the south east of the survey area, around 26°02' S 13°51' W, which is also the least faulted section of the area covered. Along the eastern edge of the survey the AUV images fairly straight parallel faults, while the western side shows a more complex pattern of faulting with faults curving westwards. There are several small highs on the surface, typically with smooth sides and summits cut by fissures. Next to one such high at 26°01' S 13°51' W the AUV imaged a series of hydrothermal chimneys and mounds (the 'Merian Vent Field'). The tallest of these chimneys is around 18 m and is shown in Fig. **5.26**.

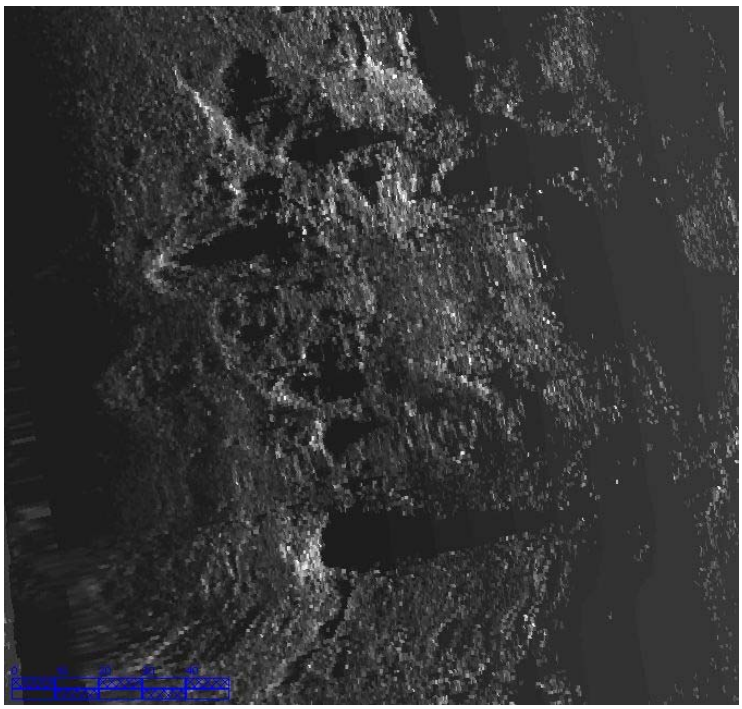

Fig. 5.26 The Merian Vent Field. Chimneys can be seen casting long, pointed shadows. Illuminated from the LHS. Bright backscatter is white and low backscatter is dark.

5.3.2.6 Segment 9 (Station 061AUV – Abyss#129)

Survey 061AUV covers a 100 km track, which goes from the centre of segment 9 across the detachment surface and then southwards towards the southern end of the segment. The surface of the detachment appears moderately backscattering and mottled in appearance. In one place a smooth area cut by E-W striations is imaged (Fig. 5.27). The detachment is separated from an area of typical hummocky volcanic terrain on the western side of the valley by a very poorly backscattering, flat area, cut by a few small faults. The southern half of the survey covers the southern end of the axial valley. The survey covers a combination of moderately backscattering hummocky and flat seafloor until 24°03' S where the seafloor is completely covered by quite poorly backscattering flat seafloor, cut by a large fault on the western side. This flow reaches as far south as 24°09' S where a combination of hummocks and patches of flat seafloor are observed again. Nothing in the southern area appears particularly young, but an area of very well defined, unfaulted volcanic hummocks are imaged at 24°14' S 13°16' W (Fig. 5.28).

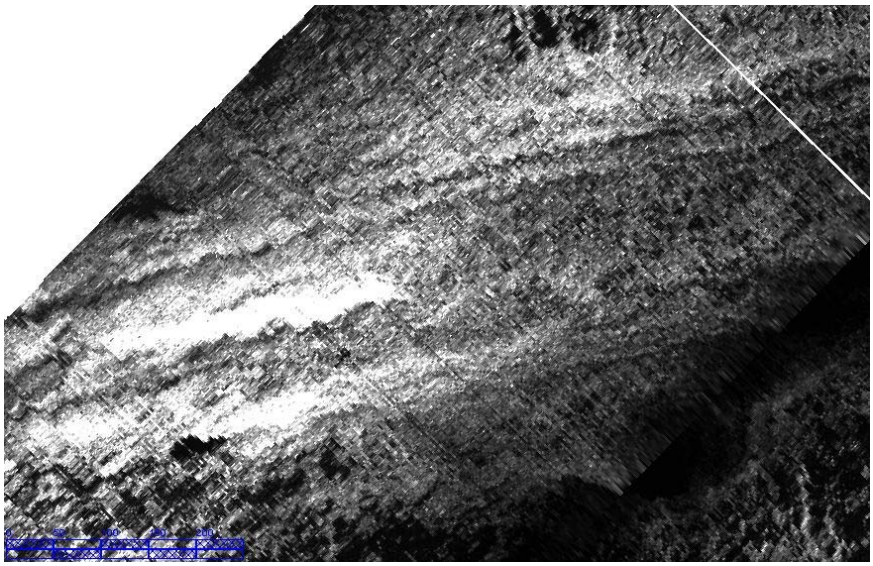

Fig. 5.27 Possible striations on the surface of the detachment. Illuminated from the bottom right. Bright backscatter is white and low backscatter is dark.

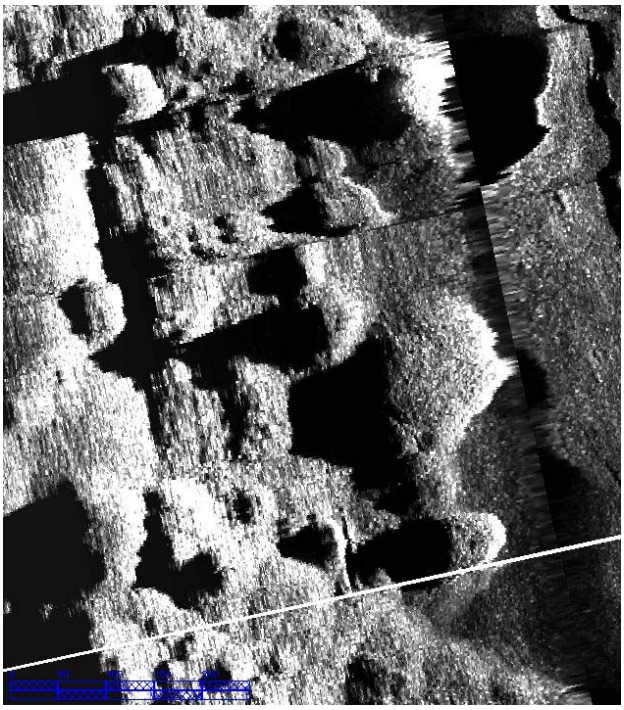

Fig. 5.28 Well defined, untectonised volcanic hummocks. Illuminated from the RHS. Bright backscatter is white and low backscatter is dark.

5.3.2.7 Segment 11 (Station 090 – Abyss#132)

Survey Abyss0132 covers a section of ridge from the north to the south of segment 11. A small section of the survey was designed to cover a good example of a cratered conical seamount (‘Brian’) imaged in the multibeam survey and described more fully in Section 5.1.2.11. The northern end of the survey is very poorly backscattering, mostly hummocky terrain. The sides of flat-topped seamounts were covered at 20°49’ S 11°40’ W and 20°51’ S 11°37’ W both of which had poorly backscattering flat summits and steep, brightly backscattering sides surrounded by large talus deposits. The axial valley is mostly filled with hummocky terrain, with the exception of one large area of flat seafloor at 20°51’ S 11°36’ W.

The cratered conical seamount is shown in Fig. **5.29**. It has a diameter of just over 1 km with a 500 m diameter, round, steep sided crater. Gullying can be seen on the flanks suggesting they are built of talus or finer material rather than pillow or lobate lavas. This combined with the very round crater could indicate an explosive origin for Brian, although in such deep water more evidence is needed to support or disprove this hypothesis.

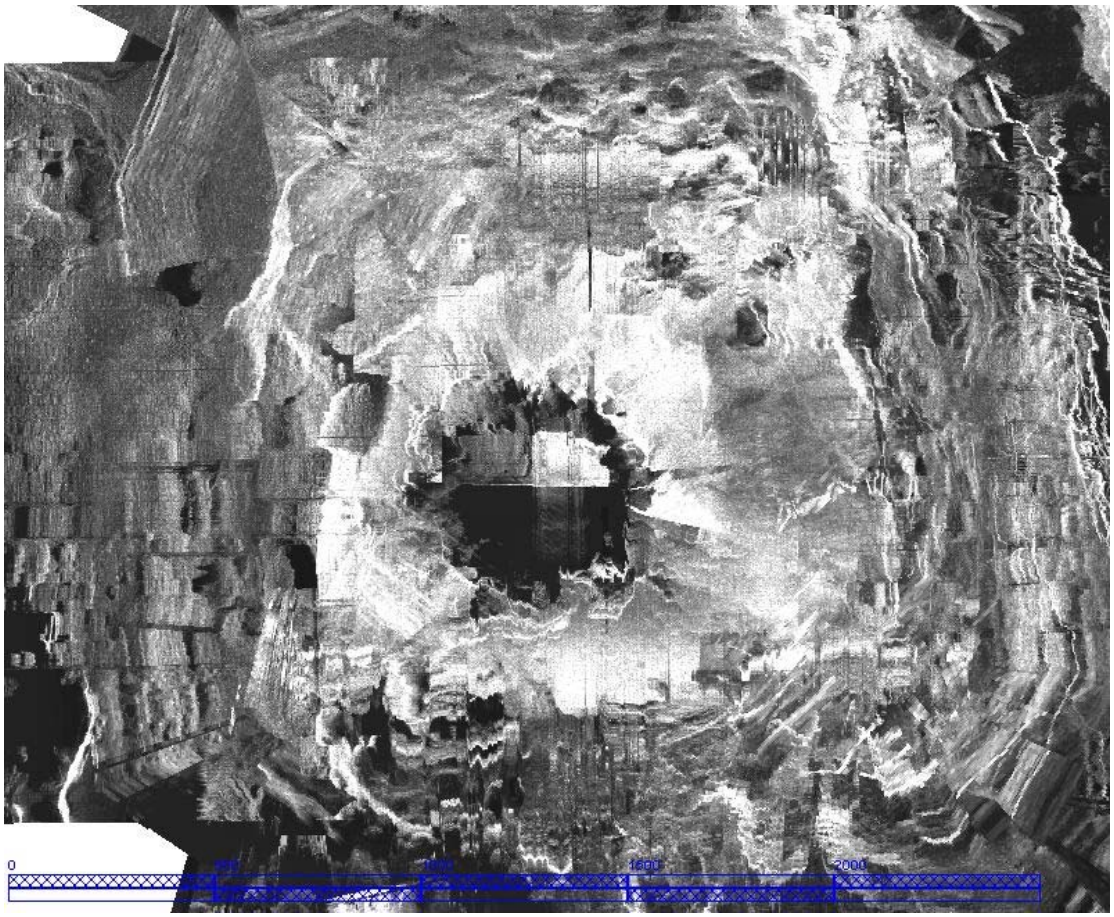

Fig. 5.29 Brian – the cratered conical seamount. Imagery is shown in 'shine through' mode, which displays the brightest areas from each swath. The seamount appears so brightly backscattering because of the slopes of the flanks, although comparison of backscatter where the AUV is travelling parallel with the slope suggest it is still more brightly backscattering than the surrounding volcanic terrains. Bright backscatter is white and low backscatter is dark.

5.3.2.8 Segment 12 (Station 101AUV – Abyss#133)

Survey 101AUV was designed to cover the northern end of segment 12 along with portions of two of the small, overlapping spreading centres, which have developed in the complex offset between segments 12 and 13 (described more fully in Section 5.1.2.12). The track is 82 km in length starting on the northern end of segment 12. The survey begins in moderately backscattering hummocky terrain, but soon reaches a moderately backscattering area of flat seafloor at 19°31' S 11°55' W. The seafloor is predominantly sheet flows until 19°20' S 11°57' W, where it becomes more hummocky and less brightly backscattering. A fairly bright area of hummocks and flat seafloor is present at 19°13' S 12°00' W, near to the end of segment 12. The AUV crossed another area of flat seafloor at 19°10' S 12°03' W as it turns toward the first small offset subsegment. The subsegment is separated by a poorly backscattering, west facing normal fault complex. The spreading segment itself is similar in backscatter intensity to segment 12 and volcanic textures are seen along its length, including a large area of smooth seafloor at 19°02' S 12°10' W and predominantly hummocky terrain in the east and west. This subsegment is separated from a second subsegment to the west by a higher area of poorly backscattering, but still volcanic looking terrain. The second segment is characterised by hummocky terrain and the AUV also covers a round area of flat seafloor, which is probably the summit of a flat-topped seamount at 18°58' S 12°15' W.

5.3.2.9 Segment 13 (Station 082AUV – Abyss#131)

Survey Abyss0131 covers a 93 km long track from the northern to the southern ends of segment 13. The northern end of the ridge is characterised by primarily hummocky terrain to 17°56' S, where the valley narrows and appears to be floored by flat seafloor. Brightly backscattering hummocky and flat seafloor can be seen around 18°00' S 12°53' W, although the pillow lavas form a slope, which may increase the backscatter on the side facing the AUV. All the lavas between the beginning of the survey and 18°06' S 12°52' W are very unfractured and unfaulted, and the overall backscatter in the area is quite high, suggesting this is an area which may have been recently volcanically active. A large area of sheet flow is observed at 18°08' S 12°51' W, flanked on its western side by a faulted area of well defined volcanic hummocks. Hummocks also fill the axial valley between this and the next large area of flat-seafloor is at 18°22' S 12°49' W. One very brightly backscattering area of hummocky terrain is imaged at 18°27' S 12°48' W, but backscatter brightness steadily increases from here towards the southern end of the survey.

5.3.2.10 Segment 15 (Station 111AUV – Abyss#134)

Survey Abyss0134 covers an 86 km long track from the mid-northern end to the mid-southern end of segment 15. The survey begins on moderately backscattering hummocky terrain at 14°40' S 13°30' W and crosses into a large (9 km wide) area of flat-seafloor at 14°41' S 13°30' W. The contact relationship between this large flat area and the seafloor to the north of it isn't clear but at 14°50' S 13°29' W it can be seen to bury the more faulted and fissured seafloor to the south. The rest of the survey covers a mixture of hummocks and patches of sheet flow, with potentially younger (untectonised and brightly backscattering) flows at 14°51' S 13°27' W, 15°03' S 13°24' W and 15°13' S 13°21' W.

5.3.2.11 Segment 16 (Station 118AUV – Abyss#135)

Station 118AUV covers a 19 km^2 area on the summit of the large axial high described in Section 5.1.2.16. The sidescan imagery was collected with 410 kHz and shows the surface of this high to be composed of flat lying lava flows, probably sheet or lobate flows. The surface is cut by a number of curving faults, which also define a boundary between brighter and probably younger flows in the centre of the survey and darker, probably older flows in the west. The flat flows are characterised by numerous fissures and collapse pits (although few tumuli), as well as areas of darker, sometimes striated looking terrain. These darker areas sometimes look like flows from fissures (Fig. **5.30**) but in other areas have less flow like outlines and form smaller patches. The fact they are so poorly backscattering despite the fact they appear to have flowed out over the brighter flows which cover most of the valley floor suggests they may have a a rougher surface and therefore are scattering the sound more.

The central area is characterised by a line of mounds, the majority of which are probably volcanic and aligned along a fault plane. Three of the 4 AUV turbidity/Eh anomalies lay along this plane, as did the large plume detected in the CTD Tow-Yo (described in Section 5.6.4).

The survey covered two known hydrothermal sites, the active Bailys Beads and the inactive Valentines Valley field discovered by Chinese scientists in 2009 and 2011 respectively (Tao et al., 2011). Both are located with west facing small faults near the center of the summit. Details of the location of turbidity and Eh anomalies during the AUV dive can be found in Section 10.12. Several sulfide structures (chimneys and mounds) have been imaged in close association with these faults and reach up to 20 m in height (Fig. **5.31**).

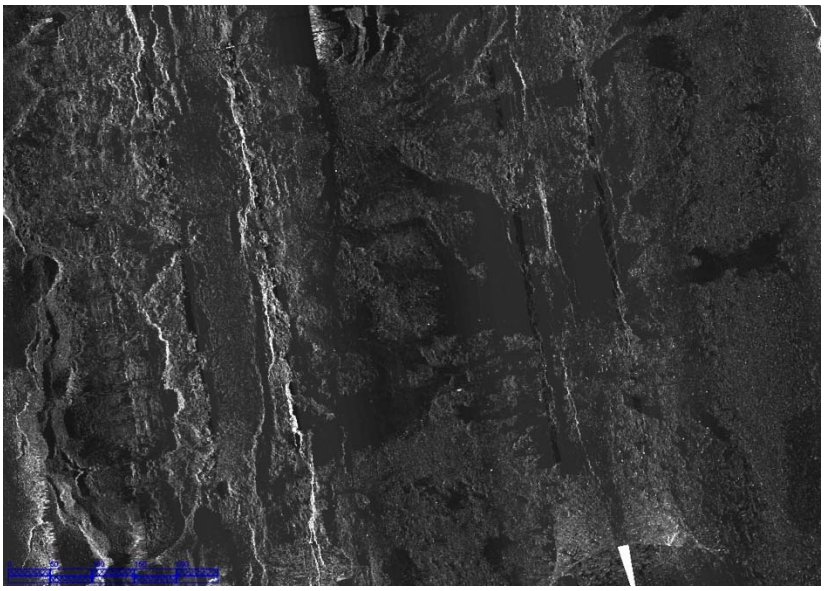

Fig. 5.30 Example of lower backscatter terrain. In this example it appears to be some kind of lava flow fed from the fissure running north to south across the picture. The sidescan data here is projected in 'shine through' mode, which displays the brightest backscattering regions from overlapping swaths. Bright backscatter is white and low backscatter is dark.

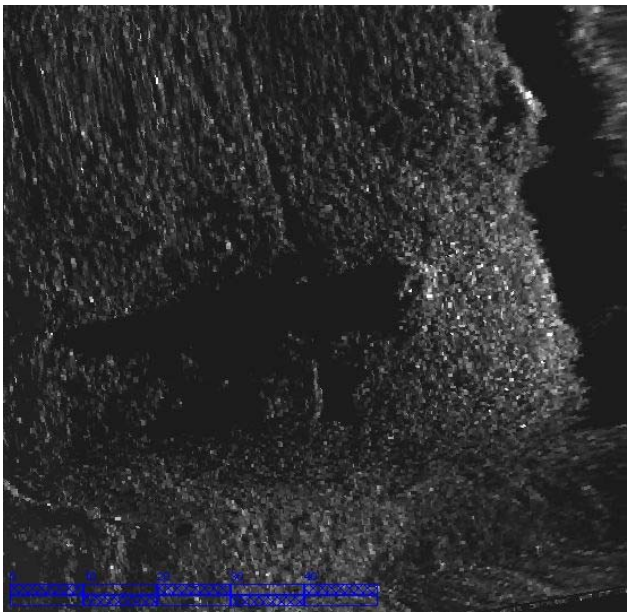

Fig. 5.31 20m tall hydrothermal chimney. The image is illuminated from the right and the chimney casts a long, t hin shadow behind it. Bright backscatter is white and low backscatter is dark.

5.4 Dredge sampling (Vishiti)

We carried out two dredge sampling stations during the cruise to recover samples from volcanic cones on Segment 11. The following samples were recovered:

Station No.: 99DS Date: 21.2.2013

* Location: Segment 11, 'The Face' lips cinder cone

* General description of dredged structure: Steep-sided cinders? cone on south end of segment 11

* Used equipment: Tonnen dredge

	Lat. (°S)	Long. (°W)	Time (UTC)	Water depth	Wire length	Tons
Start	20° 49. 211	11°36.582	11:45:20	3511m	0	
On bottom	20° 49.215	11°.36.577	12:38:10	3512m	3650	3.4
Off bottom	20°49.381	11°36.251	13.36	3358	3170	~3.7
On deck	20°49.380	11°36.251	14.18	3349	3350	1.2

Rocks found:

* Total volume: Few rocks

* General description: Two old pillow fragment many small fresh pillow buds

sample no.	Rock description:
99DS-1	15×13×5cm in size Fresh with 2-3m flow banded glass crust Fe-staining 20% vesicular. Vesicles range in size from 0.1-6cm No visible sediments
99DS-2	20×15×10cm in size Fine grain with 0.1cm size plagioclase microphenocrysts 5% vesicular Vesicles are mm in size Fe-staining Dark MnO coating
99DS-3	10×9×7cm in size Fresh with 4-5mm banded glass crust Fe-staining 10% vesicular. Vesicles are 0.1-0.8cm in size Presence of a lava tube No visible microphenocrysts, and sediments
99DS-4	9×6×4cm in size Fresh with 2mm banded glass crust Fe-staining 5% vesicular. Vesicles are 0.1-0.5cm in size No visible mirophenocrysts and sediments
99DS-5	12×9×6cm in size Fresh 1mm glass crust Fine grain with 0.1cm plagioclase and probably olivine microphenocrysts 5% vesicular. Vesicles are mm in size Fe-staining No visible sediments Dark MnO coating
99DS-Extra	Small fresh basaltic glass Some are vesicular. Vesicles range from 0.1-0.5cm in size Some of the samples are complete glass while others show about 2mm of glass. Glass is banded No visible Fe-staining and sediments.

Station No.: 100DS Date: 21.2.2013

* Location: "Smoke ring" of face in segment 11

* General description of dredged structure: Flat-topped volcano west of steep volcano dredged during the previous station
* Used equipment: Tonnen dredge

	Lat. (°S)	Long. (°W)	Time (UTC)	Water depth	Wire length	Tons
Start	20° 48. 652	11°37.402	15:22:00	3503m		2.2kn
On bottom			16:02:20	3503m	3345	
Off bottom	20°48.869	11°37.018	16.56	3458	3350	
On deck	20°44.868	11°37.016	17.38	3460		

Rocks found:

* Total volume: Few rocks

* General description: Few pillow buds and many fresh sheet lava

sample no.	Rock description:
100DS-1	22×15×5cm in size Fresh, fine grain sheet lava flow 5mm glass crust with a fresh cooling (devitrification) coating 5% vesicular. Vesicles are mm to 0.2cm in size Fe-staining Visible sediments in cooling cracks
100DS-2	13×13×10cm in size Fresh pillow lava with 2-3mm of banded glass crust Fine grain 4% vesicular Vesicles are mm in size Fe-staining No evidence of sediments and cooling coating
100DS-3	21×19×9cm in size Fresh, fine grain sheet lava flow 0.5cm glass crust with a cooling coating. 4% vesicular. Vesicles are mm in size Fe-staining No visible microphenocrysts and sediments

100DS-4	23×11×7.5cm in size Fresh, fine grain sheet lava flow 2.5cm banded glass crust with a cooling coating 5% vesicular. Vesicles are mm in size Fe-staining No visible mirophenocrysts and sediments
100DS-5	10×7×5cm in size Fine grain, fresh sheet lava flow with a 0.5cm glass crust 2% vesicular. Vesicles are mm in size Plagioclase microphenocrysts Fe-staining No evidence of sediments and cooling coating
100DS-6	14×12×9cm in size Fresh pillow lava with 2mm glass crust Fine grain 2% are vesicular. Vesicles are mm in size Fe-staining No evidence of sediments and cooling coating on glass

5.5 Hydrography

(Walter, Köhler)

5.5.1 Introduction

Currents, tides, internal waves and diapycnal mixing control the dispersal of hydrothermal products in the deep ocean. During Maria S. Merian cruise MSM25, the scientific goal of the hydrographic measurements was twofold: Firstly to detect hydrothermal plumes in the water column and study their dispersal, and secondly, to estimate the vertical mixing of the water above the ridge crest and in the axial valley in dependence of the ridge morphology. We employed the following sampling and measurements strategy: On each ridge segment, CTD casts were conducted at both ends of the segment, as well as between one to four casts inside the segment. Thus, it is possible to observe gradients along the individual segments, as well as obtain a relatively close-spaced survey on plume signals inside the segment. A hydrothermal plume signal can be identified either by negative anomalies in temperature and salinity and/or an increase in turbidity and drop of oxygen reduction potential (Eh). Hence, measurements of temperature, salinity, turbidity, and velocity were made to study the plume dispersal. Additionally, water samples with high vertical resolution were taken to be analyzed for helium and neon isotopes later in the noble gas lab (Univ. Bremen). During most of the casts, Miniature Autonomous Plume Recorder (MAPR) were attached to the CTD to capture possible signals in Eh. Towed see-sawing transects (tow-yo) were conducted at sites where either the geologic setting from the ships multibeam looked favorable for hydrothermal venting (e.g. axial volcanic heights), or the AUV had recorded a promising plume signal during surveying. During the tow-yo casts, up to five MAPR were attached to the CTD and the sea cable, typically 50, 100, 150, and 200m above the CTD, to cover a large vertical range with turbidity, temperature, and redox potential recordings.

To address the second aim of the survey, the fine structure of the temperature and density field, as well as the vertical shear of the horizontal velocity field, will be analyzed to determine the strength and distribution of turbulent vertical mixing using finescale shear and strain parameterizations (Gregg et al., 2003; Kunze et al., 2006) and density inversions (Thorpe, 1977).

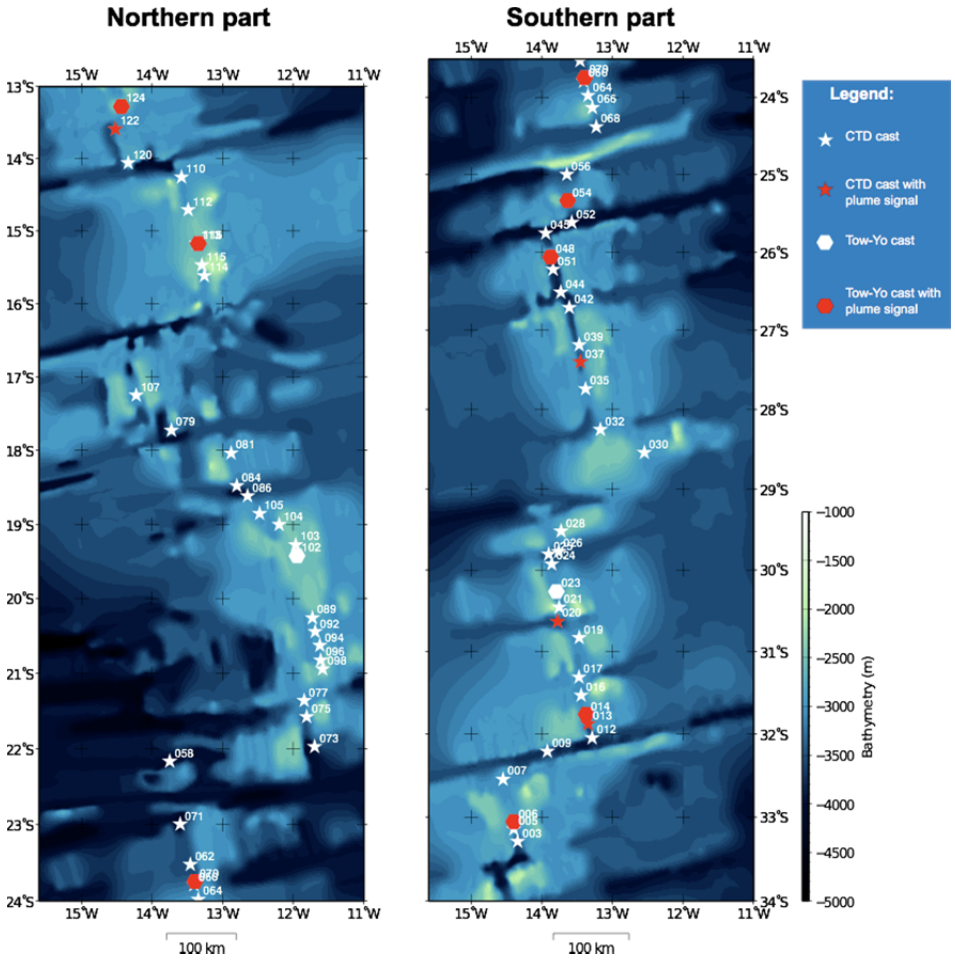

Fig. 5.32 Map of all CTD and Tow-yo stations.

5.5.2 Data

Conductivity-temperature-depth (CTD) casts were carried out using a Sea-Bird Electronics, Inc. SBE911plus system that was initially equipped with a custom build Seapoint Turbidity Meter (5x normal gain), the same sensor that is used on MAPR. The underwater unit was attached to a SBE 32 carousel water sampler with 22 Niskin bottles. The two remaining spaces for bottles were taken up by the lowered acoustic Doppler current profiler system (LADCP). The complete system worked properly throughout the cruise, except for the turbidity sensor, that started to fail under pressure beginning on station 20, and was replaced by the ships' own WetLabs Combination Fluorometer and Turbidity Sensor (ECO FLNTU) from station 30 onward. This instrument uses a similar range of wavelength for the measurement, but has a slightly higher different background (dark counts) and higher noise level. A comparison between the plume signal recorded by both the MAPR and the WetLabs instrument showed however good agreement in sensitivity and magnitude of the signal (cf. Chapter MAPR). In total 60 salinity samples, typically three to five on each cast at one station per ridge segment, were collected for later analysis at home. In total 65 CTD casts were carried out, including 8 tow-yo transects (Fig. **5.32**).

5.5.3 Hydrography

The working area spans over 20° of latitude along the ridge crest, giving a large scale view of the propagation of southern and northern hemispheric water masses along the ridge. The Antarctic Intermediate Water (AAIW), characterized by a salinity minimum and relative cold temperatures (Fig. **5.33**) is generally present along the ridge at a depth range centered around 1000 m (Fig. **5.34**). The layer becomes thinner and less fresh towards the north, indicating a gradual mixing

with the North Atlantic Deep Water (NADW) below. The NADW, that is formed in the subpolar North Atlantic enters the study area from the north mainly at the western boundary of the Atlantic, but can be found throughout the whole South Atlantic. It has a maximum in salinity compared to the water masses formed in the Southern Ocean.

The deepest and coldest water mass in the area is the Antarctic Bottom Water (AABW), with potential temperatures below 2.1°C and a relative minimum in salinity, compared to the NADW (Fig. **5.33**). Interestingly, the northward progression of the AABW is nonuniform along the ridge axis. It is present in several but not all segments below 3000 m (Fig. **5.33**), thus the intrusion apparently depends not on the actual depth of the segments axial valley, but on the sill depths to the fracture zones connecting the valley with the Argentine and Brazil basins to the west of the ridge.

Station 58 (22°20'S, 13°45'W) serves as off-axis background, but will also allow to compare finescale mixing results to the mixing rates observed in the Brazil basin during a large scale mixing experiment that included microstructure survey and a tracer release (Polzin et al., 1997; Ledwell et al., 2000; Rye et al., 2012).

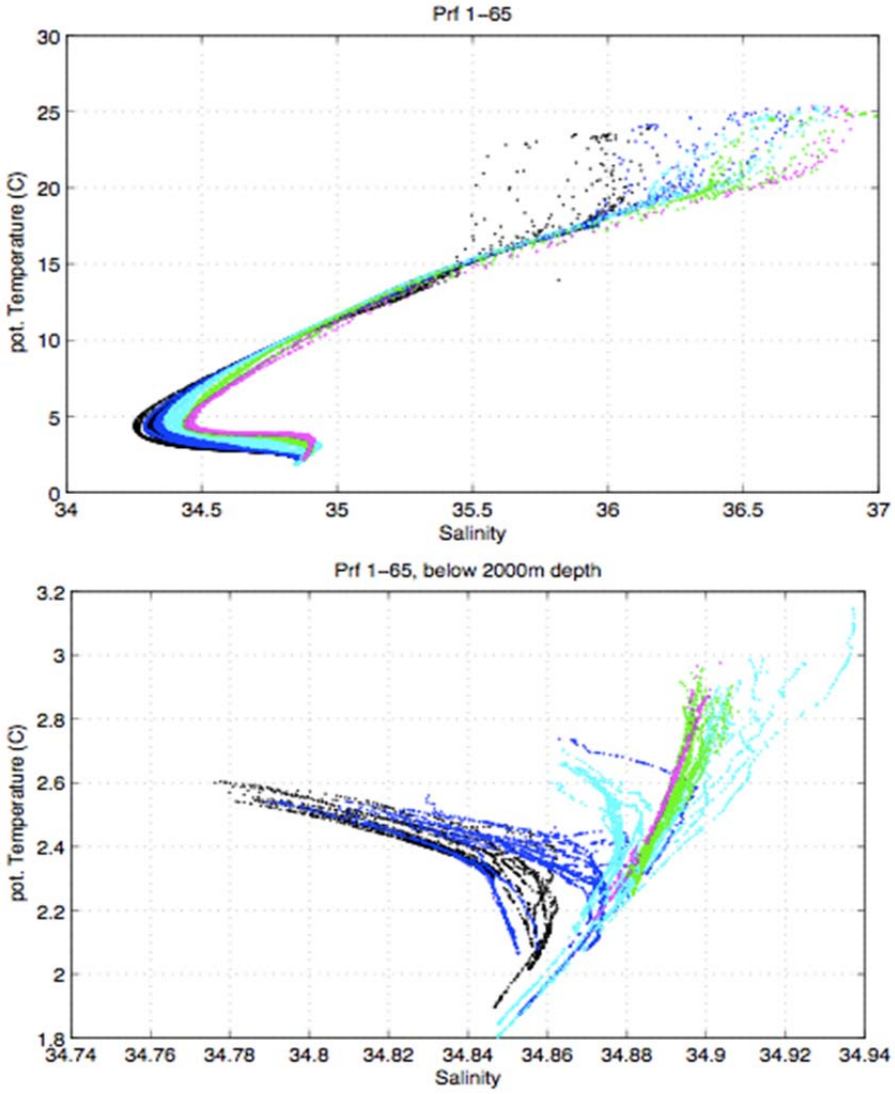

Fig. 5.33 T/S diagrams for latitude bands (black: 35-30°S; blue 30-25°S; light blue: 25-20°S; green: 20-15°S; magenta: 15-10°S). Upper panel: total water column; lower panel: below 2000m.

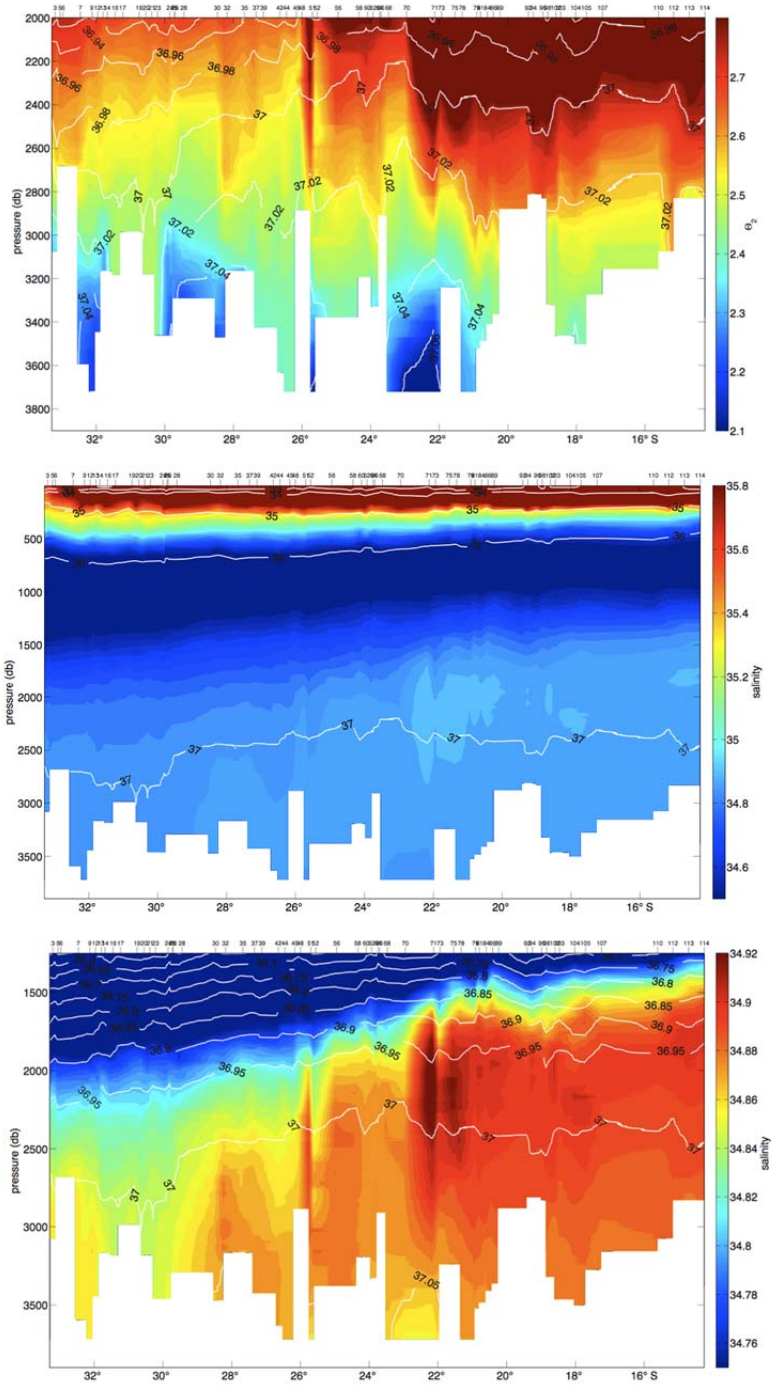

Fig. 5.34 North-south transects of potential temperature (upper panel), salinity (middle panel) and salinity below 1500dbar (lower panel).

5.5.4 Plume signals

4 of the single-cast CTD profiles and 7 of the total 9 tow-yo casts showed signals of hydrothermal particle plumes (**Fig. 5.32**). Shown here are four examples of the CTD tow-yo casts (**Fig. 5.35** - **Fig. 5.38**), all of which were recorded over axial volcanic highs, and represent different stages of proximity to a vent source (for a comprehensive overview of the turbidity as well as the concurrent Eh signals and the location of the tow-yo tracks, see Section 5.6.4). On segment 1 (**Fig. 5.35**), a patchy plume signal with a magnitude of 0.03 NTU above background level was observed, indicative of high hydrographic variability and a distal plume. In segment 7, on the other hand, the tow-yo track crossed directly over the newly discovered Merian vent field (**Fig. 5.36**), with a horizontal plume extent of ~1.5 km, and a turbidity anomaly of 0.1 NTU.

Station 116 on segment 14 was slightly to the south of an Eh signal mapped by the AUV, and shows the weak (0.05 ΔNTU) and well mixed signal of a distal plume (**Fig. 5.37**). Finally, station 124 covered the area of the known vent site Baily's Beads (Tao et al., 2011), and shows a strong plume signal of large horizontal extent (**Fig. 5.38**). During the track, the buoyant plume was crossed, which showed a temperature anomaly of 0.2°C, as well as a turbidity signal of more than 0.2 NTU above the background.

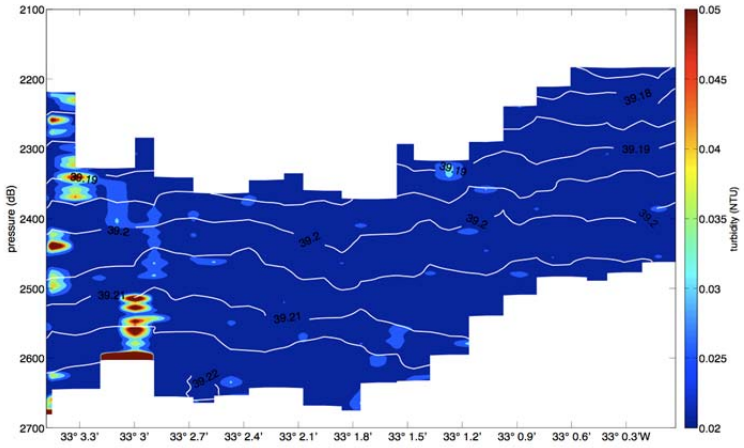

Fig. 5.35 Plume signal in turbidity; towyo station 6 (Segment 1).

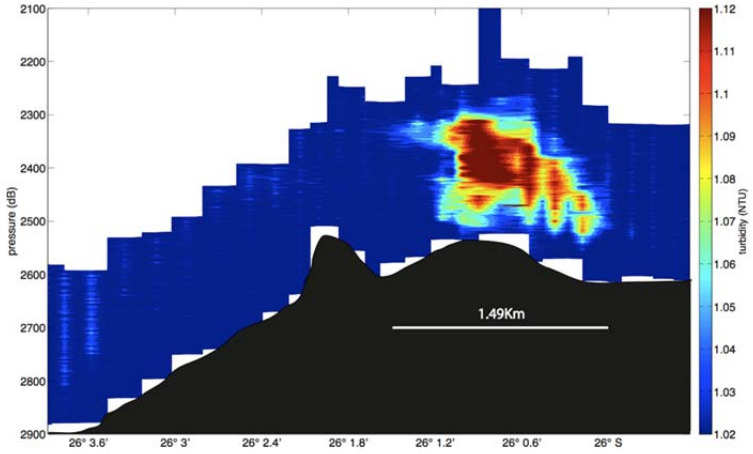

Fig. 5.36 Plume signal in turbidity of Merian vent field; towyo station 48 (Segment 7).

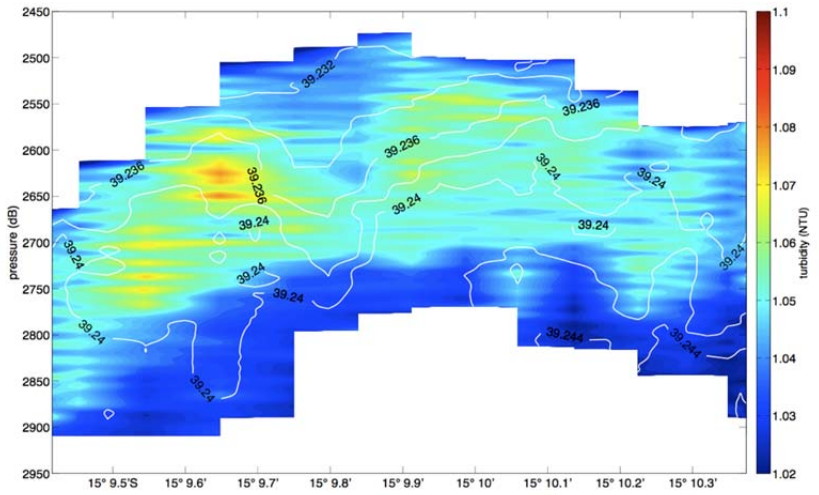

Fig. 5.37 Plume signal in turbidity; towyo station 116 (Segment 15)

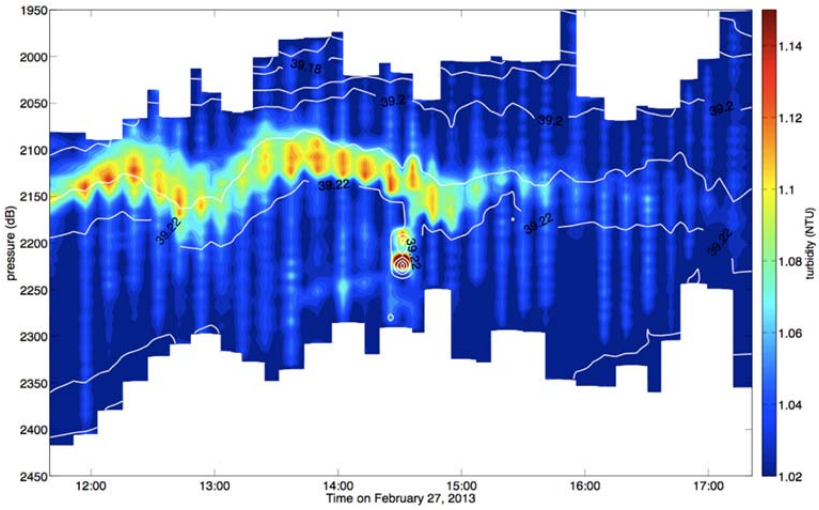

Fig. 5.38 Plume signal in turbidity of Bailey's Beads; towyo station 124 (Segment 16).

5.5.5 Literature

Gregg, M.C., T.B. Sanford, and D.P. Winkel, 2003: Reduced Mixing from the Breaking of Internal Waves in Equatorial Waters. Nature, **422**, 513–515.

Kunze, E., E. Firing, J.M. Hummon, T.K. Chereskin, and A.M. Thurnherr, 2006: Global Abyssal Mixing Inferred from Lowered ADCP Shear and CTD Strain Profiles. J. Phys. Oceanogr., **36**(8), 1553–1576.

Ledwell, J. R., E.T. Montgomery, K.L. Polzin, L.C. St. Laurent, R.W. Schmitt, and J.M. Toole, 2000: Evidence for enhanced mixing over rough topography in the abyssal ocean. Nature, **403**, 179–182.

Polzin, K.L., J.M. Toole, J.R. Ledwell, and R.W. Schmitt, 1997: Spatial Variability of Turbulent Mixing in the Abyssal Ocean. Science, **276**, 93–96.

Rye, C.D., M.-J. Messias, J.R. Ledwell, A.J. Watson, A. Brousseau, and B.A. King , 2012: Diapycnal Diffusivities from a Tracer Release Experiment in the Deep Sea, Integrated over 13 Years. Geophys. Res. Lett., **39**, L04603.

Tao, C. and Coauthors, 2011: Two Hydrothermal Fields Found on the Southern Mid-Atlantic Ridge. Sci. Chin. Earth Sci., **54**(9), 1302–1303.

Thorpe, S.A., 1977: Turbulence and Mixing in a Scottish Loch. Philos. Trans. R. Soc., **A286**, 125–181.

5.6 MAPR studies during MSM25 South Atlantic

(Vishiti, Schmid)

5.6.1 Introduction

In search for evidence of hydrothermal activity in the water column, Miniature Autonomous Plume Recorders (MAPR) were used to record temperature, pressure, optical backscatter (in nepheloid turbidity unit - NTU) and oxidation-reduction potential (Eh) along 16 ridge segments. Five MAPR units were hired from the National Oceanographic and Atmospheric Association (NOAA) Pacific Marine Environmental Laboratories (PMEL) for the duration of the cruise. The five units had the following serial numbers: 47, 48, 49, 50 and 64. For deployment, the MAPRs were either attached to the CTD during regular CTD stations (54 casts) or to the wire above the CTD for Tow-Yo stations (9 casts). At the regular CTD stations only one obvious plume anomaly was detected. However, slight deviations were recorded at some additional casts. Tow-Yo stations recorded remarkable anomalies in turbidity and Eh. The Tow-Yo stations include: 006 (segment 1), 048 (segment 7), 054 (segment 8), 070 (segment 9), 116 (segment 15) and 124 (segment 16). MAPRs where deployed at 63 casts in total. Except for one station, there was data recovery at all stations.

5.6.2 Method

During regular CTD casts, a single MAPR was attached to the CTD cage. At Tow-Yo stations, one MAPR was attached to the CTD and four additional MAPRs were tied on the wire above the CTD 50 m apart (at 50, 100, 150, 200m) with an exception of the first Tow-Yo in segment 1 where no MAPR was attached to the CTD. During these deployments, the MAPRs reached variable depths Table 1. Since plumes are expected to appear not more than a couple of hundred meters above the seafloor, only the relevant depth ranges are presented. For the data recording a recording interval of 5 seconds was chosen and after each station graphs of turbidity (NTU), temperature (^{o}C) and Eh (mV) were plotted versus depth (m) in order to quickly identify the presence of plumes. For the sake of quality control, turbidity measurements from the CTD and the MAPRs were compared. Before the beginning of the first CTD station there was a test station where one MAPR was deployed, for testing and educational purposes. For plotting of the data, the neph and Eh data where filtered with a moving average filter, of window size 5. NTU was calculated from the raw data (Volts) by:

$$\boldsymbol{Delta\ NTU} = (\boldsymbol{V_r} - \boldsymbol{V_b})/\boldsymbol{a_n}$$

Where $\boldsymbol{V_r}$ is the raw voltage, $\boldsymbol{V_b}$ is the background voltage of ambient seawater, not affected by hydrothermal plumes and $\boldsymbol{a_n}$ is a factor unique for each backscatter sensor, which has been determined by the NOAA labs, servicing the MAPR units.

5.6.3 Regular CTD casts

MAPRs were deployed at 54 CTD stations. The stations spread across segments 1-16. While some segments had only one station (4, 5 and 14) others had up to 6 stations. For the locations of the stations, see the CTD data description section of this report. All regular MAPR deployments are listed in the table below. After a few casts it was discovered that the Eh sensor of MAPR 50 was not working properly. Station 021 was used for testing the MAPRs to find out if all the remaining sensors are operational. At this station all five MAPRs were attached to the wire above the CTD, 10m apart. At station 025 two MARPs were deployed. MAPR 50 on the CTD and 64 tied to the wire. Background data was collected off axis between segment 8 and 9 (station

058). The MAPR went down to 4108m. Amongst the 54 regular MAPR deployments, only one showed a significant plume anomaly (Station 122) above the Tai Chi hydrothermal field. Some of the stations showed a small deviation in the turbidity signal (075, 077, 098, 114) and Eh (098) but generally no significant plume anomalies.

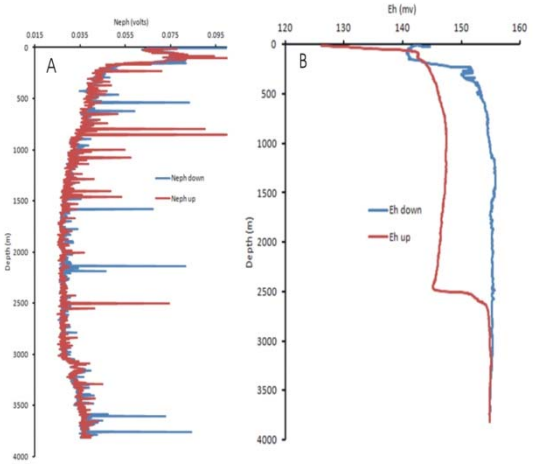

Fig. 5.39 Variation in neph and Eh Vs. depth at station 098. A) Notice a slight variation in Neph at 3000m. A few spikes in neph in both the up and down casts B) Eh jump at 2500m. Down cast is represented by blue and up cast by red.

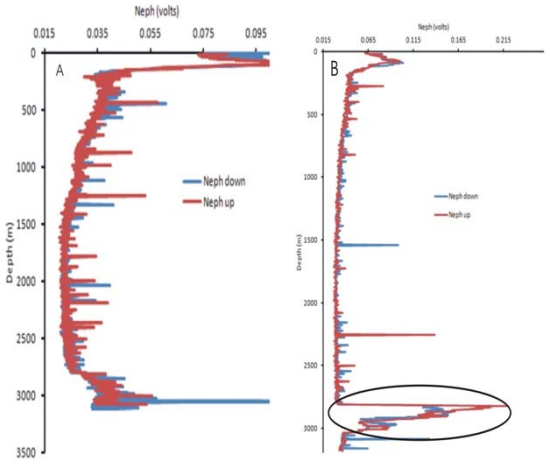

Fig. 5.40 Variations in neph Vs. depth at station 114 (left) and 122 (right) respectively. A)Notice a slight deviation in neph at 2800m and a few spikes in both the down and up casts. B)At station 122 a turbidity anomaly was recorded between 2800 and 3010m (black circle). Down cast is represented in blue and up cast in red.

Table 5.4: Summary of MAPR deployments at CTD stations. The time interval begins, as the MAPRs started logging on the deck and ends with the recovery of data.

Segment No	MAPR No	Station ID	Date and Time	GPS coordinates	Water Depth (m)	comment
1	49	003	03.02.2013 08:39-11:21	33°17.515' S 14°20.502' W	3718	Large turbidity spikes in both down and up cast
	49	005	03.02.2013 14:59-17:01	32°08.705' S 14°23.697' W	3042	Small turbidity spikes in down and up cast and no Eh anomaly
	50	007	04.02.2013 02:53-05:33	32°33.005' S 14°32.998' W	3551	No turbidity and Eh anomalies
2	49	009	04.02.2013 19:36-22:21	32°12.728' S 13°35.233' W	4109	Small turbidity spikes in down cast, no Eh anomaly
	50	012	05.02.2013 00:24-02:53	32°02.990' S 13°17.215' W	3703	No turbidity and Eh anomalies
	47	016	05.02.2013 15:32-17:46	31°32.202' S 13°26.498' W	3304	Many spike for neph in both casts (2000-3300m)
	64	017	05.02.2013 19:43-21:57	31°18.988' S 13°28.520' W	3169	Shift and scattered turbidity up cast. No Eh anomaly.
	47	019	06.02.2013 18:16-10:27	30°49.965' S 13°28.136' W	2980	No anomalies
3	49	020	06.02.2013 12:41-14:49	30°38.002' S 13°40.700' W	3903	No anomalies
	47,48,49, 50, 64	021	06.02.2013 18:16-20:46	30°27.595' S 13°45.311' W	3137	MAPR test station. Turbidity spikes in both casts, but no anomalies
	64	024	07.02.2013 03:44-07:30	29°55.604' S 13°51.600' W	3450	Tiny spikes in turbidity but no anomalies
	50,64	025	07.02.2013 08:44-11:15	29°48.277' S 13°54.033' W	3524	Few single large values for neph in down cast
	50	026	07.02.2013 12:25-14:49	29°46.492' S 13°45.741' W	3479	No anomalies
4	50	028	07.02.2013 16:58-19:04	29°31.285' S 13°43.601' W	3252	Small scatter in turbidity
5	49	030	08.02.2013 07:00-09:18	28°32.394' S 12°32.855' W	3436	Large scatter in neph only in the down cast
6	47	032	08.02.2013 14:26-17:00	28°15.171' S 13°10.079' W	4095	Many neph spikes in both casts
	47	035	09.02.2013 01:50-03:52	27°44.306' S 10°22.898' W	3165	Many neph spikes in both casts
	47	037	09.02.2013 06:06-08:45	27°24.001' S 13°27.202' W	3937	Many neph spikes in both casts
	47	039	09.02.2013 10:13-12:39	27°10.99' S 13°28.11' W	3373	Many neph spikes in both casts
	47	042	09.02.2013 21:19-23:58	26°42.576' S 13°36.593' W	3594	Many neph spikes in both casts
7	47	044	10.02.2013 01:37-04:01	26°30.939' S 13°43.873' W	3721	Many neph spikes in both casts
	47	047	10.02.2013 08:53-11:55	25°45.364' S 13°56.647' W	4248	Many neph spikes in both casts
8	47	052	12.02.2013 02:23-04:52	25°37.102' S 13°34.602' W	3948	Few neph spikes in both casts
	47	056	12.02.2013 19:55-22:17	24°59.946' S 13°38.798' W	3369	Few neph spikes in the upcast
0ff axis	48	058	13.02.2013 18:03-20:48	22°09.997' S 13°44.984' W	4108	Background data for comparison
9	47	060	14.02.2013 08:42-12:12	23°47.408' S 13°24.404' W	3290	Few neph spikes in both casts
	47	062	14.02.2013 16:15-18:35	23°31.304' S 13°27.418' W	3805	No anomalies
	64	064	14.02.2013 22:09-00:30	23°58.601' S 13°20.600' W	3552	Few neph spikes in down cast
	48	066	15.02.2013 02:33-04:40	24°08.115' S 13°17.078' W	3155	Few neph spikes in down cast
	47	068	15.02.2013 07:21-09:43	24°23.104' S 13°13.800' W	3671	Few neph spikes in the up cast
	47	071	16.02.2013 00:32-03:30	22°59.07' S 13°36.28' W	4322	Few neph spikes in both casts
10	47	073	16.02.2013 19:13-21:49	21°58.402' S 11°41.807' W	3921	Few neph spikes in the down cast
	47	075	16.02.2013 00:25-02:33	21°34.707' S 11°48.601' W	3211	Small deviation in neph at 3000m

Segment No	MAPR No	Station ID	Date and Time	GPS coordinates	Water Depth (m)	comment
	47	077	17.02.2013 04:10-06:34	21°21.707' S 11°50.799' W	3813	Small deviation in neph at 3000-3500m
	47	079	18.02.2013 10:28-13:07	17°43.701' S 13°01.811' W	3446	No data collected due to battery failure.
13	48	081	18.02.2013 16:10-18:39	18°02.303' S 12°53.003' W	3636	Few neph spikes in the up cast
	48	084	19.02.2013 04:06-06:16	18°29.007' S 12°48.000' W	3454	Few neph spikes in the up cast
	49	086	19.02.2013 07:41-10:23	18°37.205' S 12°39.899' W	3708	Few neph spikes in both casts
11	49	089	20.02.2013 08:05-10:35	20°15.572' S 11°43.791' W	3343	No anomalies
	48	092	20.02.2013 14:53-17:08	20°26.707' S 11°41.396' W	3373	Few neph spikes in the up cast
	47	094	20.02.2013 18:39-21:21	20°37.691' S 11°37.416' W	3437	MAPR battery check
	48	094	20.02.2013 18:35-21:21	20°37.691' S 11°27.416' W	3445	Few neph spikes in the down cast
	48	096	20.02.2013 23:02-01:36	20°49.503' S 11°36.603' W	3430	Few neph spikes in the up cast
	48	098	21.02.2013 03:00-05:52	20°56.505' S 11°35.102' W	3838	Neph deviation at 3000m and a big jump in Eh
12	49	103	22.02.2013 10:16-12:15	19°16.702' S 11°57.901' W	2787	Few neph spikes in the down cast
	48	104	22.02.2013 14:05-16:06	19°00.207' S 12°12.101' W	2855	Few neph spikes in the up cast
	49	105	22.02.2013 20:50-23:16	18°51.508' S 12°28.697' W	3291	Few neph spikes in both casts
14	49	107	23.02.2013 11:40-15:05	15°15.125' S 14°13.624' W	3300	Few neph spikes in the up cast
15	49	110	24.02.2013 13:23-15:40	14°15.356' S 13°35.063' W	3335	Few neph spikes in both casts
	49	112	24.02.2013 20:35-22:37	14°42.505' S 13°29.299' W	2816	Few neph spikes in both casts
	49	113	25.02.2013 01:03-03:16	15°10.207' S 13°22.199' W	3042	Few neph spikes in both casts
	49	114	25.02.2013 05:52-08:06	15°37.002' S 13°15.604' W	3115	Neph deviation at 2800m
	48	115	25.02.2013 08:53-11:02	15°28.150' S 13°17.600' W	2839	Few neph spikes in both casts
16	48	120	26.02.2013 22:41-00:16	14°03.605' S 14°20.406' W	1854	No plume anomaly at Rainbow
	48	122	27.02.2013 03:26-05:53	13°35.406' S 14°31.205' W	3161	Large plume anomaly at Tai Chi

5.6.4 Tow-Yo casts

MAPRS were deployed at 9 Tow-Yo stations. For these stations the IXSEA Posidonia underwater navigational system was used to determine the precise position of the CTD and MAPR units. Tow-Yo stations where done in segments 1, 2, 3, 7, 8, 9, 12, 15 and 16. Hydrothermal activity was found in the MAPR Tow-Yo data of segment1, 7, 8, 9, 15 and 16. No hydrothermal anomalies were detected by the MAPRs at the Tow-Yo stations in segments 2, 3 and 12. In order to identify any anomalies in the data, Eh and turbidity where plotted against the water depth and time or geographical coordinates, after the recovery of instruments. For all Tow-Yo stations, showing a hydrothermal plume anomaly, a bathymetric map with the Tow-Yo track, as well as the Eh and turbidity profiles are provided below.

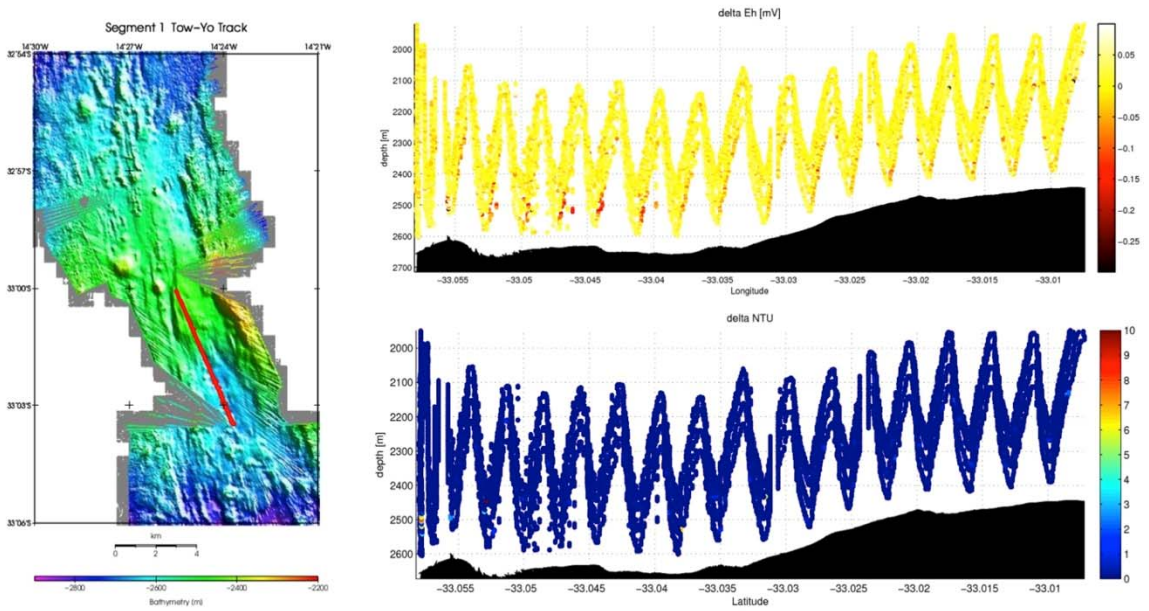

Fig. 5.41 Bathymetric map of the segment 1 Tow-Yo track (red line). Eh and turbidity profiles at the right. The Eh and turbidity data indicate the presence of a weak plume anomaly at the very southern end of the profile.

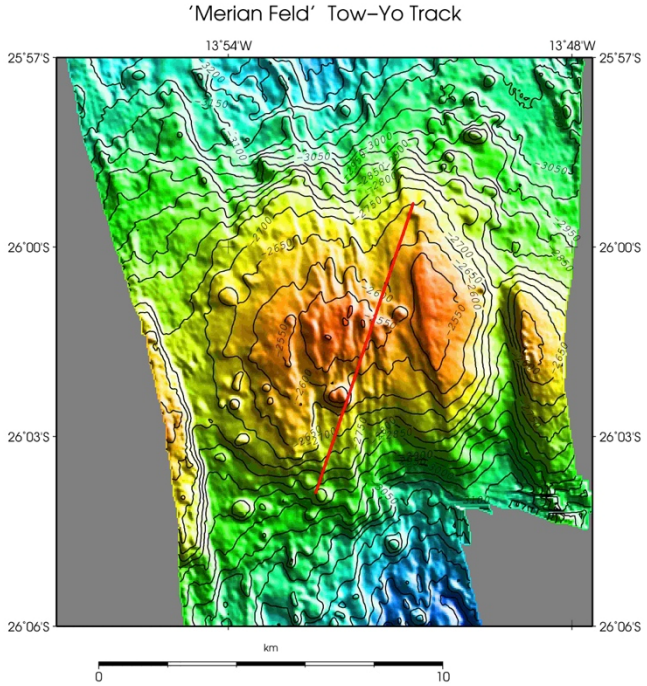

Fig. 5.42 Bathymetric map showing NE-SW trending Tow-Yo track (red line) over the axial high in the northern part of segment 7.

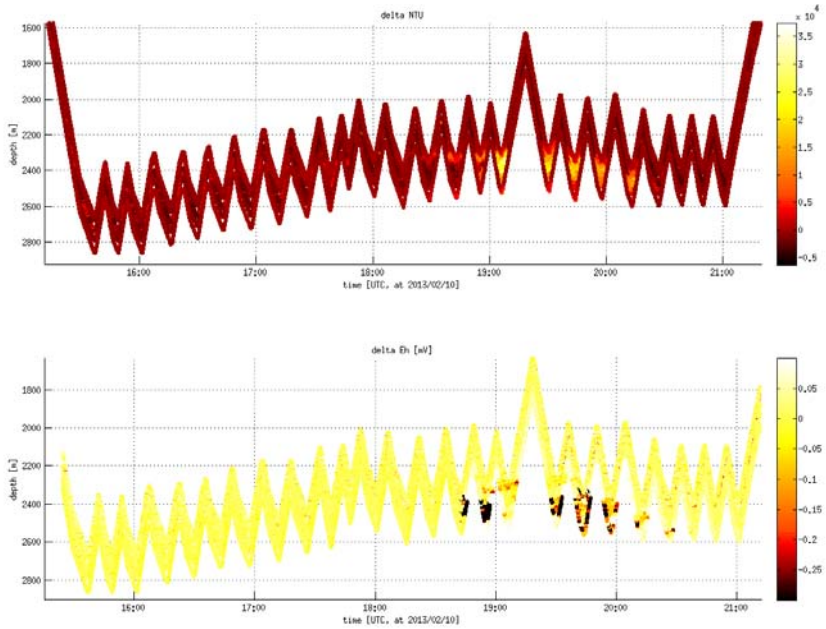

Fig. 5.43 Eh and Turbidity profiles across the axial high of segment 7, indicating the presence of a strong plume signal.

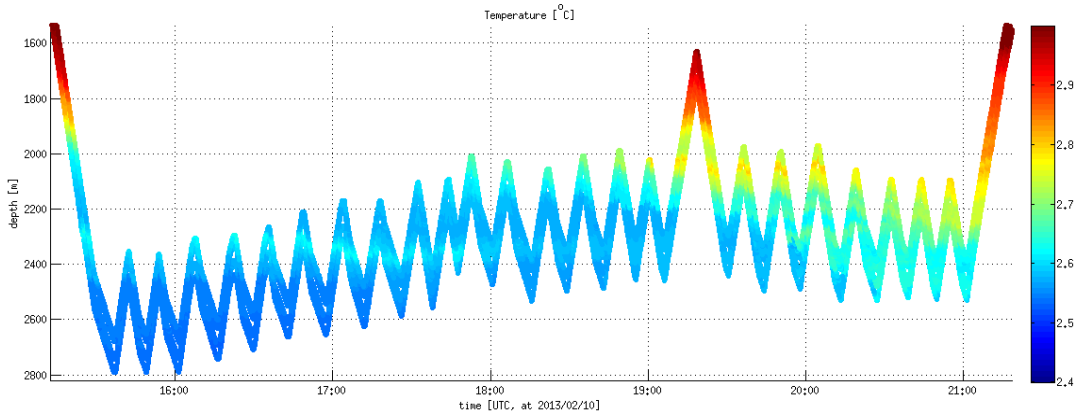

Fig. 5.44 Variation in temperature across the axial high in segment 7. Notice the inverse temperature profiles at several points of the profile, indicating an unstable temperature stratification.

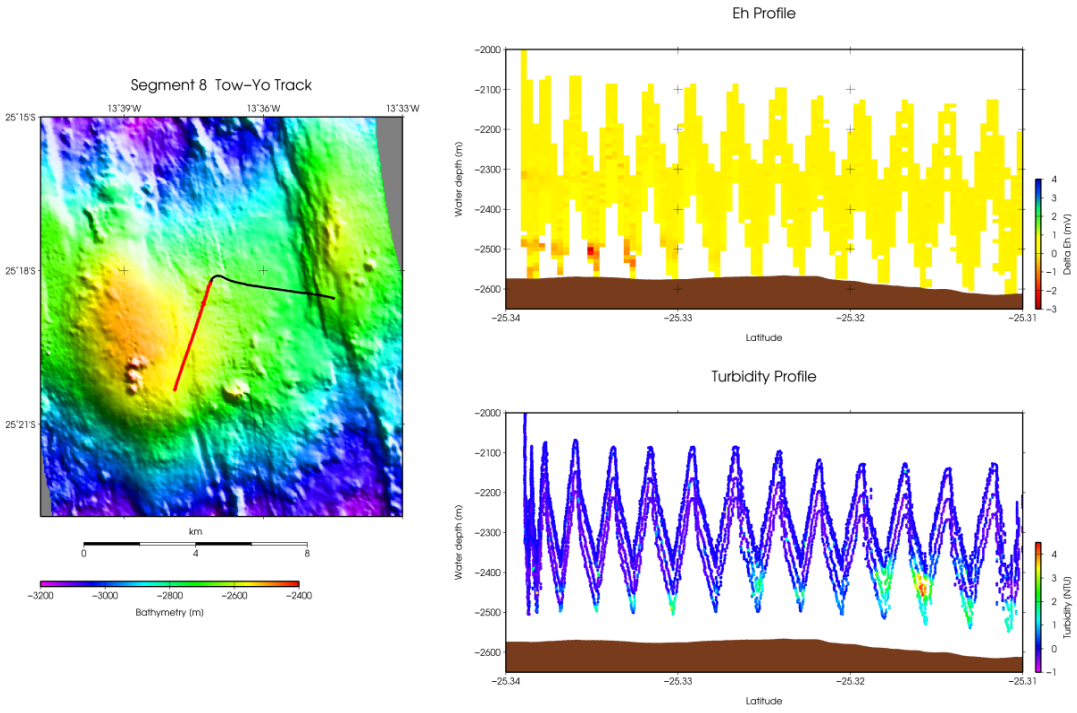

Fig. 5.45 Bathymetric map of a well developed axial high in segment 8 showing the Tow-Yo track. The first part of the track is marked by a red line and the second by a black line. The profiles to the right display the Eh and turbidity distribution along the first part. Notice a small anomaly in Eh and a turbidity anomaly indicating a plume signal. In the second part of the Tow-Yo profile, no plume signal was detected. Note, the unit of turbidity data is arbitrary.

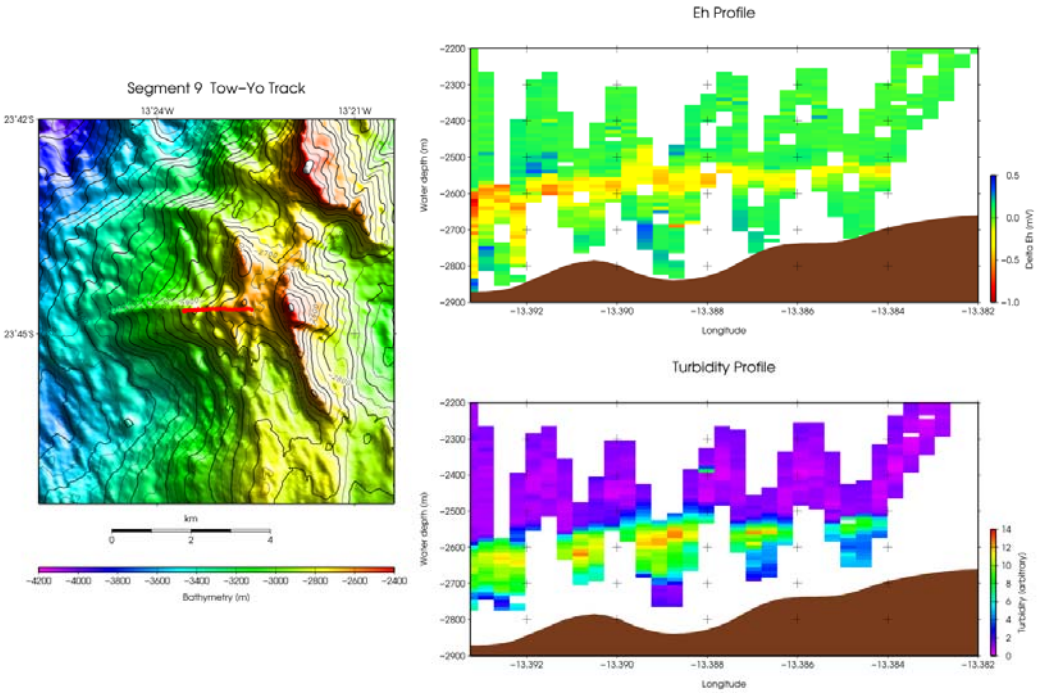

Fig. 5.46 Bathymetric map across a volcanic high in segment 9 showing the Tow-Yo track (red line) and gridded profiles of Eh and turbidity along the Tow-Yo track, indicating strong hydrothermal signals.

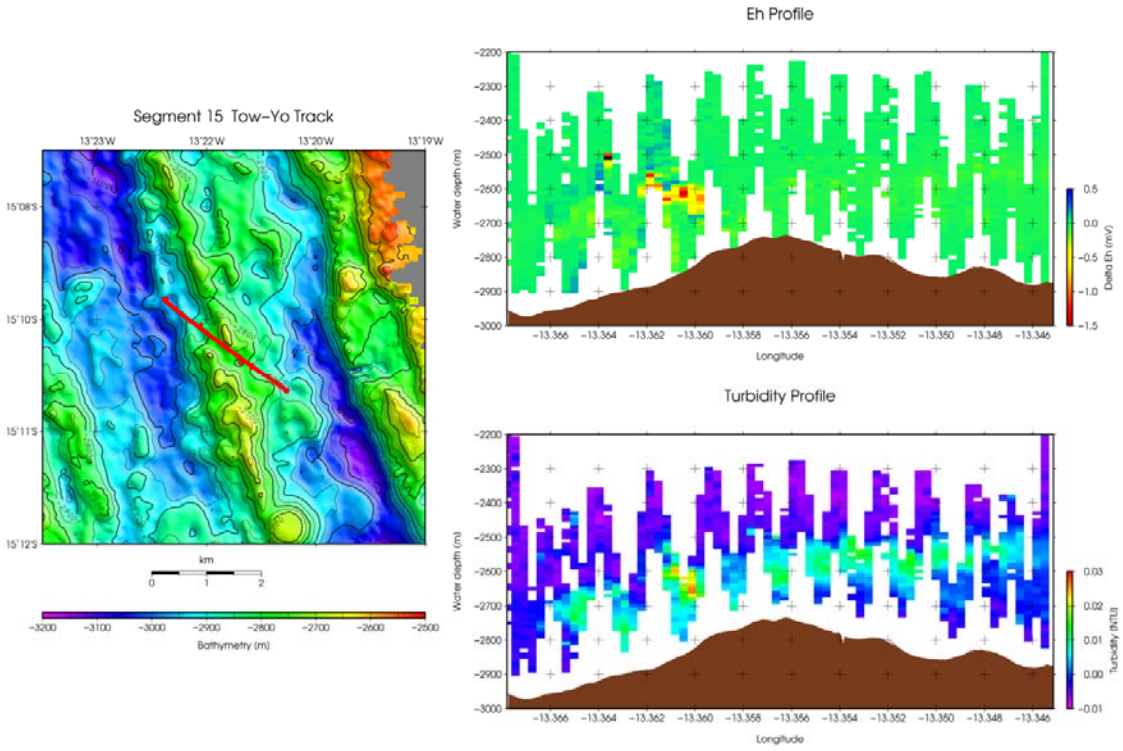

Fig. 5.47 Bathymetric map showing the Tow-Yo track (red line) at segment 15 and gridded profiles of Eh and turbidity indicating the presence of a scattered hydrothermal plume.

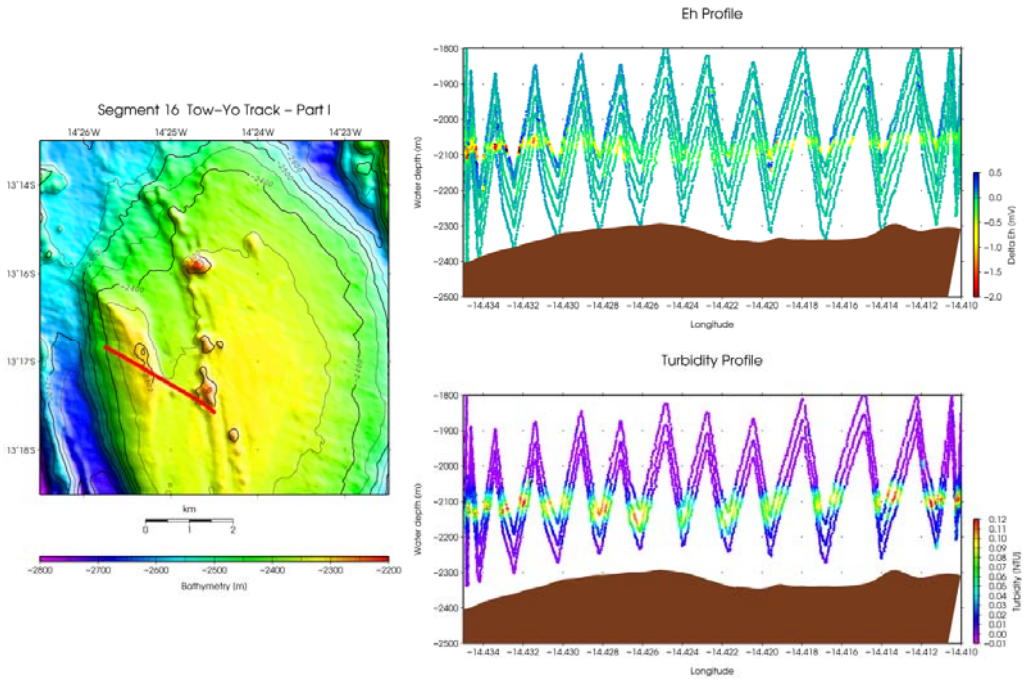

Fig. 5.48 Bathymetric map, indicating the first part of the Tow-Yo track on segment 16. Eh and turbidity along the this part of the Tow-Yo track indicate strong hydrothermal plume signals throughout the Tow-Yo track.

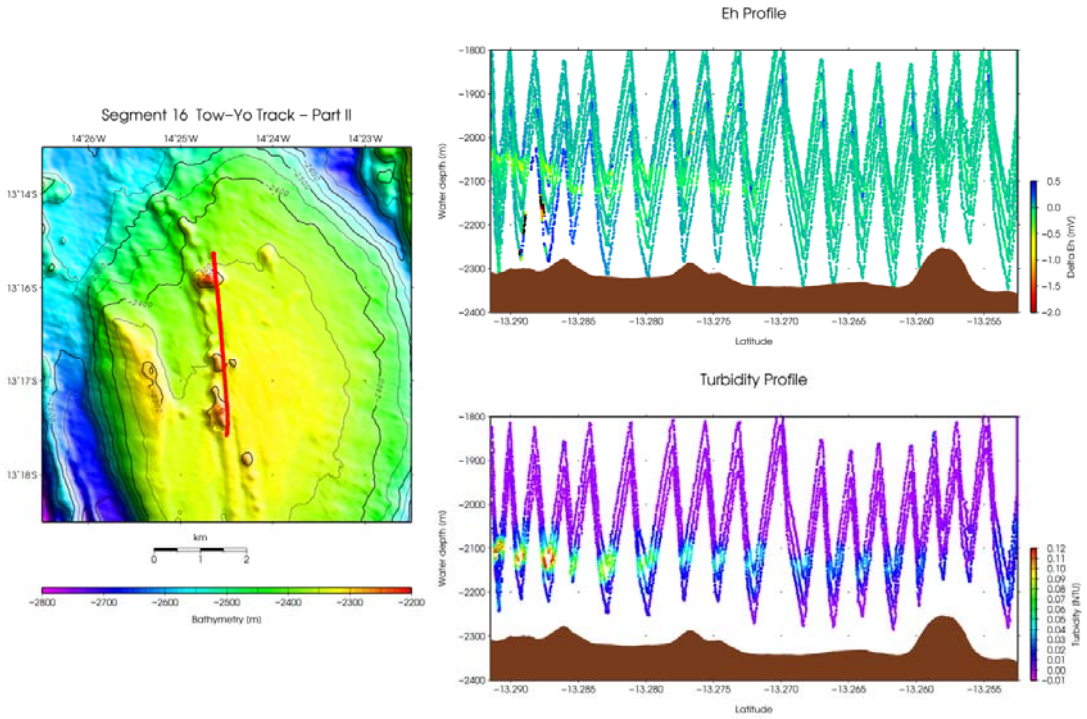

Fig. 5.49 Bathymetric map, indicating the second part of the Tow-Yo track on segment 16. Eh and turbidity along the this part of the Tow-Yo track indicate strong hydrothermal plume anomalie

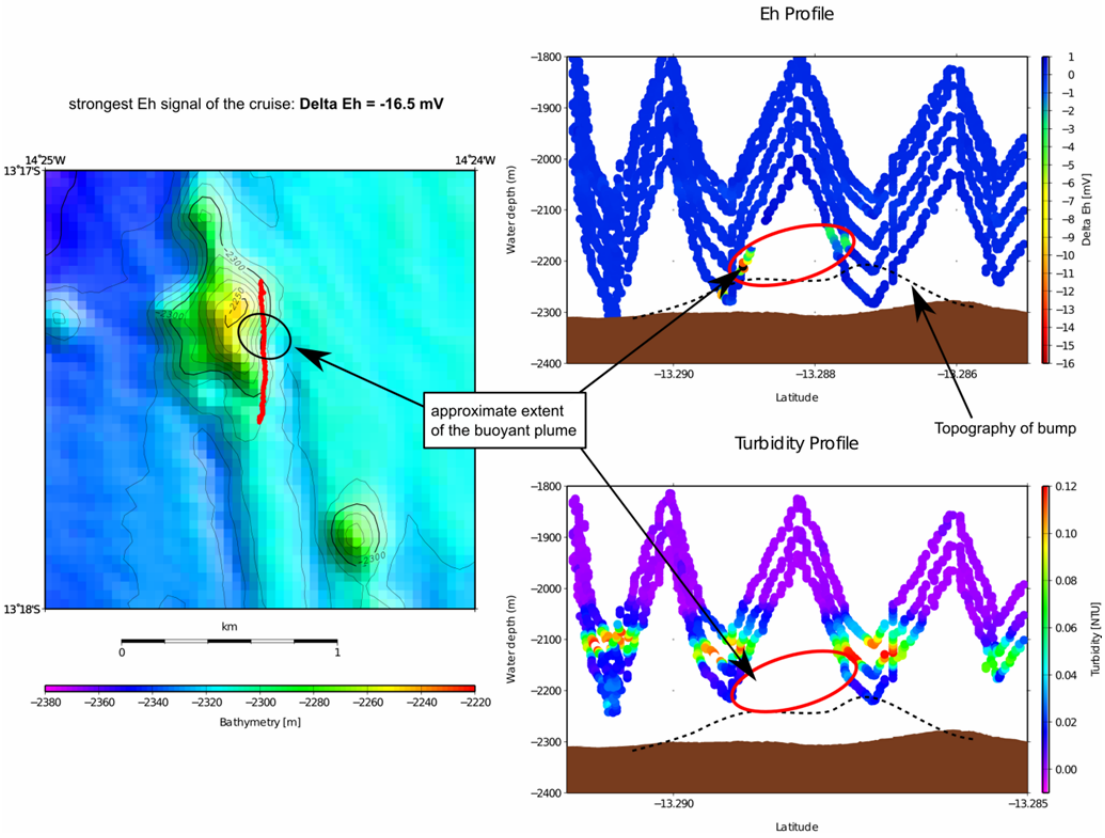

Fig. 5.50 Bathymetric map of a small bump on the seafloor of segment 16, were the Eh signal and the CTD turbidity showed exceptionally strong anomalies, indicating the presence of a buoyant plume.

Table 5.5: Summary of MAPR deployments at Tow-Yo stations. Time interval range from when the MAPRs started logging on deck to recovery.

Segment No	MAPR No	Station ID	Date and Time	GPS coordinates start	GPS coordinates end	Water Depth (m)	Comment
1	50,47,48, 49,64	006	03.02.2013 18:23-00:09	32°03.529' S 14°28.752' W	32°59.529' S 14°25.752' W	2518	Slight evidence of a plume
2	50,47,48, 49,64	014	05.02.2013 10:26-14:14	31°45.99' S 13°22.32' W	31°44.127' S 13°65.659' W	3133	No plume anomaly
3	50,47,48, 49,64	023	06.02.2013 22:19-02:33	30°17.706' S 13°47.197' W	30°15.000' S 13°47.665' W	2938	No plume anomaly
7	50,47,48, 49,64	048	10.02.2013 13:46-22:01	26°03.88' S 13°52.47' W	25°59.38' S 13°50.80' W	2858	Strong plume anomaly
8	50,47,48, 49,64	054	12.02.2013 08:10-16:54	25°20.306' S 13°37.895' W	25°18.55' S 13°34.51' W	2557	Two plume anomalies
9	50,47,48, 49,64	070	15.02.2013 16:36-20:43	23°44.680' S 13°23.580' W	23°44.677' S 13°23.585' W	2878	Plume anomaly
12	50,47,48, 49,64	102	22.02.2013 03:14-09:06	19°25.704' S 11°56.901' W	19°24.104' S 11°54.901' W	2858	No plume anomaly
15	50,47,48, 49,64	116	25.02.2013 15:18-20:51	15°10.365' S 13°20.713' W	15°09.380' S 13°22.061' W	2873	Small plume anomaly
16	50,47,48, 49,64	124	27.02.2013 10:05-18:00	13°16.609' S 14°26.116' W	13°14.937' S 14°24.753' W	2390	Plume anomaly

5.6.5 Comparison between MAPR and CTD turbidity measurements

For the Tow-Yo station 048, up-cast measurements of the MAPR turbidity sensor and the CTD mounted turbidity sensor (Eco Wet Labs) where compared for quality control. For the comparison an up-cast was chosen, where both sensors showed a strong plume anomaly in the water column. As the MAPR, chosen for the comparison, was mounted on the wire 50m above the CTD, the pressure was used as a common reference. The figure below gives the results of the comparison. The correlation of the 133 measurement of common depth, is described by the coefficient correlation of R^2 = 0.8885. Both sensors indicate the maximum turbidity of the hydrothermal plume to be in the order of 0.18 NTU. The background levels slightly differ, with the CTD mounted turbidity sensor showing a slightly increased noise level and the MAPR turbidity data figuring a spike at 2000 dbar.

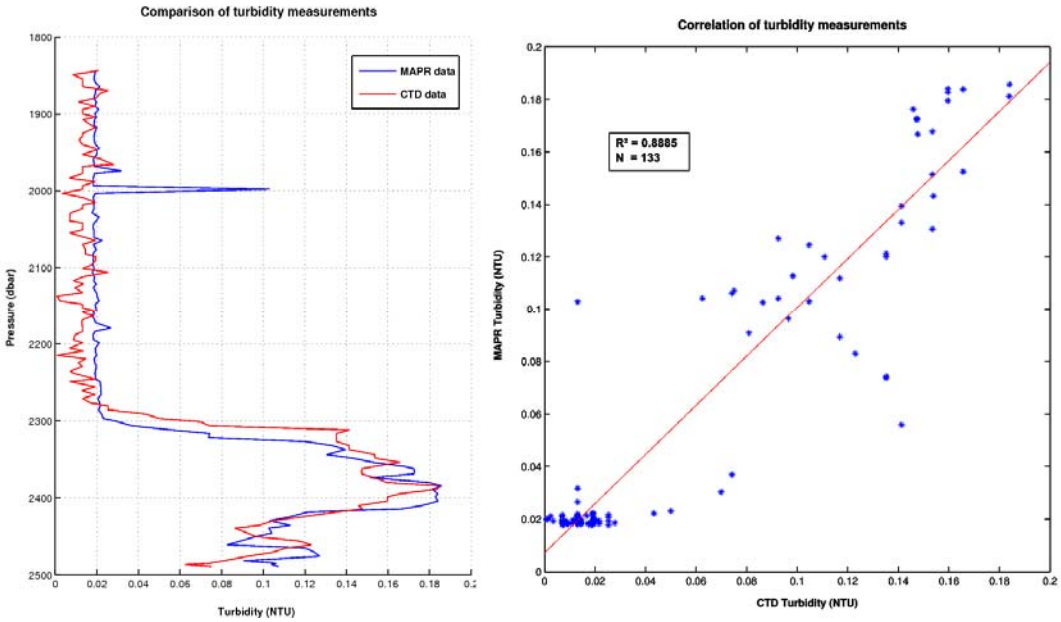

Fig. 5.51 Left, comparison between the CTD turbidity measurements and MAPR turbidity measurement of up cast measurements through a strong plume anomaly in the Tow-Yo profile at segment 7. Right, correlation of the data plotted in the left hand graph.

5.7 Current measurements

(Köhler, Walter)

5.7.1 Introduction

During MSM25, the focus of the direct current measurements was on obtaining profiles of velocity parallel to the CTD casts with a lowered Acoustic Doppler Current Profiler (LADCP) system. These velocity data will be used for the calculation of finescale velocity shear to estimate diapycnal mixing above the ridge crest, and to interpret the dispersal of plume signals in the axial valley.
In addition to the lowered ADCP, upper ocean velocity data were collected during the transits between the individual stations with the ships' two vessel mounted ADCPs, a 75kHz and a 38kHz instrument.

5.7.2 LADCP

Two RD Instruments 300kHz Workhorse Monitor ADCPs were attached to a carousel water sampler and operated in a synchronized master-slave configuration in which the downward looking master triggers the upward looking slave. Both instruments were used with a ping rate of 1Hz and a 10m depth cell size. Power for both instruments was supplied by 35 commercial quality 1.5V batteries, externally assembled in a modified Aanderaa pressure housing. A compass calibration was carried out prior to the cruise.

Additional weights of about 300 kg in total were mounted to the water sampler, ensuring a stable movement of the instruments with very little tilt and generally steady vertical velocity. CTD pressure profiles were used for exact depth information.
During the cruise three different ADCPs were used. Two of the instruments were calibrated as masters (SN 7915 and 2161), one as slave (SN 1973). Independent of the combination of the used instruments a heading-dependent compass offset between master and slave of up to 20% was found especially for profiles during which the carousel water sampler was spinning strongly. To test for sources of the compass offset between master and slave instrument all combinations of instruments were tested but the offset was found to be independent on the used instruments (including using a master instrument as slave). As a successful calibration of all instruments was carried out immediately before the cruise and the offset is independent of the used instrument combinations, it is probably induced by interferences between the water sampler carousel and the ADCP compasses. After station 7 the winch was changed which lead to a decrease in the spinning of the water sampler.

After station 79 instrument SN7915 was used as master in combination with the slave (SN1973) since the beam quality of instrument SN2161 (calibrated as master but used as slave) slightly decreased. The instrument configuration was changed to master (SN2161) with slave (SN1973) after station 116 as the beam quality of instrument SN7915 decreased, instrument 2161 recorded good data.

Due to cable problems station 20 was just carried out with the master instrument.
As the number of scatterers strongly decreased with depth (**Fig. 5.52**), the lowering and heaving velocity of the water sampler carousel was lowered from 1m/s to 0.8m/s in depths below 2000m from station 79 onwards in order to increase the number of shear estimates in each depth bin. With the lowered winch speed the number of shear estimates slightly increased and a minimum of 100 shear estimates per bin could be achieved for most profiles with some exception were just approximately 80 shear estimates are available below 2000m.

Some weak high frequency noise can be seen in all data sets which probably results from interferences of the altimeter with the ADCPs. As also signals of the Posidonia system can be seen in the ADCP data, it was turned off for stations 105, 107 and 110 but were found to not significantly influence the data quality.

The raw data (except those listed in *Fischer, J. and M. Visbeck, 1993: Deep Velocity Profiling With Self-Containing ADCPs. J. Atmos. Oceanic Technol., 10, 764--773.*
M. Visbeck, 2002: Deep Velocity Profiling Using Lowered Acoustic Doppler Profilers: Bottom Track and Inverse Solutions. J. Atmos. Oceanic Technol., 19(5), 794--807.
Table 5.6) have been processed with an inverse method (Visbeck, 2002) using barotropic, bottom track and smoothness constraints, as well as external pressure from the CTD system, with a threshold for the standard deviation between down- and upcast of 2.8. When the inverse solution was not sufficiently determined (mostly because of lack of scatterers at depth), a shear solution (Fischer and Visbeck, 1993) was applied.
Fischer, J. and M. Visbeck, 1993: Deep Velocity Profiling With Self-Containing ADCPs. J. Atmos. Oceanic Technol., 10, 764--773.
M. Visbeck, 2002: Deep Velocity Profiling Using Lowered Acoustic Doppler Profilers: Bottom Track and Inverse Solutions. J. Atmos. Oceanic Technol., 19(5), 794--807.

Table 5.6: Profiles that were not processed using the inverse solution with a threshold for the standard deviation between down- and upcast of 2.8.

Stationnr.	Profilnr.	comments
3	1	Shear solution
19	11	shear solution, threshold 2
20	12	Master only, shear solution
24	15	shear solution, threshold 2
25	16	inverse solution, threshold 2.3
35	21	shear solution, threshold 2
51	28	shear solution, threshold 2
60	33	inverse solution, threshold 2.0
68	37	shear solution, threshold 2
71	39	both shear and inverse solution give no satisfying results
75	41	shear solution, threshold 2
92	48	inverse solution, threshold 2.3
96	50	inverse solution, threshold 2.0
104	54	inverse solution, threshold 2.3
105	55	inverse solution, threshold 2.3
110	57	inverse solution, threshold 2.0
113	59	inverse solution, threshold 2.0
115	61	inverse solution, threshold 2.3

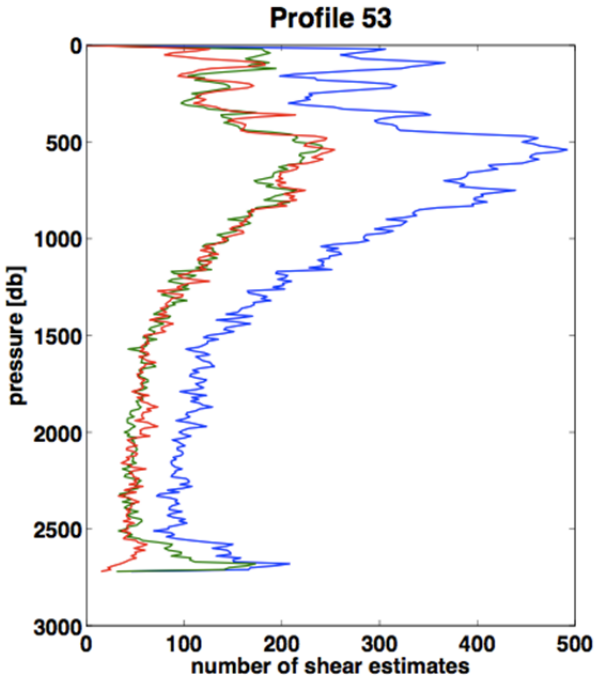

Fig. 5.52 Number of shear estimates during down- (green), upcast (red) and total (blue). Below 2000m sparse scatterers only allow for approximately 80 estimates per bin with reduced winch speed of 0.8m/s.

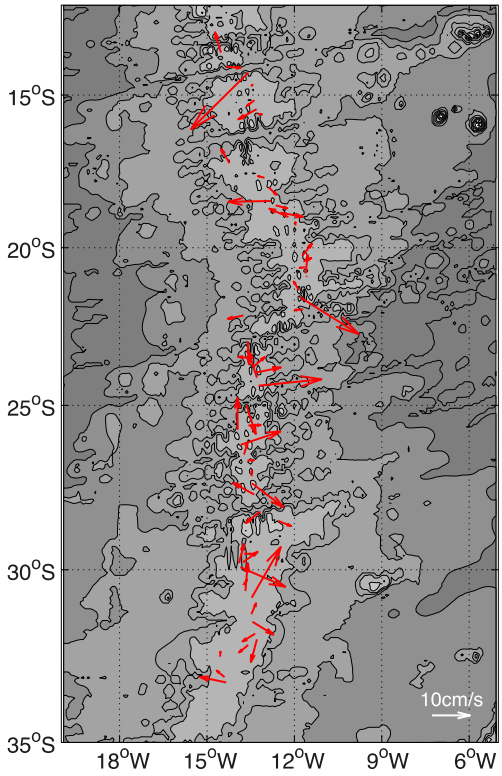

Fig: 5.53 Mean velocities in the bottommost 500m. The flow direction is strongly steered by the local topography.

5.7.3 vmADCP

Data from the two vessels mounted ADCP were recorded during the transits to and from the work area, as well as along the 16 surveyed segments. One, the RD Instruments 75 kHz Ocean Surveyor, is mounted permanently into the hull of the ship, while the 38 kHz Ocean Surveyor was lowered into the sea chest of the ship. Both instruments were configured to collect narrow bandwidth water-profile data throughout the cruise. The 75 kHz OS data were recorded in 8 m bins to get high vertical resolution data in the upper water column. The 38 kHz OS data were collected in 32 m bins to achieve maximum range. The ship's Doppler log that is well known to cause considerable reduction in data quality in the 75 kHz OS was switched off to avoid the severe interferences that would result in strongly reduced range and poor data quality. Navigation as well as heading, pitch, and roll data were obtained from ship's SeaTex Seapath 200 system that, in combination with the Motion Reference Unit, provides differential GPS and attitude data.

The calm sea state was calm resulted in a profiling range of typically 700 to 800 m for the 75kHz and 1400 to 1500 m for the 38kHz instrument, except for transits were the ship was moving with a velocity of 15 kn, which resulted in a reduction of range and data quality. A water-track calibration of the transducer alignment will be carried out post-cruise.

5.8 Noble gas sampling (Buss)

The primordial components of helium isotopes are ideal tracers for large-scale distribution of vent fluids in the water column also in the South Atlantic. The sampling strategy during MSM25 was to sample 12-22 depth levels, with the highest resolution in the lowermost 500m of the water column, in order to provide a picture of a more regional distribution of dispersing vent fluids in the water column along the mid Atlantic ridge.

5.8.1 Sampling and analysis

For measurements of the helium concentrations and isotopic signature, water samples were collected from the Niskin bottles. In total 973 samples were taken, 522 of them were sealed free of head space and gas tight in copper tubes and 451 of them were taken with the Ampoule-based Water Sampler (AWS) were water is drawn into evacuated glass ampoules with subsequent flame sealing (**Fig: 5.54**, Roether et al., 2013).

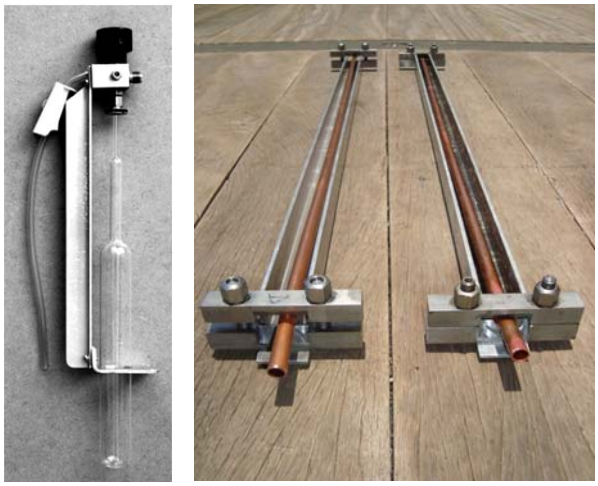

Fig: 5.54 (left) Ampoule-based Water Sampler (AWS). The glass-ampoule is connected to the valve which sits in an aluminium holder to stabilize the glass-ampoule. (right) Two Copper tubes in aluminium holder used for the classical sampling. Left one still open end empty, the right one is closed and filled with water.

Helium isotope measurements will be carried at University of Bremen with a fully automated UHV mass spectrometric system. For the Cu-tubing samples, the preparation includes gas extraction in a controlled high vacuum system, the AWS method saves the gas extraction step prior to admission to the mass spectrometer. Helium and neon are separated from permanent gases in a cryo system at 25 K. A split of the sample is analyzed for 4He, 20Ne and 22Ne with a quadrupole mass spectrometer. At 14 K helium is separated from neon and released into the sector field mass spectrometer for analysis of 3He and 4He. The facility achieves about ± 0.2% precision for 3He/4He ratios, and ± 0.5% or better for helium and neon concentrations (Sültenfuß et al., 2009).

The AWS method is a new method which was developed to replace the classical Cu-tubing sampling to minimize the delay between sampling and measurement by combining sample collection and gas extraction in one step. The AWS was successfully tested at sea in comparison to the Cu tubing sampling in 2011; during MSM25 also 20 duplicate samples were taken to study the precision of the measured helium isotope values for both sampling systems.

Roether, W., M. Vogt, S. Vogel, and J. Sültenfuss, 2013: Combined sample collection and gas extraction for the measurement of helium isotopes and neon in natural waters Deep-Sea Res. I, subm.

Sültenfuss, J., M. Rhein, and W. Roether, 2009: The Bremen Mass Spectrometric Facility for the Measurement of Helium Isotopes, Neon, and Tritium in Water. Isotopes Environ.

5.9 Trace Metals and Proteomics

(Held)

5.9.1 Introduction and Sampling Overview

Trace metal and protein samples were collected across the 16 studied segments between 33 degrees South and 13 degrees South along the Mid-Atlantic Ridge. These micronutrient samples will be analyzed for trace metal concentrations (primarily iron and manganese) to study the importance of slow spreading regions and hydrothermal vent fields such as the Southern MAR on global iron inputs. Previous work has generated a profile of dissolved metals in the East→ West direction across the ridge (approximately 13 degrees South)[1]. The goal of this sampling is primarily to generate a dissolved metal profile in the North→ South direction along the entire studied area. Trace metal concentrations will be compared with ^{3}He data also collected on this cruise to help us understand the chemical make-up of the hydrothermal systems, as well as the ridge's impact on global biogeochemical cycles.

Microbial biomass samples were also collected to characterize the functions of the vent-field microbial community. These samples will also be used in the development of new techniques for protein analysis. Given their importance in biogeochemical processes, marine microbes are of particular interest in understanding the chemistry of the Mid-Atlantic ridge vent fields[2].

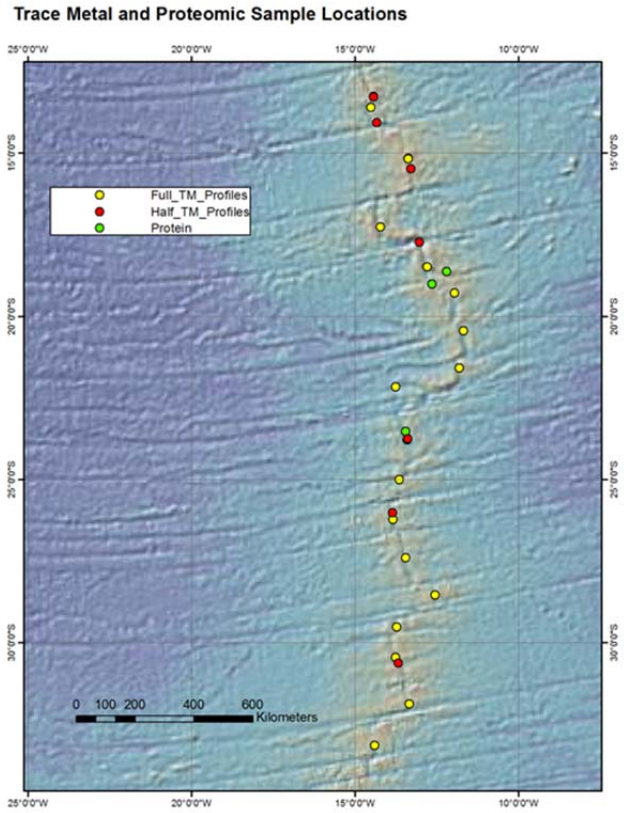

Fig. 5.55 Trace Metal and Protein Sampling Overview

Table 5.7: Sampling Details

Section	Profile	Station	TM Profiles	Protein Samples
1	1	002	Full	
2	2	013	Full	
3	3	020		1 at 3200m (Plume Signal)
	4	021	Full	
4	5	025	Full	
5	6	030	Full	
6	7	037	Full	
7	8	048	Half	1 at 2400m (Plume Signal)
	9	051	Full	
8	10	055	Full	
9	12	059	Full	
	13	062		1 at 2800m
	14	070	Half	1 at 2650 (Plume Signal)
10	15	075	Full	
11	19	092	Full	
12	20	103	Full	
	21	104		1 at 2100m (Plume Signal)
13	16	079	Half	
	17	084	Full	
	18	086		1 at 3000m
14	22	107	Full	
15	23	113	Full	
	24	115	Half	
	25	116		1 at 2800m (Plume Signal)
16	26	120	Half	
	27	122	Full	
	28	123	Half	1 at 350m (oxygen min zone?)
Background	11	057	Full	

5.9.2 Trace Metal Sampling

Trace metal (TM) samples were obtained in each of the segments surveyed during this cruise. Full water profiles (10m to bottom) were acquired at least once each segment, supplemented with half profiles (2000m to bottom) in areas of particular interest, usually over areas with CTD and/or AUV plume hits. Profiles were usually taken mid-segment, though efforts were made to match trace metal profiles with full helium profiles for later comparison. Discrete trace metal samples were also obtained at protein sampling locations, see section 5.9.3. For a complete listing of profiles taken at each station, see

Table 5.7. In total, 422 TM samples were obtained.

All sample work was conducted in a positive pressure environment that met or exceeded Class 100 standards (affectionately coined the "bubble"). A HEPA filter provide dust-free air to the "bubble," and particulate counts were monitored regularly (see **Fig. 5.56**)

Samples were collected using acid washed, trace metal clean low-density polyethylene sample bottles. Approximately one-half of the collected sample water was filtered through Teflon tubing and an acid washed 0.2uM polycarbonate plastic filter into trace metal clean LDPE sample bottles. All sample bottles and filter rigs were rinsed with sample water prior to collection or processing. Care was taken to prevent cell lyses, and therefore inaccurate dissolved/particulate metal distributions, by maintaining a gentle vacuum during the filtration process. In most cases, both dissolved (filtered) and particulate (unfiltered) samples were retained, though particulate samples were discarded at some stations to conserve supplies. Filters were also retained for analysis.

Fig. 5.56 Shipboard TM Clean environment – the "bubble" - during filtration operations

5.9.3 Protein Sampling

Protein samples were obtained whenever possible at plume locations identified by CTD profiles. Because trace metal distributions are not always visible in CTD data, protein samples were also taken at two "non-plume" locations. One set of samples was collected in the oxygen-minimum zone (~350m) in the northernmost area of the survey.

Biomass samples were collected by filtering approximately 10L of water evenly through four 0.2uM polycarbonate plastic sandwich filters. The filters were folded twice with the biomass facing inward, then inserted into pH-neutral 1.2mL cryovials and covered completely in preservative solution (Ambien, RNAlater). In total, 32 protein samples were collected (four filters each in eight separate locations, see

Table 5.7) Samples were kept cool in a refrigerator for the duration of the cruise. Discrete trace metal samples were collected at each location selected for protein analyses, using the techniques outlined in section 0.

Fig. 5.57 Staining on hydrothermal plume location protein sample filter after approximately 1.5L of seawater has passed through (Station 048, 2400m depth)

5.9.4 Planned Analyses

Trace metal samples will be acidified to pH 1.7 with clean HCl upon return, and will be stored at room temperature until analysis to preserve the trace metal contents. Total dissolved iron and manganese will be measured via inductively coupled mass spectrometry (ICP-MS) to generate a North-South trace metal profile of the axis. Particulate metal concentrations will also be calculated to investigate the rate of spreading/scavenging of these micronutrients.

Proteins will be extracted from the biomass samples using procedures described in previous publications. Proteins will be identified and proteomic profiles generated using LC-Mass Spectroscopy. It should be noted that this is a somewhat new method for protein analysis; as a result, these samples will contribute to the development of these techniques.

6 Summary of Science Achievements

By the end of the cruise we had successfully carried out hydrothermal exploration along 3000 km of the Southern Mid-Atlantic Ridge (representing almost 5% of the total length ((64,000km: Bird, 2003)) of the global mid-ocean ridge system and over 8% of the economically more interesting slow-spreading (<40mm/yr) ridges (Baker, 2007; Bird, 2003)). Our results show that all "Turtle Pits-like" segments are presently hydrothermally active, providing support for the model which we were aiming to test. We also have been able to show that such segments have characteristic and quantifiable bathymetric features and will use this information in the post-cruise studies to develop the first remote-sensing method for predicting the locations of chronic hydrothermal systems on slow-spreading ridges based on multibeam bathymetric measurements alone. Application of this method to off-axis regions should allow us to estimate the metal endowment of the Atlantic plate as a whole. We were also successful in acquiring mixing information from almost all segments. This data still requires much post-processing work before any conclusions can be drawn about the relationship between ridge morphology and the strength of dipycnal mixing.

7 Data and Sample Storage and Availability

Water samples will be analysed for helium isotope ratios in Bremen, no long-term sample storage for water samples is envisaged. Rock samples will be placed in the GEOMAR Lithothek sample repository immediately post-cruise. All multibeam, backscatter and side-scan data will be archived in the GEOMAR data management system where it will, after expiry of the proprietary period, be accessible via the WDC network (Pangaea-integration). CTDS and LADCP data will be uploaded to PANGAEA when post-processing is completed. Samples and data will be openly available 2 years from the end of the project (available as of 04.2015). Lithothek and Data Management contacts at Geomar are available on www.geomar.de.

8 Acknowledgements

We would like first and foremost to thank Captain Günther and his crew for their exceptional support during MSM25. Both on a professional and personal level they made this cruise a hugely successful and memorable venture. Participation on the cruise was made possible by funding from the DFG and WHOI. The NOAA Vents program provided the MAPR equipment. Ko-ichi Nakamura (AIST, Japan) kindly provided the Eh electrode for ABYSS.

9 Station List MSM25

Station #	CTD #	Start time (UTC)	Start Date (UTC)	Start Lat.	Start Long.	Action*	End time (UTC)	End Date (UTC)	End Lat.	End Long.
MSM025/001	0	7:54:01	31.01.13	33°31.31´S	2°1.19´E	CTD and AUV test	12:35.59	31.01.13	33°31.04´S	2°01.80´E
MSM025/002		17:00:00	02.02.13	33°27.17´S	11°39.13´W	Posidonia calibration	18:42:59	02.02.13	33°27.54´S	11°40.04´W
MSM025/003	1	9:09:00	03.02.13	33°17.515 S	14°20.502 W	CTD; 2 ADCP's, 1 MAPR on CTD, turbidity-sensor, depth: 3718m	11:21:30	03.02.13	33°17.518 S	14°20.501 W
MSM025/004		11:54:00	03.02.13	33°16.43´S	14°21.00´W	Aborted AUV dive	13:43:00	03.02.13	33°16.22´S	14°21.01´W
MSM025/005	2	15:14:21	03.02.13	33°08.705 S	14°23.697 W	CTD; 2 ADCP's, 1 MAPR on CTD, turbidity-sensor, depth: 3042m	17:01:10	03.02.13	33°08.703 S	14°23.699 W
MSM025/006	3	18:30:15	03.02.13	33°03.486 S	14°23.703 W	CTD - Tow-Yo; 2 ADCP's, 4 MAPR (50m, 100m, 150m and 200m), turbidity-sensor, depth:2432m - 2641m	0:11:44	04.02.13	32°59.529 S	14°25.752 W
MSM025/007	4	3:24:00	04.02.13	32°33.005 S	14°32.998 W	CTD; 2 ADCP's, 1 MAPR on CTD, turbidity-sensor, depth: 3552m	5:33:50	04.02.13	32°33.007 S	14°33.002 W
MSM025/008						Posidonia calibration				
MSM025/009	5	19:58:15	04.02.13	32°12.728 S	13°35.233 W	CTD; 2 ADCP's, 1 MAPR on CTD, turbidity-sensor, depth: 4109m	22:21:30	04.02.13	32°12.730 S	13°35.231 W
MSM025/010										
MSM025/011		22:34:00	04.02.13	32°12.66 S	13°35.10 W	Multibeam, ~ 7,2 kn	0:13:00	05.02.13	32°05.62 S	13°18.12 W
MSM025/012	6	0:42:45	05.02.13	32°02.990 S	13°17.215 W	CTD; 2 ADCP's, 1 MAPR on CTD, turbidity-sensor, depth: 3703m	2:53:00	05.02.13	32°03.004 S	13°17.200 W
MSM025/012-2		4:30:00	05.02.13	32°02.98 S	13°17.20 W	AUV dive #125 with microstructure sensor and 120 kHz sidescan sonar	0:07:00	06.02.13	31°20.40 S	13°28.25 W
MSM025/013	7	7:46:09	05.02.13	31°52.997 S	13°20.607 W	CTD; 2 ADCP's, turbidity-sensor, depth: 3392m	9:47:10	05.02.13	31°52.993 S	13°20.604 W
MSM025/014	8	11:10:30	05.02.13	31°46.994 S	13°22.277 W	CTD - Tow-Yo; 2 ADCP's, 1 MAPR on CTD plus 4 MAPR at cable (50m, 100m, 150m, 200m), turbidity-sensor, depth: 3014m - 3134m	14:13:10	05.02.13	31°44.127 S	13°65.659 W
MSM025/015		14:21:00	05.02.13	31°44.09 S	13°22.72 W	Multibeam, 1,9 kn	15:44:00	05.02.13	31°32.20 S	13°25.51 W
MSM025/016	9	15:51:10	05.02.13	31°32.202 S	13°26.498 W	CTD; 2 ADCP's, 1 MAPR on CTD, turbidity-sensor, depth: 3304m	17:46:10	05.02.13	31°32.208 S	13°26.498 W
MSM025/017	10	19:58:30	05.02.13	31°18.988 S	13°28.520 W	CTD; 2 ADCP's, 1 MAPR on CTD, turbidity-sensor, depth: 3169m	21:47:20	05.02.13	31°18.990 S	13°28.518 W
MSM025/018		0:17:00	06.02.13	31°20.38 S	13°28.32 W	Multibeam, 1,1 kn	11:49:00	06.02.13	30°39.67 S	13°31.78 W

Station #	CTD #	Start time (UTC)	Start Date (UTC)	Start Lat.	Start Long.	Action*	End time (UTC)	End Date (UTC)	End Lat.	End Long.
MSM025/019	11	8:41:00	06.02.13	30°49.965 S	13°28.139 W	CTD; 2 ADCP's, 1 MAPR on CTD, turbidity-sensor, depth: 2980m	10:27:00	06.02.13	30°49.962 S	13°28.139 W
MSM025/020	12	12:50:40	06.02.13	30°38.002 S	13°40.700 W	CTD; 1 ADCP (Master), 1 MAPR on CTD, turbidity-sensor, depth: 3903m	14:49:00	06.02.13	30°38.005 S	13°40.699 W
MSM025/020-2		14:55:00	06.02.13	30°38.00 S	13°40.70 W	AUV dive #126 with Eh sensor and 120 kHz sidescan sonar	11:36:00	07.02.13	29°48.46 S	13°54.39 W
MSM025/021	13	18:41:44	06.02.13	30°27.595 S	13°45.311 W	CTD; 2 ADCP's, 5 MAPR at cable (all approx. 10m above CTD) for calibration, turbitity-sensor, depth: 3137m	20:46:40	06.02.13	30°27.597 S	13°45.310 W
MSM025/022		20:55:00	06.02.13	30°27.60 S	13°45.30 W	Multibeam, 1,3 kn	22:25:00	06.02.13	30°17.72 S	13°47.20 W
MSM025/023	14	22:37:50	06.02.13	30°17.706 S	13°47.197 W	CTD - Tow-Yo; 2 ADCP's, 1 MAPR on CTD plus 4 MAPR at cable (50m, 100m, 150m, 200m), turbidity-sensor, depth: 2938m - 3460m	2:33:43	07.02.13	30°15.000 S	13°47.665 W
MSM025/024	15	5:28:30	07.02.13	29°55.604 S	13°51.600 W	CTD; 2 ADCP's, turbidity-sensor, depth: 3450m	7:30:20	07.02.13	29°55.603 S	13°51.602 W
MSM025/025	16	9:01:00	07.02.13	29°48.277 S	13°54.033 W	CTD; 2 ADCP's, 1 MAPR on CTD plus 1 MAPR at cable (10m), turbidity-sensor (did not work), depth: 3524m	11:09:00	07.02.13	29°48.279 S	13°54.034 W
MSM025/026	17	12:46:00	07.02.13	29°46.492 S	13°45.741 W	CTD; 2 ADCP's, turbidity-sensor (did not work properly), depth: 3479m	14:49:20	07.02.13	29°46.505 S	13°45.741 W
MSM025/027		14:52:00	07.02.13	29°46.50 S	13°45.74 W	Multibeam, ~ 9,9 kn	17:05:00	07.02.13	29°31.28 S	13°43.60 W
MSM025/028	18	17:12:15	07.02.13	29°31.285 S	13°43.601 W	CTD; 2 ADCP's, turbidity-sensor, depth: 3252m	19:04:15	07.02.13	29°31.279 S	13°43.605 W
MSM025/029		19:13:00	07.02.13	29°31.27 S	13°43.61 W	Multibeam, ~ 7,7 kn				
MSM025/030	19	7:17:20	08.02.13	28°32.394 S	12°32.855 W	CTD; 2 ADCP's, 1 MAPR on CTD, turbidity-sensor, depth: 3436m	9:18:00	08.02.13	28°32.390 S	12°32.862 W
MSM025/031		9:28:00	08.02.13	28°32.41 S	12°32.86 W	Multibeam, ~ 9,8 kn	11:53:00	08.02.13	29°09.64 S	12°41.13 W
MSM025/032	20	14:42:00	08.02.13	28°15.171 S	13°10.079 W	CTD; 2 ADCP's, new / different turbidity-sensor, depth: 4095m	17:00:31	08.02.13	28°15.172 S	13°10.085 W
MSM025/033		17:12:00	08.02.13	28°15.18 S	13°10.13 W	Multibeam, ~ 7,2 kn	22:06:00	08.02.13	27°53.42 S	13°21.05 W
MSM025/034		22:13:00	08.02.13	27°53.48´S	13°21.01´W	AUV dive #127 with Eh sensor and 120 kHz sidescan sonar	18:59:59	09.02.13	27°03.95´S	13°29.80´W

Station #	CTD #	Start time (UTC)	Start Date (UTC)	Start Lat.	Start Long.	Action*	End time (UTC)	End Date (UTC)	End Lat.	End Long.
MSM025/035	21	2:04:18	09.02.13	27°44.306 S	13°22.898 W	CTD; 2 ADCP's, turbidity-sensor, depth: 3165m	3:52:00	09.02.13	27°44.302 S	13°22.899 W
MSM025/036		4:04:00	09.02.13	27°44.12 S	13°22.90 W	Multibeam, ~ 4,4 kn	6:12:00	09.02.13	27°23.97 S	13°27.21 W
MSM025/037	22	6:24:17	09.02.13	27°24.005 S	13°27.195 W	CTD; 2 ADCP's, 1 MAPR on CTD, turbidity-sensor, depth: 3937m	8:49:10	09.02.13	27°24.006 S	13°27.198 W
MSM025/038		9:06:00	09.02.13	27°23.64 S	13°27.08 W	Multibeam, ~ 5,2 kn	10:28:00	09.02.13	27°10.99 S	13°28.13 W
MSM025/039	23	10:41:30	09.02.13	27°11.000 S	13°28.106 W	CTD; 2 ADCP's, 1 MAPR on CTD, turbidity-sensor, depth: 3373m	12:40:20	09.02.13	27°10.989 S	13°28.102 W
MSM025/040		12:44:00	09.02.13	27°10.99 S	13°28.11 W	Multibeam, ~ 9,4 kn	16:52:00	09.02.13	27°03.28 S	13°29.81 W
MSM025/041		19:15:00	09.02.13	27°03.46 S	13°29.73 W	Multibeam, ~ 9,3 kn	21:45:00	09.02.13	26°42.58 S	13°36.59 W
MSM025/042	24	21:52:25	09.02.13	26°42.576 S	13°36.583 W	CTD; 2 ADCP's, 1 MAPR on CTD, turbidity-sensor, depth: 3594m	23:58:00	09.02.13	26°42.577 S	13°36.583 W
MSM025/043		0:05:00	10.02.13	26°42.58 S	13°36.59 W	Multibeam, ~ 9,5 kn	1:43:00	10.02.13	26°30.94 S	13°43.86 W
MSM025/044	25	1:53:00	10.02.13	26°30.939 S	13°43.873 W	CTD; 2 ADCP's, turbidity-sensor, depth: 3721m	4:01:09	10.02.13	26°30.938 S	13°43.873 W
MSM025/045	26	9:17:50	10.02.13	25°45.365 S	13°56.653 W	CTD; 2 ADCP's, 1 MAPR on CTD, turbidity-sensor, depth: 4248m	11:44:00	10.02.13	25°45.367 S	13°56.646 W
MSM025/046										
MSM025/047		11:56:00	10.02.13	25°45.32 S	13°56.32 W	Multibeam, ~ 9,7 kn	14:26:00	10.02.13	26°03.91 S	13°52.48 W
MSM025/048	27	14:36:00	10.02.13	26°03.881 S	13°52.467 W	CTD - Tow-Yo; 2 ADCP's, 1 MAPR on CTD plus 4 MAPR at cable (50m, 100m, 150m, 200m), turbidity-sensor, depth: 2484m - 2858m	21:59:30	10.02.13	25°59.324 S	13°50.774 W
MSM025/049		22:35:00	10.02.13	25°57,02´S	13°51.80´W	AUV dive #128 at Merian vent field with Eh sensor and 410 kHz sidescan sonar	18:52:59	11.02.13	26°0,51´S	13°52.77´W
MSM025/050		0:20:00	11.02.13	25°57.02 S	13°51.80 W	Multibeam, ~ 9,5 kn	16:08:00	11.02.13	26°00.23 S	13°51.98 W
MSM025/051	28	20:26:00	11.02.13	26°13.231 S	13°50.474 W	CTD; 2 ADCP's, turbidity-sensor, depth: 3834m	22:35:40	11.02.13	26°13.233 S	13°50.473 W
MSM025/052	29	2:40:00	12.02.13	25°37.102 S	13°34.602 W	CTD; 2 ADCP's, 1 MAPR on CTD, turbidity-sensor, depth: 3948m	4:52:35	12.02.13	25°37.098 S	13°34.601 W
MSM025/053		5:01:00	12.02.13	25°37.09 S	13°34.61 W	Multibeam, ~ 10,1 kn	7:58:00	12.02.13	25°18.97 S	13°39.62 W

Station #	CTD #	Start time (UTC)	Start Date (UTC)	Start Lat.	Start Long.	Action*	End time (UTC)	End Date (UTC)	End Lat.	End Long.
MSM025/054	30	8:21:20	12.02.13	25°20.306 S	13°37.895 W	CTD - Tow-Yo; 2 ADCP's, 1 MAPR on CTD plus 4 MAPR at cable (50m, 100m, 150m, 200m), turbidity-sensor, depth: 2550m - 2744m	16:52:45	12.02.13	25°18.553 S	13°34.507 W
MSM025/055		17:00:00	12.02.13	25°18.55 S	13°34.51 W	Multibeam, ~ 9,5 kn	19:29:00	12.02.13	25°00.93 S	13°46.24 W
MSM025/056	31	20:23:10	12.02.13	24°59.946 S	13°38.798 W	CTD; 2 ADCP's, 1 MAPR on CTD, turbidity-sensor, depth: 3364m	22:17:00	12.02.13	24°59.947 S	13°38.802 W
MSM025/057		22:32:00	12.02.13	24°59.75 S	13°38.41 W	Multibeam, ~ 9,6 kn	18:13:00	13.02.13	22°10.16 S	13°45.09 W
MSM025/058	32	18:27:20	13.02.13	22°09.997 S	13°44.984 W	CTD; 2 ADCP's, 1 MAPR on CTD, turbidity-sensor, depth: 4168m	20:48:25	13.02.13	22°09.992 S	13°44.982 W
MSM025/059		21:43:00	13.02.13	22°17.26 S	13°45.86 W	Multibeam, ~ 9,8 kn	8:50:00	14.02.13	23°53.73 S	13°25.23 W
MSM025/060	33	10:18:50	14.02.13	23°47.403 S	13°24.404 W	CTD; 2 ADCP's, 1 MAPR on CTD, turbidity-sensor, depth: 3290m	12:12:30	14.02.13	23°47.402 S	13°24.402 W
MSM025/061		13:03:00	14.02.13	23°44.75´S	13°23.62´W	AUV dive #129 with Eh sensor and 120 kHz sidescan sonar	11:08:59	15.02.13	24°23,16´S	13°13.80´W
MSM025/062	34	16:27:35	14.02.13	23°31.304 S	13°27.418 W	CTD; 2 ADCP's, 1 MAPR on CTD, turbidity-sensor, depth: 3805m	18:35:10	14.02.13	23°31.304 S	13°27.416 W
MSM025/063		18:42:00	14.02.13	23°31.30 S	13°27.41 W	Multibeam, ~ 9,3 kn	21:41:00	14.02.13	23°56.37 S	13°16.38 W
MSM025/064	35	22:33:15	14.02.13	23°58.601 S	13°20.600 W	CTD; 2 ADCP's, 1 MAPR on CTD, turbidity-sensor, depth: 3552m	0:36:40	15.02.13	23°58.605 S	13°20.604 W
MSM025/065		0:47:00	15.02.13	23°58.60 S	13°20.48 W	Multibeam, ~ 8,5 kn	2:40:00	15.02.13	24°08.02 S	13°16.89 W
MSM025/066	36	2:50:28	15.02.13	24°08.115 S	13°17.078 W	CTD; 2 ADCP's, 1 MAPR on CTD, turbidity-sensor, depth: 3155m	4:40:16	15.02.13	24°08.108 S	13°16.998 W
MSM025/067		4:49:00	15.02.13	24°08.10 S	13°17.00 W	Multibeam, ~ 9,5 kn	7:21:00	15.02.13	24°23.11 S	13°13.61 W
MSM025/068	37	7:38:40	15.02.13	24°23.104 S	13°13.800 W	CTD; 2 ADCP's, 1 MAPR on CTD, turbidity-sensor, depth: 3671m	9:47:30	15.02.13	24°23.105 S	13°13.800 W
MSM025/069		11:20:00	15.02.13	24°23.47 S	13°13.74 W	Multibeam, ~ 9,5 kn	17:30:00	15.02.13	23°44.68 S	13°23.59 W
MSM025/070	38	17:37:30	15.02.13	23°44.680 S	13°23.580 W	CTD - Tow-Yo; 2 ADCP's, 1 MAPR on CTD plus 4 MAPR at cable (50m, 100m, 150m, 200m), turbidity-sensor, depth: 2701m - 2878m	20:43:10	15.02.13	23°44.659 S	13°22.563 W
MSM025/071	39	1:01:52	16.02.13	22°59.603 S	13°36.199 W	CTD; 2 ADCP's, 1 MAPR on CTD, turbidity-sensor, depth: 4322m	3:27:48	16.02.13	22°59.604 S	13°36.203 W
MSM025/072		3:32:00	16.02.13	22°59.60 S	13°36.20 W	Multibeam, ~ 9,6 kn	19:28:00	16.02.13	21°58.41 S	11°41.83 W

Station #	CTD #	Start time (UTC)	Start Date (UTC)	Start Lat.	Start Long.	Action*	End time (UTC)	End Date (UTC)	End Lat.	End Long.
MSM025/073	40	19:35:30	16.02.13	21°58.402 S	11°41.807 W	CTD; 2 ADCP's, 1 MAPR on CTD, turbidity-sensor, depth: 3921m	21:49:15	16.02.13	21°58.396 S	11°41.808 W
MSM025/074		22:06:00	16.02.13	21°58.00 S	11°41.87 W	Multibeam, ~ 9,5 kn	0:38:00	17.02.13	21°34.70 S	11°48.61 W
MSM025/075	41	0:43:42	17.02.13	21°34.707 S	11°48.601 W	CTD; 2 ADCP's, 1 MAPR on CTD, turbidity-sensor, depth: 3211m	2:33:10	17.02.13	21°34.706 S	11°48.599 W
MSM025/076		2:41:00	17.02.13	21°34.71 S	11°48.60 W	Multibeam, ~ 9,7 kn	4:15:00	17.02.13	21°21.69 S	11°50.83 W
MSM025/077	42	4:21:35	17.02.13	21°21.707 S	11°50.799 W	CTD; 2 ADCP's, 1 MAPR on CTD, turbidity-sensor, depth: 3813m	6:34:55	17.02.13	21°21.707 S	11°50.802 W
MSM025/078		6:41:00	17.02.13	21°21.70 S	11°50.80 W	Multibeam, ~ 10,0 kn	10:28:00	18.02.13	17°43.65 S	12°59.84 W
MSM025/079	43	10:58:05	18.02.13	17°43.701 S	13°01.811 W	CTD; 2 ADCP's, 1 MAPR on CTD (did not work - no avaible data), turbidity-sensor, depth: 3446m	13:07:47	18.02.13	17°43.703 S	13°01.801 W
MSM025/080		13:58:00	18.02.13	17°46.70´S	12°55,70´W	AUV dive #130 (aborted due to leak detection in main electronics bottle)	14:38:59	18.02.13	17°46,09´S	12°55,83´W
MSM025/081	44	16:20:31	18.02.13	18°02.303 S	12°53.003 W	CTD; 2 ADCP's, 1 MAPR on CTD plus 1 at cable (10m), turbidity-sensor, depth: 3636m	18:39:55	18.02.13	18°02.305 S	12°53.002 W
MSM025/082		20:23:00	18.02.13	17°46.37´S	12°55,72´W	AUV dive #131 with Eh sensor and 120 kHz sidescan sonar	17:42:59	19.02.13	18°36,60´S	12°44,56´W
MSM025/083		23:03:00	18.02.13	17°46.55 S	12°55.84 W	Multibeam, ~ 9,4 kn	4:03:00	19.02.13	18°28.98 S	12°48.03 W
MSM025/084	45	4:13:11	19.02.13	18°29.007 S	12°48.000 W	CTD; 2 ADCP's, 1 MAPR on CTD, turbidity-sensor, depth: 3454m	6:16:10	19.02.13	18°29.007 S	12°48.002 W
MSM025/085		6:24:00	19.02.13	18°29.00 S	12°48.00 W	Multibeam, ~ 2,6 kn	7:51:00	19.02.13	18°37.17 S	12°38.94 W
MSM025/086	46	8:03:10	19.02.13	18°37.205 S	12°38.899 W	CTD; 2 ADCP's, 1 MAPR on CTD, turbidity-sensor, depth: 3708m	10:23:30	19.02.13	18°37.205 S	12°38.900 W
MSM025/087		10:36:00	19.02.13	18°37.34 S	12°38.80 W	Multibeam, ~ 8,7 kn	15:43:00	19.02.13	18°36.53 S	12°44.59 W
MSM025/088		17:46:00	19.02.13	18°36.60 S	12°44.56 W	MUltibeam survey	8:16:59	20.02.13	20°15,57´S	11°43.67´W
MSM025/089	47	8:29:20	20.02.13	20°15.572 S	11°43.791 W	CTD; 2 ADCP's, 1 MAPR on CTD, turbidity-sensor, depth: 3343m	10:35:55	20.02.13	20°15.570 S	11°43.797 W
MSM025/090		10:55:00	20.02.13	20°15.91´S	11°43.59´W	AUV dive #132 with Eh sensor and 120 kHz sidescan sonar	8:04:00	21.02.13	20°56,43´S	11°34.99´W
MSM025/091						Multibeam				
MSM025/092	48	15:00:00	20.02.13	20°26.707 S	11°41.396 W	CTD; 2 ADCP's, 1 MAPR on CTD, turbidity-sensor, depth: 3373m	17:08:40	20.02.13	20°26.709 S	11°41.402 W

Station #	CTD #	Start time (UTC)	Start Date (UTC)	Start Lat.	Start Long.	Action*	End time (UTC)	End Date (UTC)	End Lat.	End Long.
MSM025/093						Multibeam				
MSM025/094	49	19:10:20	20.02.13	20°37.691 S	11°37.416 W	CTD; 2 ADCP's, 1 MAPR on CTD plus 1 at cable (10m), turbidity-sensor, depth: 3444m	21:21:15	20.02.13	20°37.691 S	11°37.409 W
MSM025/095										
MSM025/096	50	23:28:30	20.02.13	20°49.505 S	11°36.603 W	CTD; 2 ADCP's, 1 MAPR on CTD, turbidity-sensor, depth: 3430m	1:36:25	21.02.13	20°49.508 S	11°36.598 W
MSM025/097						Multibeam				
MSM025/098	51	3:23:00	21.02.13	20°56.505 S	11°35.102 W	CTD; 2 ADCP's, 1 MAPR on CTD, turbidity-sensor, depth: 3838m	5:52:11	21.02.13	20°56.505 S	11°35.101 W
MSM025/099		start: 11:45	21.02.13	20°49.211 S	11°36.582 W	Dredging;Tonnen-Dredge, depth: 3511m (start), 3349m (on deck)	on deck: 14:18	21.02.13	20°49.380 S	11°36.251 W
MSM025/100		start: 15:22	21.02.13	20°48.652 S	11°37.402 W	Dredging;Tonnen-Dredge, depth: 3503m (start), 3460m (on deck)	on deck: 17:38	21.02.13	20°48.868 S	11°37.016 W
MSM025/101		0:39:00	22.02.13	19°33.50 S	11°53.93 W	AUV dive #133 with Eh sensor and 120 kHz sidescan sonar	19:44:00	22.02.13	18°58.05 S	12°15.74 W
MSM025/102	52	3:38:30	22.02.13	19°25.704 S	11°56.901 W	CTD - Tow-Yo; 2 ADCP's, 1 MAPR on CTD plus 4 MAPR at cable (50m, 100m, 150m, 200m), turbidity-sensor, depth: 2554m - 2858m	9:06:40	22.02.13	19°24.104 S	11°54.901 W
MSM025/103	53	10:30:50	22.02.13	19°16.702 S	11°57.901 W	CTD; 2 ADCP's, 1 MAPR on CTD, turbidity-sensor, depth: 2787m	12:14:22	22.02.13	19°16.705 S	11°57.905 W
MSM025/104	54	14:20:10	22.02.13	19°00.207 S	12°12.101 W	CTD; 2 ADCP's, 1 MAPR on CTD, turbidity-sensor, depth: 2855m	16:06:10	22.02.13	19°00.205 S	12°12.104 W
MSM025/105	55	21:15:15	22.02.13	18°51.508 S	12°28.697 W	CTD; 2 ADCP's, 1 MAPR on CTD, turbidity-sensor, depth: 3291m	23:16:00	22.02.13	18°51.508 S	12°28.700 W
MSM025/106						Multibeam				
MSM025/107	56	13:03:30	23.03.13	17°15.125 S	14°13.624 W	CTD; 2 ADCP's, 1 MAPR on CTD, turbidity-sensor, depth: 3300m	15:05:17	23.02.13	17°15.126 S	14°13.621 W
MSM025/108						Multibeam				
MSM025/109						Multibeam				
MSM025/110	57	13:34:30	24.02.13	14°15.356 S	13°35.063 W	CTD; 2 ADCP's, 1 MAPR on CTD, turbidity-sensor, depth: 3335m	15:40:00	24.02.13	14°15.354 S	13°35.063 W
MSM025/111		18:09:00	24.02.13	14°38.80 S	13°30.23 W	AUV dive #134 with Eh sensor and 120 kHz sidescan sonar	13:35:00	25.02.13	15°24.00 S	13°16.28 W

Station #	CTD #	Start time (UTC)	Start Date (UTC)	Start Lat.	Start Long.	Action*	End time (UTC)	End Date (UTC)	End Lat.	End Long.
MSM025/112	58	20:55:30	24.02.13	14°42.505 S	13°29.299 W	CTD; 2 ADCP's, 1 MAPR on CTD, turbidity-sensor, depth: 2816m	22:37:45	24.02.13	14°42.503 S	13°29.302 W
MSM025/113	59	1:21:45	25.02.13	15°10.207 S	13°22.199 W	CTD; 2 ADCP's, 1 MAPR on CTD, turbidity-sensor, depth: 3042m	3:16:40	25.02.13	15°10.205 S	13°22.202 W
MSM025/114	60	6:08:26	25.02.13	15°37.002 S	13°15.604 W	CTD; 2 ADCP's, 1 MAPR on CTD, turbidity-sensor, depth: 3115m	8:06:35	25.02.13	15°37.002 S	13°15.603 W
MSM025/115	61	9:18:30	25.02.13	15°28.103 S	13°17.605 W	CTD; 2 ADCP's, 1 MAPR on CTD, turbidity-sensor, depth: 2839m	11:02:15	25.02.13	15°28.104 S	13°17.605 W
MSM025/116	62	15:55:00	25.02.13	15°10.365 S	13°20.713 W	CTD - Tow-Yo; 2 ADCP's, 1 MAPR on CTD plus 4 MAPR at cable (50m, 100m, 150m, 200m), turbidity-sensor, depth: 2740m - 2953m	20:51:15	25.02.13	15°09.380 S	13°22.061 W
MSM025/117						Multibeam				
MSM025/118		14:34:00	26.02.13	13°17.41 S	14°23.92 W	AUV dive #135 over Baileys Beads vent field with Eh sensor and 410 kHz sidescan sonar	9:54:00	27.02.13	13°17.52 S	14°25.88 W
MSM025/119						Multibeam				
MSM025/120	63	23:07:10	26.02.13	14°03.605 S	14°20.406 W	CTD; 2 ADCP's, 1 MAPR on CTD, turbidity-sensor, depth: 1854m	0:16:28	27.02.13	14°03.603 S	14°20.401 W
MSM025/121						Multibeam				
MSM025/122	64	3:53:20	27.02.13	13°35.406 S	14°31.205 W	CTD; 2 ADCP's, 1 MAPR on CTD, turbidity-sensor, depth: 3161m	5:53:59	27.02.13	13°35.408 S	14°31.209 W
MSM025/123						Multibeam				
MSM025/124	65	10:53:15	27.02.13	13°16.606 S	14°26.101 W	CTD - Tow-Yo; 2 ADCP's, 1 MAPR on CTD plus 4 MAPR at cable (50m, 100m, 150m, 200m), turbidity-sensor, depth: 2216m - 2390m	18:00:05	27.02.13	13°14.937 S	14°24.753 W

10 Appendix - AUV Dive descriptions

10.1 Station 004AUV - dive #124

Date: Feb 03rd/04th, 2013 Launch: 11:57 UTC Recovery: 06:42 UTC
Survey time: 14.7 hours Distance travelled: 96.3 km

Mission on segment 1 using Eh sensor while collecting sidescan data (120 kHz). Mission was flown at an altitude of 150 m and a range of 600m. Mission went fine and three discrete plume signals were recorded over a strike length of 6 km near the segment high. The strongest signal is detected north of the high. This signal is the strongest Eh-anomaly observed during this cruise even when considering the mission in the Merian vent field. Sidescan images show evidence for disturbence by vehicle movement, likely related to the high altitude of the mission and loss of bottom lock with strong counterreaction of the vehicle.

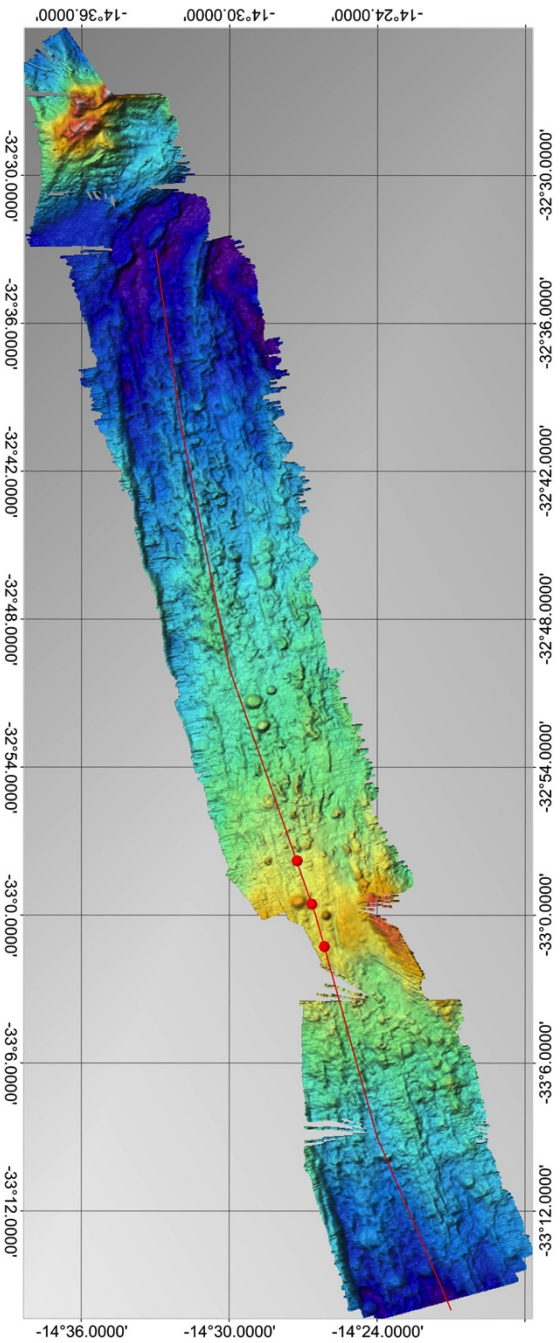

Uncorrected track and redox (Eh) hits of AUV Abyss along segment 1 (33°S). Underlying bathymetry is from this cruise.

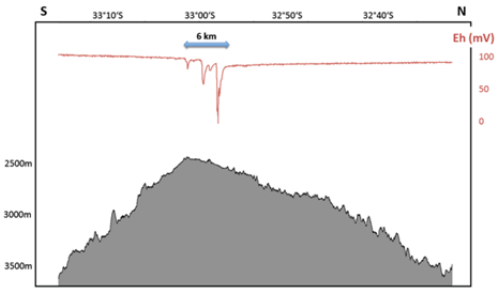

Navigation (offsets over time):
Checks with Posidonia were possible at the beginning and during two CTD stations.
offset at start (13:40 UTC): 276m/159°;
offset at 16:04 (UTC): 365m/158°;
offset at 04:47 (UTC): 556m/159°

10.2 Station 012AUV - dive #125

Date: Feb 05th/06th, 2013 Launch: 04:30 UTC Recovery: 00:07 UTC
Survey time: 14.3 hours Distance travelled: 88.1 km

Mission on segment 2 using the oceanography microstructure sensor and sidescan (120 kHz). Mission was flown at an altitude of 150 m and a sidescan range of 600m. Mission went fine, but water in the external data logger prevented collecting current information.

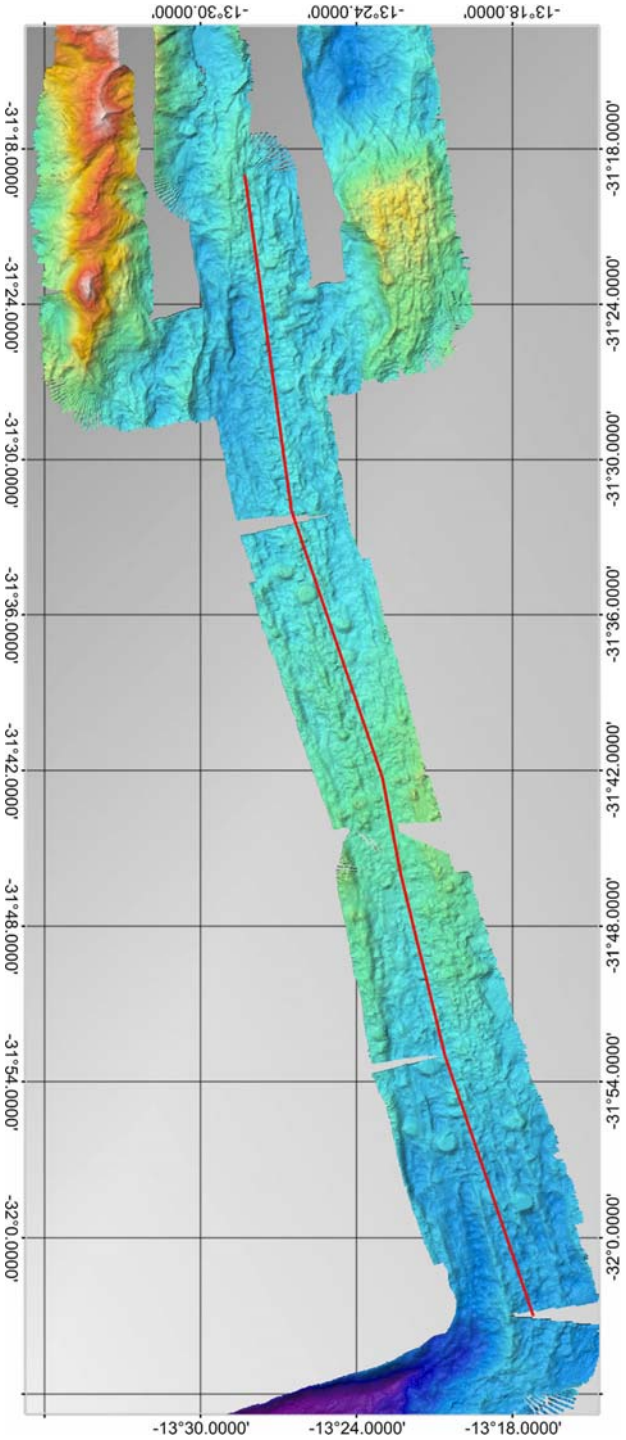

Uncorrected track of AUV Abyss along segment 2 (31°30'S). Note that no Eh-sensor was deployed during this survey. Underlying bathymetry is from this cruise.

Navigation (offsets over time):
Checks with Posidonia were possible at the beginning and during three CTD stations
offset at start (06:08 UTC): 122m/140°;
offset at 09:12 (UTC): 240m/166°;
offset at 11:55 (UTC): 364m/167°;
offset at 17:10 (UTC): 569m/167°

10.3 Station 020AUV - dive #126

Date: Feb 06th/07th, 2013 Launch: 15:05 UTC Recovery: 11:36 UTC
Survey time: 17.3 hours Distance travelled: 108.7 km

Mission on segment 3 using the Eh-sensor and sidescan (120 kHz). Mission was flown at an altitude of 150 m and a range of 600m. A small redox anomaly was encountered near a segment high in the northern part of the survey area. Sidescan data is only fair due to strong fin movement.

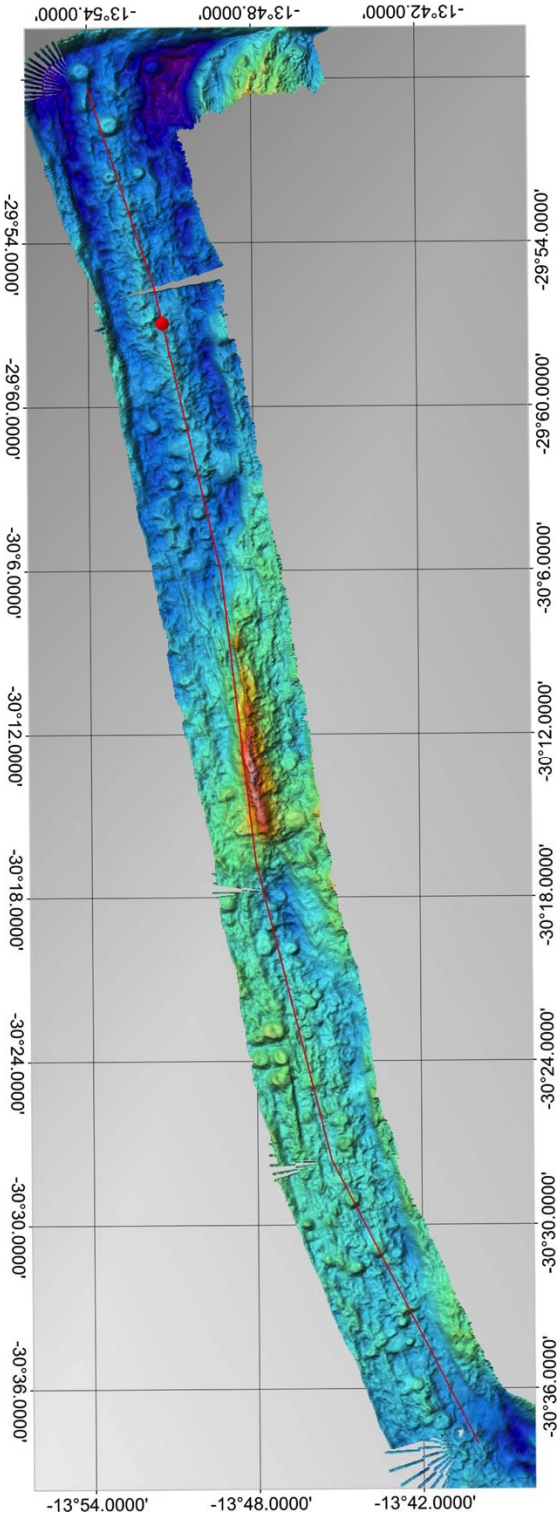

Uncorrected track and redox (Eh) hits of AUV Abyss along segment 3 (30°S). Underlying bathymetry is from this cruise.

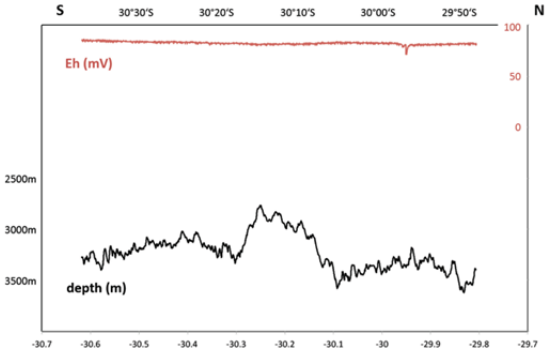

Navigation (offsets over time):
Checks with Posidonia were possible at the beginning and during three CTD stations
offset at start (16:46 UTC): 352m/247°;
offset at 20:29 (UTC): 361m/231°;
offset at 07:05 (UTC): 691m/204°;
offset at 17:10 (UTC): 908m/195°

10.4 Station 034AUV - dive #127

Date: Feb 08th/09th, 2013 Launch: 22:24 UTC Recovery: 18:55 UTC
Survey time: 17.1 hours Distance travelled: 108.1 km

Mission on segment 6 using the Eh-sensor and sidescan (120 kHz). Mission was flown at an altitude of 150 m and a range of 600m. Mission went fine and two redox anomalies were encountered near segment highs. The southern anomaly is quit pronounced while the northern one is very small. Sidescan data is fair.

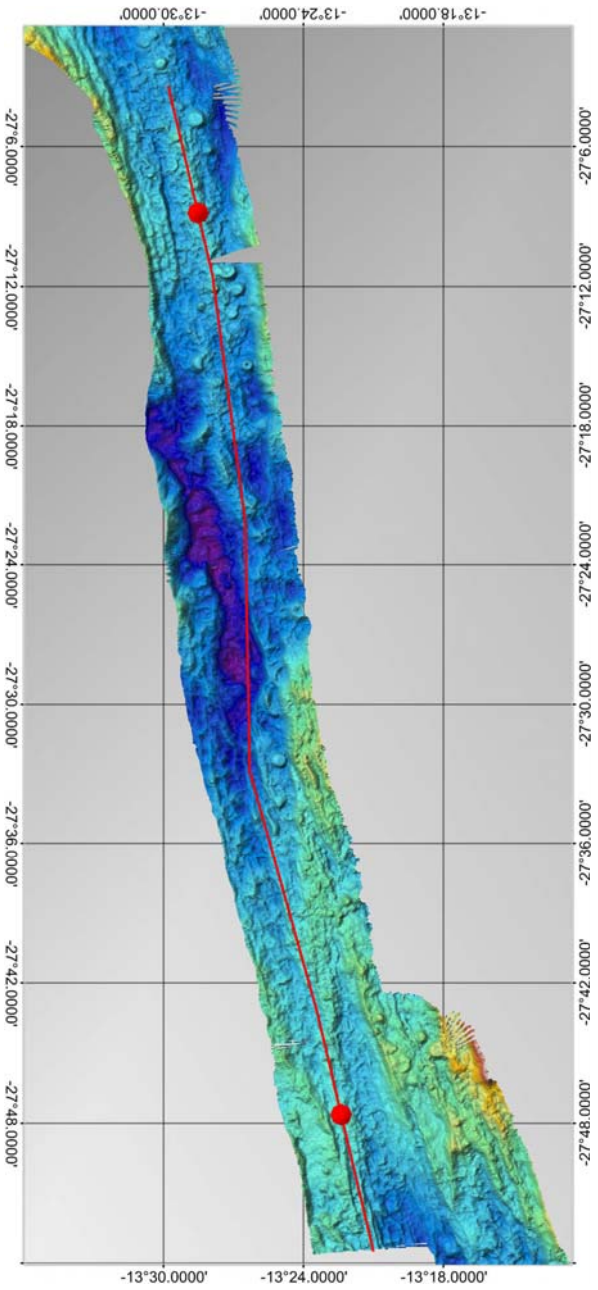

Uncorrected track and redox (Eh) hits of AUV Abyss along segment 6 (27°30'S). Underlying bathymetry is from this cruise.

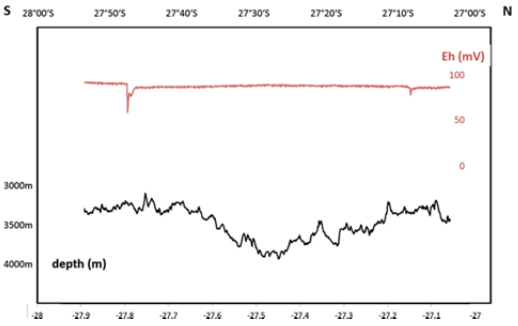

Navigation (offsets over time):
Checks with Posidonia were possible at the beginning and during two CTD stations.
offset at start (00:21 UTC): 260m/095°;
offset at 03:24 (UTC): 269m/115°;
offset at 17:24 (UTC): 464m/185°

10.5 Station 049AUV - dive #128

Date: Feb 10th/11th, 2013 Launch: 22:43 UTC Recovery: 18:57 UTC
Survey time: 17.7 hours Distance travelled: 108.7 km

Mission on segment high near 26°S using the Eh-sensor/turbidity and high-resolution sidescan (410 kHz) to identify and map possible hydrothermal fields at this summit. Mission was flown at an altitude of 50 m and a line spacing of 200m. Sidescan data is very good quality and imaged abundant sulfide structures the tallest ones tentatevily calculated as being > 20m in height. Sulfide structures are associated with faults in the eastern part of the volcanic edifice. The largest Eh hit is in the nadir line of the survey and therefore not visible in the sidescan data, but there are abundant chimneys visible in the sidescan images indicating a vigorous hydrothermal field.

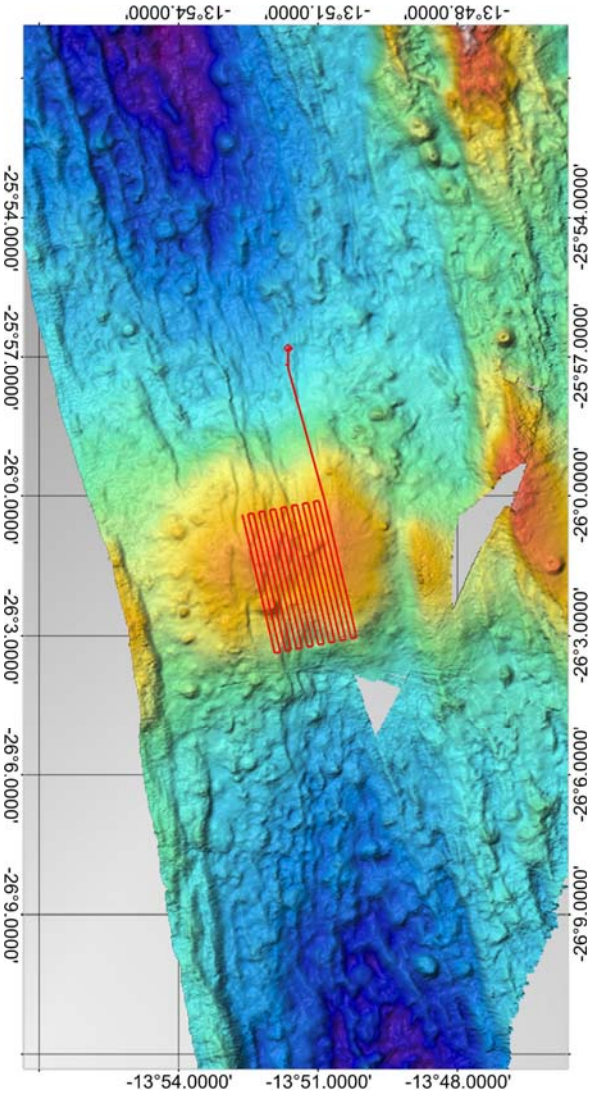

Left: Corrected track of AUV Abyss over the summit of the axial high at segment 7 (26°S). Dive is devoted to high-resolution sidescan and Eh/turbidity mapping of hydrotherml fields near the summit. Underlying bathymetry is from this cruise.

Below:
Map of the interpolated Eh values along track.

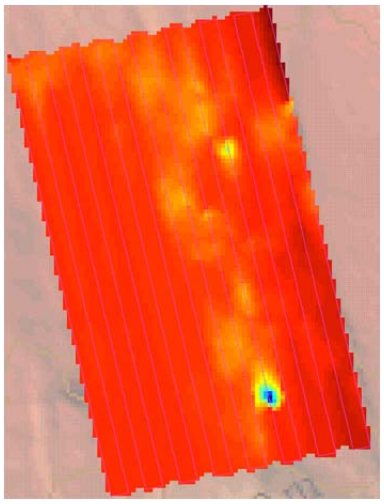

Navigation:
Checks with Posidonia were only possible during start and end of the survey
offset at start of survey was ca. 431m/162°;
offset at end 18:00 (UTC): ca. 358m/179°

10.6 Station 061AUV - dive #129

Date: Feb 14th/15th, 2013 Launch: 13:05 UTC Recovery: 11:08 UTC
Survey time: 19.2 hours Distance travelled: 113.1 km

Mission on segment 9 using the Eh-sensor and low-resolution sidescan (120 kHz). Mission was flown at an altitude of 100 m and covered a core complex in the center of the segment as well as the transition to the basaltic floor as well as the southern part of this segment. Sidescan data is good to fair. Still, vehicle movement due to high/low pitch is visible in the data record. A strong Eh and a weaker turbidity anomaly is visible at the starting point of the dive close to N/S-trending faults cutting the core complex near two east-west trending ridges. Dive is cut short due to failing battery capacity shortly before the final waypoint

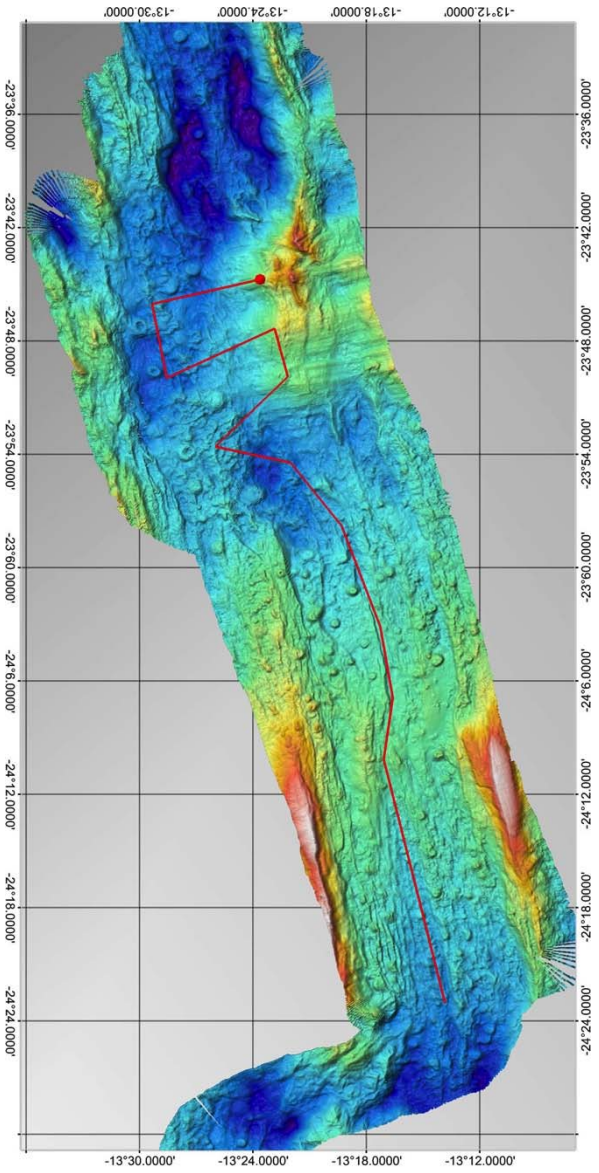

Uncorrected track and redox (Eh) hit of AUV Abyss along segment 9 (24°S). First part of the dive is devoted to few transects over the transition betwenn the core complex to the basaltic floor. Second part of the dive is along the southern part of this segment. Underlying bathymetry is from this cruise.

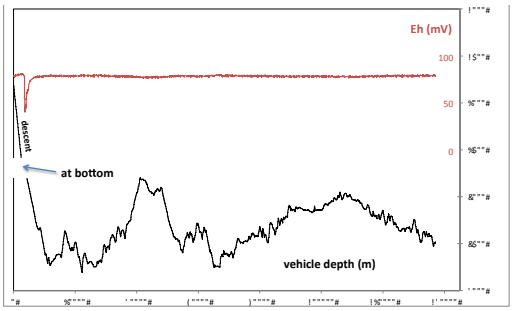

Navigation (offsets over time):
Checks with Posidonia were possible at the beginning and during a CTD station.
offset at start (14:35 UTC): 241m/173°;
offset at 04:31 (UTC): 224m/169°;

10.7 Station 080AUV - dive #130

Date: Feb 18th, 2013 Launch: 14:00 UTC Recovery: 14:39 UTC
Survey time: - hours Distance travelled: 0.7 km
Mission was aborted shortly after the start due to leak in the main junction box.

10.8 Station 082AUV - dive #131

Date: Feb 18th/19th, 2013 Launch: 20:16 UTC Recovery: 17:41 UTC
Survey time: 17.6 hours Distance travelled: 107.5 km

Mission on segment 13 using the Eh-sensor and low-resolution sidescan (120 kHz). Mission was flown at an altitude of 120 m and covered almost the entire segment. No Eh or turbidity anomalies were found during the survey. Mission was aborted at the ascent position due to low battery capacity (<5%).

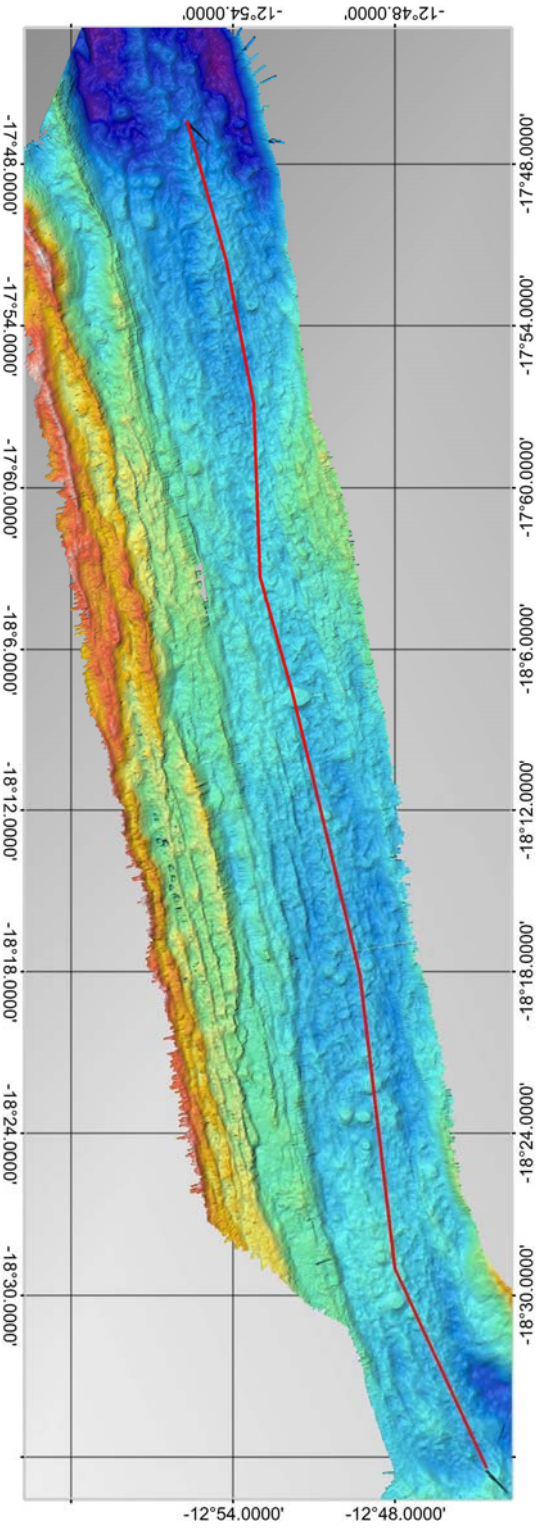

Uncorrected track of AUV Abyss along segment 13 (18°S). Neither Eh or turbidity anomaly were detected during this dive. Underlying bathymetry is from this cruise.

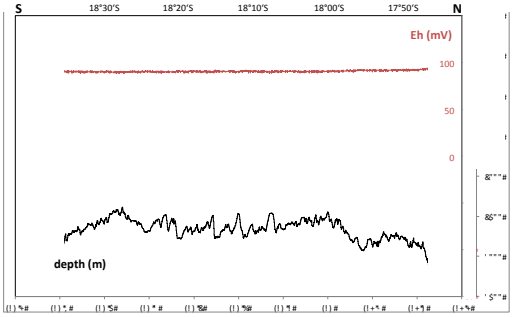

Navigation (offsets over time):
Checks with Posidonia were possible at two locations.
offset at start of survey (22:16 UTC) was 214m/232°;
offset at the end of the survey (cross at 16:04 (UTC) was: 423m/136°;

10.9 Station 090AUV - dive #132

Date: Feb 20th/21st, 2013 Launch: 10:57 UTC Recovery: 08:04 UTC
Survey time: 17.5 hours Distance travelled: 105.6 km

Mission on segment 11 using the Eh-sensor and low-resolution sidescan (120 kHz). Mission was flown at an altitude of 120 m and covered large parts of the segment. A survey with 3 boxes surrounding a steep-sided, cratered volcanic cone was included in the mission. Sidescan data is good to fair. No Eh or turbidity anomalies were found during the survey. Mission was aborted at the ascent position due to low battery capacity (<5%).

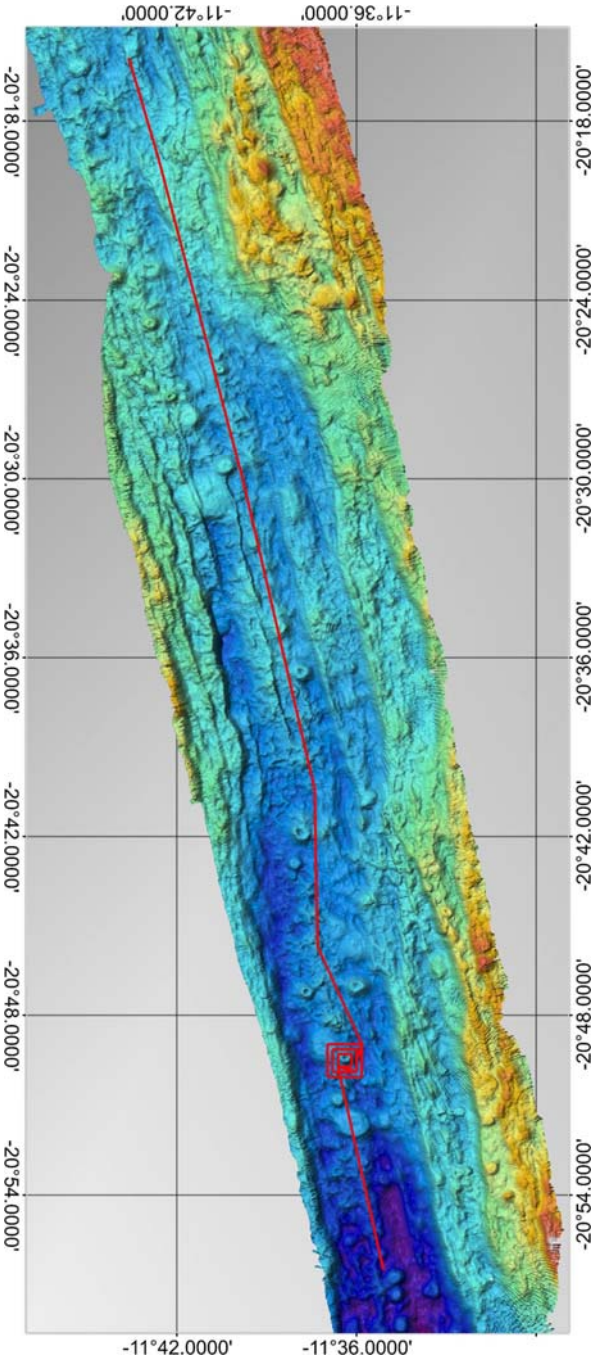

Uncorrected track of AUV Abyss along segment 11 (20°30'S). Neither Eh or turbidity anomaly were detected during this dive. Underlying bathymetry is from this cruise.

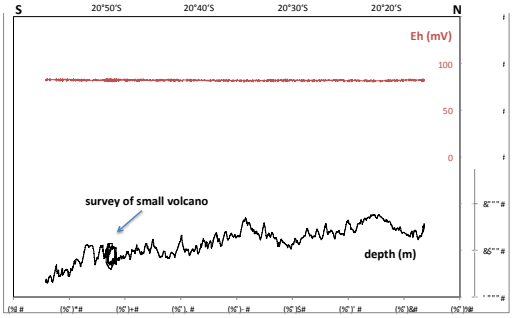

Navigation:
Checks with Posidonia were possible during some intervals (offsets over time)
offset at start of survey (12:29 UTC) was 122m/114°;
offset during mapping of the volcano at 01:00 (UTC) was: 447m/029°

Example of USBL/INS position offset during survey of steep-sided volcano:

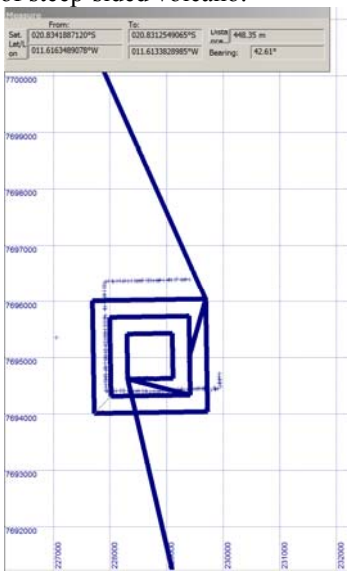

10.10 Station 101AUV - dive #133

Date: Feb 22nd, 2013 Launch: 00:41 UTC Recovery: 19:43 UTC
Survey time: 15.9 hours Distance travelled: 102.4 km

Mission on segment 12 using the Eh-sensor and low-resolution sidescan (120 kHz). Mission was flown at an altitude of 120 m and covered the northern, shallower parts of the segment with two small subsegments showing curved volcanic highs with elongated spines. An Eh and turbidity anomaly were both detected in the main rift valley, however, they do not coincide. The turbidity maximum is located on top of a small volcano while the pronounced Eh-anomaly occurs 2 km to the north. The turbidity anomaly is not associated with the vehicle flying at low altitude and related possible disturbense of local sediments. There is no turbidity anomaly associated with the Eh-peak. Also, there is no evidence for hydrothermal activity in the bend parts of the two subsegments or near the small volcanic high where the CTD towyo was flown (near 19°25'S). Sidescan data is good to fair.

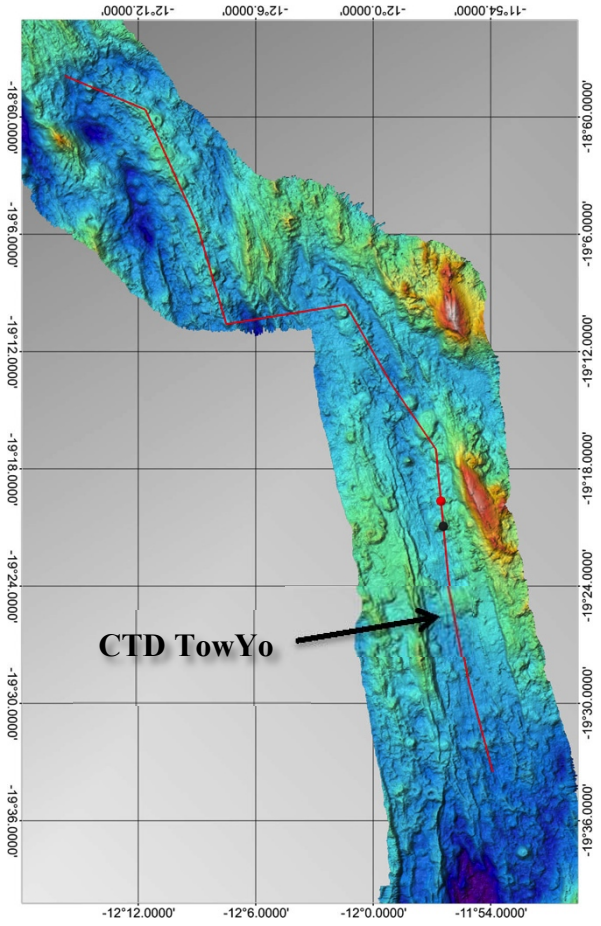

Uncorrected track and Eh anomaly of AUV Abyss along segment 12. Red dot and black dot indicate position of Eh and turbidity on the track, respectively. Underlying bathymetry is from this cruise.

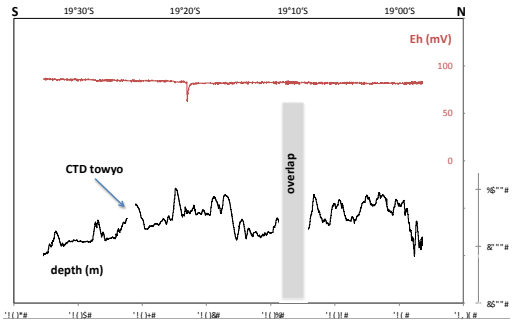

Navigation:
Checks with Posidonia were possible during 4 time intervals
offset at start of survey was ca. 102m/256°;
offset at 05:30 (UTC): ca. 141m/267°
offset at 16:34 (UTC): ca. 131m/170°
offset at end 18:19 (UTC): ca. 330m/145°

10.11 Station 111AUV - dive #134

Date: Feb 24th/25th, 2013 Launch: 18:14 UTC Recovery: 13:34 UTC
Survey time: 16.3 hours Distance travelled: 103.4 km

Mission on segment 15 using the Eh-sensor and low-resolution sidescan (120 kHz). Mission was flown at an altitude of 120 m and detected a small Eh anomaly near a short volcanic high in the southern part of the track. Sidescan data is good to fair.

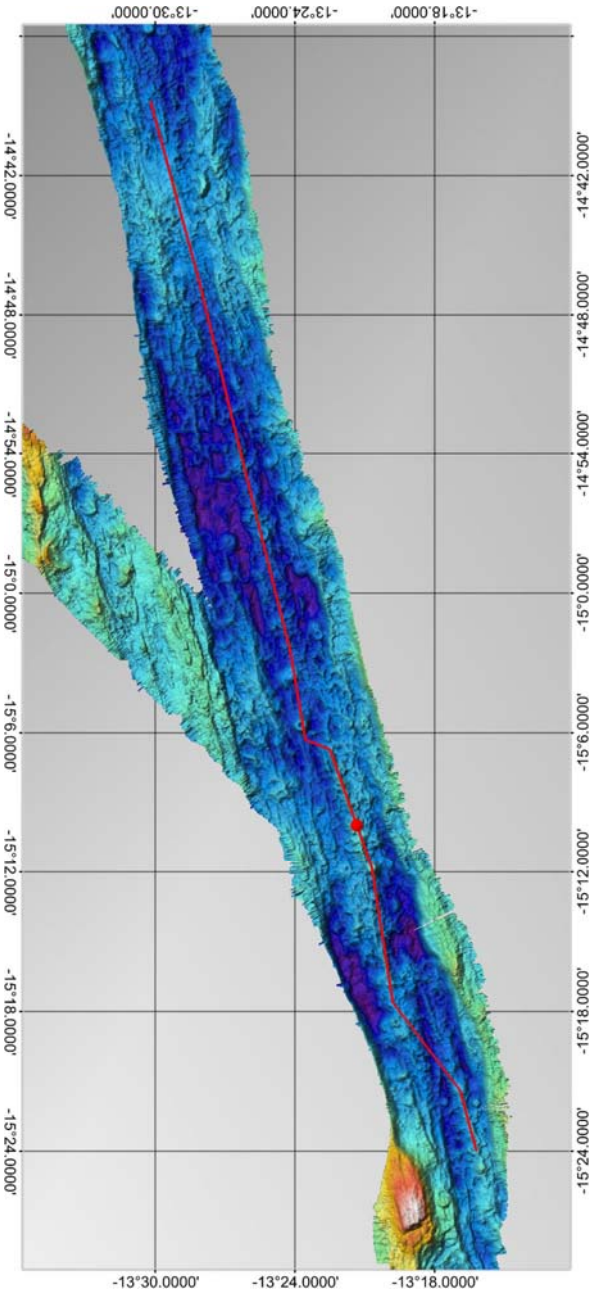

Uncorrected track and Eh anomaly of AUV Abyss along segment 15. Underlying bathymetry is from this cruise.

Navigation:
Checks with Posidonia were possible during 3 time intervals
offset at start of survey (19:38 UTC): 326m/224°;
offset at 21:12 (UTC): ca. 287m/220°
offset at end 12:12 (UTC): ca. 102m/133°

10.12 Station 118AUV - dive #135

Date: Feb 26th/27th, 2013 Launch: 14:36 UTC Recovery: 09:52 UTC
Survey time: 16.3 hours Distance travelled: 102.4 km

Mission on segment 16 using the Eh-sensor and high-resolution sidescan (410 kHz) over areas of known hydrothermal fields (Valentines Valles and Baileys Beads. Mission was flown at an altitude of 40 m (range 200m) and a line spacing of 100/300 m to achieve full overlap and no gaps. Comparison with USBL position data indicates that the survey was flown 400m north of the intended position. Eh anomalies and turbidity signals in the water column are widespread but Eh signals are surprisingly small (minimum of 76.8mV) when compared to many other surveys during this cruise. Sidescan data is very good.

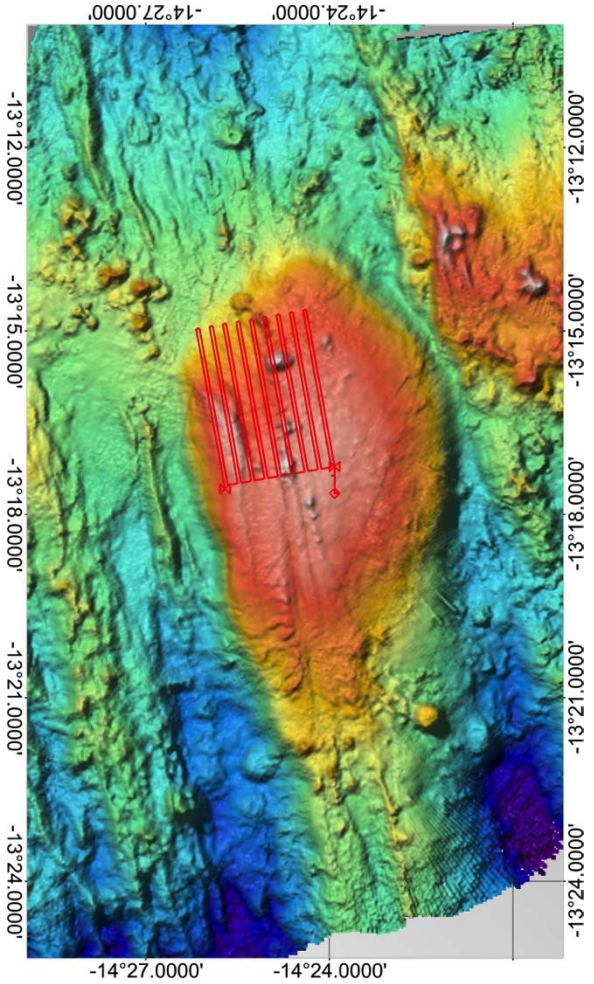

Left: Uncorrected track of AUV Abyss survey at segment high of segment 16. Underlying bathymetry is from this cruise.

Below: Eh and turbidity anomalies along track.

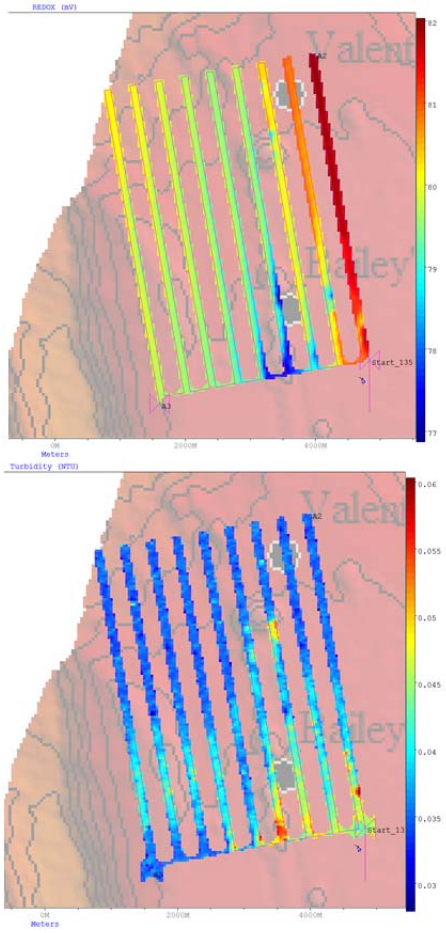

Navigation:
Checks with Posidonia were only possible during start and end of the survey
offset at start of survey was ca. 386m/351°;
offset at end 08:29 (UTC): ca. 486m/350°